UNIVERSITY OF READING

Department of Meteorology

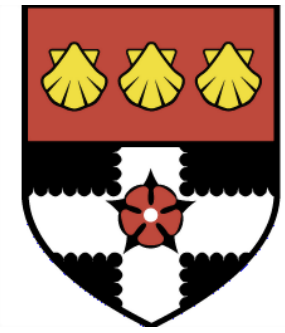

Modelling Melt Lake Formation on an Ice Shelf

Samantha Claire Buzzard

A thesis submitted for the degree of Doctor of Philosophy

February 2017

Declaration

I confirm that this is my own work and the use of all material from other sources has been properly and fully acknowledged.

Samantha Buzzard

Abstract

The accumulation of surface meltwater on ice shelves can lead to the formation of melt lakes. Melt lakes have been implicated in crevasse propagation and ice shelf collapse; the Larsen B ice shelf on the Antarctic Peninsula was observed to have a large amount of melt lakes present on its surface just before its collapse in 2002. Such collapse can affect ocean circulation and temperature, and cause a loss of habitat. Additionally, it can cause a loss of the buttressing effect that ice shelves can have on their tributary glaciers, thus allowing the glaciers to accelerate, contributing to sea level rise.

We present results of a 1-D mathematical model of surface melt on an idealised ice shelf. The model incorporates a calculation of the surface energy balance of an ice shelf, heat transfer through the upper ice shelf, the production and percolation of meltwater into the firn, the formation of ice lenses in the firn and the formation, development and refreezing of surface melt lakes on the ice shelf.

The melt lake model is applied to the Larsen C Ice Shelf, located on the Antarctic Peninsula, where melt lakes have been observed. The Antarctic Peninsula has warmed several times the global average over the last century and Larsen C has been suggested as a candidate for becoming fully saturated with meltwater by the end of the current century.

When forced with automatic weather station data from Larsen C, our model produces surface melting, meltwater accumulation, melt lake development and refreezing consistent with current observations. We examine the sensitivity of lake formation to uncertain parameters, and provide evidence of the importance of processes such as the lateral transport of meltwater (and thus ice shelf topography) to the formation of surface lakes, a process without which lakes were not found to form. Furthermore, we investigate the impact on melt lakes and the surface energy balance of possible future atmospheric conditions.

This thesis is dedicated to the memory of

Megan Davison (1989 – 2017)

the original maths partner in crime.

Acknowledgements

Firstly I would like to thank my supervisors at the University of Reading, Prof Daniel Feltham and Dr Daniela Flocco, for their contributions to this project. They have given me invaluable scientific guidance and support in allowing me to develop as a researcher. I would also like to thank my co-supervisor Prof. Peter Sammonds and his group at UCL for always going out of their way to make me feel welcome and assisting me when I needed and the rest of the CPOM group at Reading for their help and advice.

I would also like to thank Prof Jonathan Gregory and Dr Remi Tailleux for acting as my monitoring committee and the advice that they have provided along the way.

I am grateful to the many people within the glaciology community have provided helpful comments or resources but especially to Allen Pope and also the MIDAS project members for providing verification for the model.

The PhD and general social community within Reading meteorology have made the process of completing a PhD far better than I could ever have hoped. Office cake makers, panto participants, Thursday quizzers, runners (and nearly triathletes), and those who have helped me out with somewhere to stay during writing up all make this a really great place to be.

Equally as important have been my friends outside of Reading for contributions of tea, food, support and of course gin.

I am particularly grateful to my family especially my parents for accepting that this was a far better thing to do than become an accountant without too many questions.

Finally I would also like to thanks James, both the band for making a key contribution to several Reading social occasions, and also, and most importantly, the person for always being supportive and never stopping believing that I could do this. He also made tea.

-Fairbro

Contents

Chapter 1

Introduction

1.1 Antarctic Ice Shelves

Antarctica is covered by an ice sheet consisting of thirty million cubic kilometers of land ice, extending over almost fourteen million square kilometers. It is fringed by ice shelves, floating tongues of ice that are attached to grounded ice which is resting on and moving over land. They interact with both the air and ocean and therefore exert control on the stability of their tributary glaciers and ice sheets as a whole (Vaughan and Arthern, 2007).

The Antarctic continent is fringed by many ice shelves, covering an area of over 1.56 million square kilometers (Rignot, 2013). They cover 75% of the continent's coastline and make up 11% of the area of Antarctica.

1.2 The Antarctic Peninsula

The Antarctic Peninsula, home of several ice shelves including the Larsen Ice Shelves, has warmed over five times the global average over the last century (Khazendar *et al.*, 2011). This warming is thought to be due to changes in atmospheric circulation, particularly in the Southern Annular Mode or SAM (the movement of the belt of westerly winds that circle Antarctica) due to anthropogenic influences such as greenhouse gas emissions and ozone depletion (Anisimov *et al.*, 2007). The level of influence of these factors has been debated. Thompson and Solomon (2002) suggest that the cooling of the Antarctic stratosphere through ozone loss leads to a pressure difference between Antarctica and the mid-latitudes which leads to a southern movement of the SAM. However this is challenged by Marshall *et al.* (2004) who state that trends in the SAM begin prior to stratospheric ozone depletion. It may be the case that greenhouse gase increases and stratospheric ozone depletion both act in combination, leading to meridional temperature gradients and movement of the SAM (Shindell and Schmidt, 2004).

Stronger winds cause advection of warmer maritime air masses over the Antarctic Peninsula mountains, resulting in warming of the Peninsula as warm, dry foehn winds descend the mountains (Barrand *et al.*, 2013). The influence of these foehn winds is discussed further in Chapter 4.

Barrand *et al.* (2013) find that the melt extent in the Peninsula is strongly correlated with the October-January averaged Southern Annular Mode index, suggesting the melt here is linked to large-scale modes of atmospheric variability.

On some of the Peninsula Ice Shelves surface melting of snow and firn (partially compacted snow) has been observed to occur and surface melt lakes have also been observed. Temperatures in the Peninsula frequently exceed 0°C and as much as 66% of the total volume of Antarctic snow melt occurs here (Kuipers Munneke *et al.*, 2012b).

The Antarctic Peninsula's glaciers and ice shelves have been shown to have large mass balance sensitivities to temperature (Hock *et al.*, 2009) and have been observed to have thinned due to both surface and basal melting (Shepherd *et al.*, 2003) during recent years.

Figure 1.1 shows the location of the Larsen C Ice Shelves on the Antarctic Peninsula. The Larsen A Ice Shelf collapsed in 1995 and the Larsen B Ice Shelf partially collapsed in 2002.

1.3 Ice shelf loss

Sudden ice shelf disintegration can lead to losses of vast areas of ice in short periods of time. For example, the dramatic collapse of the Larsen B Ice Shelf in 2002 has been well documented, with 3200 km^2 of ice being lost during a small number of weeks (Scambos *et al.*, 2004). The loss of the buttressing effect of these ice shelves has been observed to lead to acceleration of glaciers that previously fed onto the ice shelves (Rignot *et al.*, 2004; De Angelis and Skvarca, 2003), which will lead to an increase in sea level. Rignot *et al.* (2004) estimated that the mass loss associated with the flow acceleration subsequent to the collapse of the Larsen B Ice Shelf exceeds 27 km^3 per year with some glaciers showing a two- to six-fold increase in centreline speed (Scambos *et al.*, 2004). Furthermore, it has been suggested that this flow acceleration is contributing to the approaching demise of the remainder of the Larsen B Ice Shelf (Khazendar *et al.*, 2015).

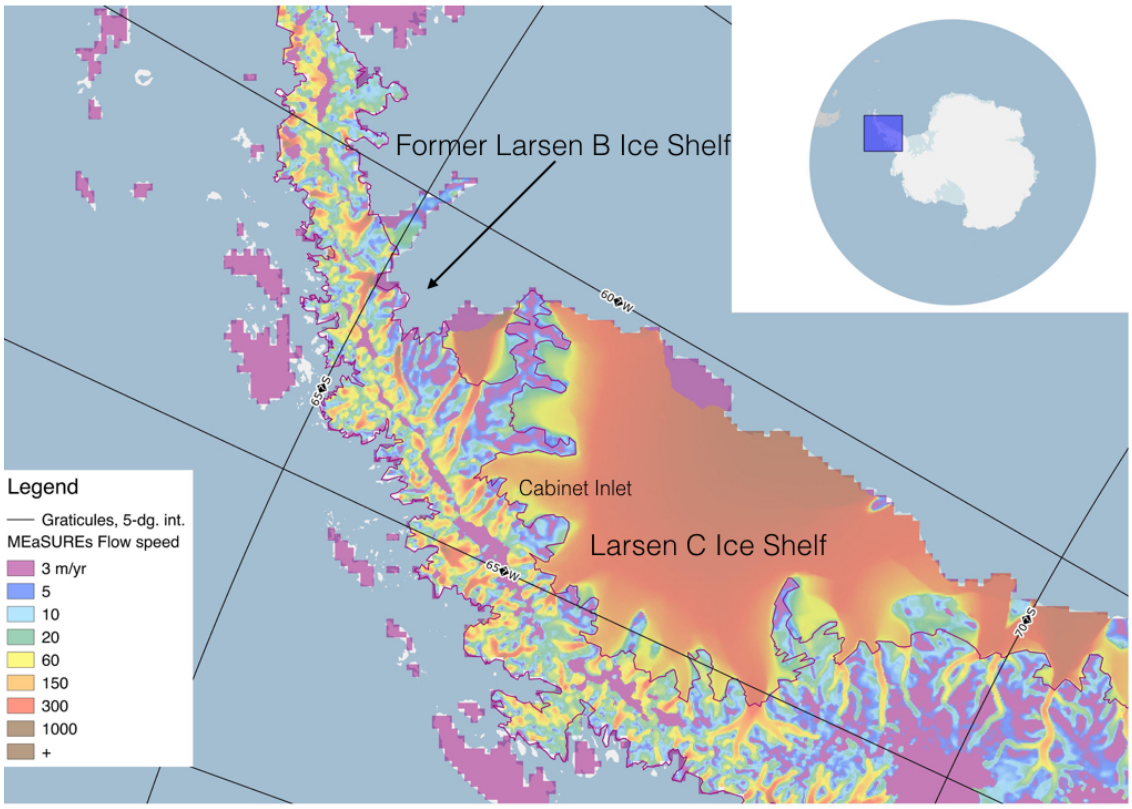

Figure 1.1: The Larsen Ice Shelves on the Antarctic Peninsula, showing the location of Larsen B before its break up and the location of the Larsen C Ice Shelf. The flow speed of the ice is shown, and the grounding line of the ice shelf (shown as a red line).

Rebesco *et al.* (2014) found that sea floor sediment at the current grounding line (the point where the ice sheet flows off of the land and becomes an ice shelf floating on the ocean) of the Larsen B Ice Shelf suggests that Larsen B's grounding line had been stable for thousands of years and thus grounding line instability was not a factor in this ice shelf's sudden collapse. This is taken to suggest that the collapse was likely a response to surface warming as opposed to thinning of the ice shelf from below due to heating from the ocean.

Most ice shelf break up events occur during longer melt seasons suggesting that melt-water, rather than just warming, is responsible (Scambos *et al.*, 2000). Melting on ice shelves and ice sheets can lead to water accumulating in certain areas which can result in the formation of melt lakes.

The 2001/02 melt season on Larsen B had a high level of melting with a total of 802 melt hours, 96% more than the average of 410 melt hours for this ice shelf previous to this

(van den Broeke, 2005). Furthermore, significant meltwater lake coverage was noted on the Larsen B Ice Shelf before its collapse, as shown in Figure 1.2. This collapse occurred during the warmest summer recorded on the northeastern Antarctic Peninsula, where Larsen B is located (Skvarca *et al.*, 2004).

One possible mechanism for meltwater playing a role in ice shelf collapse is that it can fill crevasses on the ice shelf and cause them to propagate both vertically and horizontally, due to the pressures caused by water having a greater density than ice. Scambos *et al.* (2000) suggest that when sufficient meltwater is present for crevasses to remain 90% filled with water then they are very likely to propagate through the full depth of the ice shelf.

The region of the Larsen B Ice Shelf that experienced sudden disintegration lay almost completely within the region of observed melt lakes on the ice shelf surface (Scambos *et al.*, 2004), which were noted to drain shortly before the break up event (Banwell *et al.*, 2013). The pattern of break up of Larsen B suggests that fracturing by surface melt played a key role in the disintegration of the ice shelf (Rack and Rott, 2004).

Crevasse propagation requires a significant amount of water as for the meltwater to penetrate into the cold ice shelf interior the process needs to happen quickly. Scambos *et al.* (2003) suggest that for a 0.5 m wide crevasse this penetration needs to happen on a timescale of hours to days. However, when penetration does occur, the ice shelf will remain weak as the refrozen ice will remain warmer (and therefore softer) than the older glacial ice for many years. Furthermore, seawater can also infiltrate the crevasse below which will create permanently weaker zones of frozen saline ice within the base of the ice shelf (Scambos *et al.*, 2003).

Decadal-scale processes in the firn layer overlying the ice shelves can lead to ice shelves reaching the conditions necessary for a sudden collapse, and thus melt lake formation and crevasse propagation should be considered the final stage for ice shelf collapse (Kuipers Munneke *et al.*, 2014). This may lead to the ice shelf reaching a critical limit at which minor disturbances may result in sudden collapse (Rott *et al.*, 1998). Therefore, the processes that lead to lake formation and the development of the lakes themselves can be key in predicting the future of ice shelves that have not yet reached the stage of significant melt lake coverage.

It has been suggested by Banwell *et al.* (2013) that lake-induced flexural stresses can produce a fracture network that can lead to a chain reaction of lake drainage and result

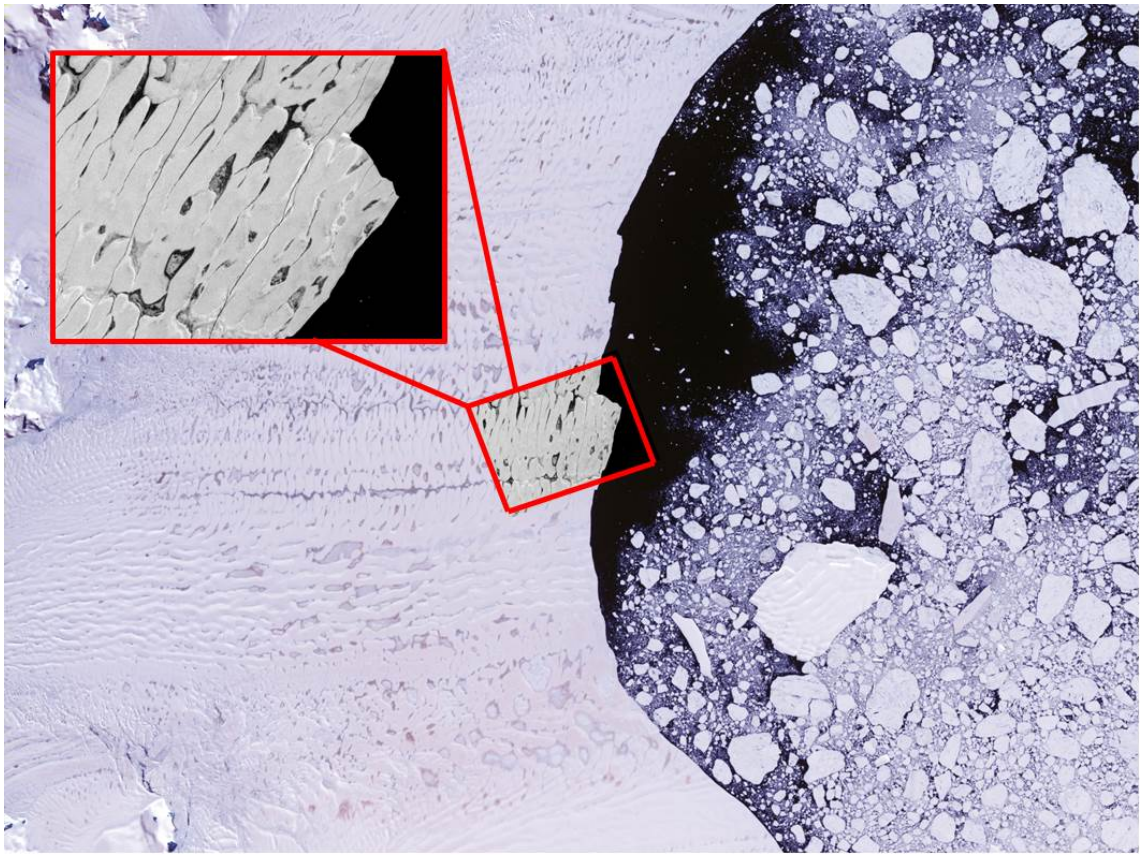

Figure 1.2: Melt lakes observed on Larsen B at the time of break up, 2002. The zoomed in area in the red box shows the presence of melt lakes on the ice shelf surface (image edited, originals copyright NASA).

in sudden ice shelf collapse. Therefore, it is possible that more than one process may lead to sudden ice shelf collapse, although it seems likely that meltwater and melt lakes play a role.

Large collapse events such as those observed on the Larsen B Ice Shelf are unprecedented in the last 10,000 years (Domack *et al.*, 2005). The collapse followed the warmest summer recorded on the ice shelf (Skvarca *et al.*, 2004). Furthermore, it is thought that even if iceberg calving were to cease it would take centuries for the ice shelf to return to its pre-collapse state (Rignot *et al.*, 2004), suggesting these sudden events are connected to the recent warming rather than being due to cyclic variations in the climate of the Peninsula.

Ice shelf collapse is important as the addition of the cold, fresh water to the ocean that results from the melting of the collapsed areas of ice can affect ocean circulation, heat budget and salinity, in addition to causing potential shipping hazards. Furthermore, ice

shelf loss can cause loss of biological habitat.

Possibly the most significant consequence of ice shelf loss can be the subsequent contribution to sea level rise. Although the ice shelves themselves do not contribute to sea level rise (as ice that is floating on the ocean they have already displaced their own weight in the water so sea level will not change following their collapse) the acceleration of their tributary glaciers as a result of the loss of the buttressing effect of the ice shelf as described above does then contribute to sea level rise. This acceleration was observed when the Larsen B Ice Shelf collapsed (Rignot *et al.*, 2004).

1.4 Surface melt lakes on the Larsen C Ice Shelf

Surface melt lakes have been observed on the Larsen C Ice Shelf, the southern neighbour of the Larsen B Ice Shelf. Alongside other Peninsula ice shelves it too has been experiencing warming, resulting in the $-9\,^{\circ}\mathrm{C}$ isotherm, which has been suggested as being the northern limit of ice shelf viability (Morris and Vaughan, 2003), having now moved far enough south to cross the Larsen C Ice Shelf. It has been suggested as one of the most susceptible ice shelves for sudden collapse based on melt activity (Scambos *et al.*, 2000), firn characteristics and melt season length (Scambos *et al.*, 2004).

Larsen C has been changing during recent years. During the extreme melt season of 1993, no melt lakes were observed on the ice shelf despite over 50 days of melting (Scambos *et al.*, 2003). However, lakes have been observed on the ice shelf in subsequent years (see Section 4.1), suggesting that some of this previous melt was retained and densified the firn, as oppose to running off of the ice shelf.

The presence of these lakes is significant for two reasons:

1. The lakes are darker than surrounding ice and so will have a lower albedo, thus absorbing more shortwave radiation in a feedback loop that can lead to further melting;

2. The lakes have been implicated in ice shelf break up as discussed above.

In addition to surface melt, it is also the case that the Larsen C Ice Shelf is thinning from underneath due to warming from the ocean (Holland *et al.*, 2015). The influence of sea ice on the ice shelf can have a stabilising effect on preventing rift or crevasse propaga-

tion (Jansen *et al.*, 2010), although the stability of the ice shelf has recently become much less certain with the discovery of a growing rift that is likely to soon lead to the loss of an iceberg of more than 5000 km^2 from the ice shelf front and may lead to the remaining ice becoming unstable (The MIDAS project, 2017). Therefore, understanding these processes alongside those taking place for surface melt are essential in gaining a full understanding of possible future conditions on the Larsen C Ice Shelf.

It is clear that surface melt and firn densification are important processes that determine future change of the Larsen C Ice Shelf. Lakes of tens of meters in width and tens of kilometres in length have been observed on the ice shelf (Luckmann *et al.*, 2015). The ice shelf is lowering and losing air content due to surface melting (Holland *et al.*, 2011) and becoming less permeable to meltwater (Khazendar *et al.*, 2011). Therefore, in order to begin to understand the conditions and possible future outcome for the Larsen C Ice Shelf an understanding of the potential for melt lake formation on the ice shelf and any effect their presence may have is essential.

The possible role of surface melt in ice shelf collapse and the observation of melt lakes on the Larsen C Ice Shelf suggest that the investigation of surface melt processes on this ice shelf is important in understanding how the ice shelf may continue to change in the future.

1.5 Modelling studies of surface melt and lake formation

A great deal of the previous work on ice melt lakes and ponds has been focussed on ponds on sea ice, for example the work of Taylor and Feltham (2004), Scott and Feltham (2010) and Ebert and Curry (1993). Although many of the principles used in these studies can be applied to melt lakes on ice shelves, a key difference is that ice shelves consist only of frozen freshwater. They have no saline content, unlike sea ice, where salinity and mushy layer theory are central to the consideration of the modelling of melt ponds. Furthermore, the processes of firn compaction and meltwater percolation will be much more important when considering ice shelves as ice shelves can have thousands of years of compacted firn transitioning into ice on their surface whereas sea ice in many cases may be less than a year old.

Some modelling studies that have specifically looked at melt lakes on ice sheets and

ice shelves have been carried out. These include Lüthje *et al.* (2006a), Leeson *et al.* (2012), Clason *et al.* (2012) and Banwell *et al.* (2012b). In addition, Sergienko and MacAyeal (2005) look at surface melt specifically on the Larsen Ice Shelves.

Several of these studies investigate surface melt on the Greenland Ice Sheet. Although this is a different situation to the Antarctic ice shelves investigated in this thesis these studies are still useful for comparison as there are many similarities between the surfaces of ice shelves and ice sheets. For example, they both consist of fresh water ice and have lakes occurring over larger spatial scales than sea ice melt ponds. Furthermore, topography plays an important role in the location of ice shelf and ice sheet melt lake formation.

1.5.1 Lüthje et al. 2006

The Lüthje *et al.* (2006a) study uses a one-dimensional model to investigate the evolution of supraglacial lakes on the West Greenland Ice Sheet margin. Their focus is on the enhanced ablation caused by the presence of these lakes.

They use the enthalpy method which tracks the total energy in the system and then use this to calculate the liquid fraction of a volume of ice and water.

They assume that heat is transferred through the ice shelf by conduction and have a Neumann condition at the bottom boundary of the model domain. The surface temperature is calculated using a surface energy balance equation which is forced using data collected from the West Greenland Ice Sheet. Sensible and latent heat fluxes are calculated using bulk formulae, although these do not include a value for wind speed which can be an important factor in the magnitude of these fluxes.

This model considers solely the processes that take place once melting has begun on the ice sheet. It is run for 30 days from the point that snow cover has disappeared.

Here lateral transport of meltwater is initiated using a drainage model from Lüthje *et al.* (2006b) which calculates runoff as proportional to the gradient of surface topography, which is obtained from a surface digital elevation model. This approach does mean that important processes such as water loss through streams or moulins is lost, but these processes would add a great deal of complication to the model.

In contrast to the modelling efforts in this thesis, the percolation of water through snow is not considered. Instead the model is run at the point that it is assumed that

all snow has disappeared and therefore the boundary between the ice and lake can be tracked without having to incorporate any processes that take place in the firn. Although this assumption may be valid for parts of Greenland and some glaciers it would limit the applications of a model like this to areas such as the Larsen C Ice Shelf where there is significantly more firn which does not disappear completely during one melt season.

The use of a vertical domain of 4 m allows Lüthje *et al.* (2006a) to use a small grid size of 1 cm. This does mean that any heat transfer below 4 m is not captured by the model, but as it is run for such short timescales (just the development of one lake) this may not be an issue. They state that 'enthalpy variations only occur in the uppermost part of the ice sheet' as a justification for their domain size, which, while this may be true for the timescales they look at, would not be valid for looking at the development of lakes over several years.

The Lüthje *et al.* (2006a) model includes the assumption that, due to the 'relatively large surface slope (0.009) of the area studied', lakes of less than 50 cm cannot form. As will be shown in Chapter 4, lakes on the Larsen C Ice Shelf are often less than 50 cm deep, and the surface there is not bare ice so this assumption would not be valid for use in the model presented in this thesis.

The study found that the lakes on the Greenland Ice Sheet play a significant role in causing enhanced ablation beneath the lake (by 110 and 170% for the years investigated), suggesting that the albedo change caused by lake presence has a high importance for the surface energy balance and overall melt rate on the ice sheet. The model results show reasonable agreement between the modelled position and satellite observations of lakes. The authors suggest that the area coverage of lakes found by the model was too large, and that the inclusion of artificial moulins was necessary for more realistic lake coverages, suggesting that these are in fact very important for the Greenland case.

1.5.2 Banwell et al. 2012

The Banwell *et al.* (2012b) study looks at supraglacial lake filling on Greenland, focussing on the Paakitsoq region. Their study uses the surface energy balance model of Rye *et al.* (2010), which is calibrated in Banwell *et al.* (2012b) for Greenland, to calculate melting and subsequent runoff. Lateral transport is then modelled using the catchment algorithm of Arnold (2010).

The surface mass balance model of Rye *et al.* (2010) couples a surface energy exchange model to a subsurface model which simulates changes in temperature, density and water content in the firn. Here, the surface energy balance is modelled by calculating the energy available for melting from the net shortwave, longwave, sensible heat, latent heat and ground heat fluxes. The subsurface model allows snow accumulation and meltwater percolation down into the firn. Refreezing of meltwater occurs where the temperature is below freezing and the density is less than the density of ice. Meltwater is allowed to percolate through cells at the freezing temperature up to the snow ice interface. It is not allowed to saturate the snow, but rather forms runoff if it reaches the snow-ice interface and does not refreeze.

The Rye *et al.* (2010) model does not include dry snow densification as it is noted that the formation of ice lenses is prevalent on the glacier the model is investigating, Midre Lovénbreen in Svalbard (Wright *et al.*, 2007).

The model was calibrated, optimising the model parameters against available mass balance measurements. It was found that although the calibrated solution performed well at locations for which measurements were available it was relatively insensitive to both superimposed ice and internal accumulation. It is suggested that this is due to the superimposed ice and firn zones only comprising a small percentage of the overall mass of Midre Lovénbreen. For the case of the Larsen C Ice Shelf it is likely that these processes are far more important, due to snow accumulating annually (areas of Midre Lovénbreen have areas that are seasonally snow free) so these processes need to be included in the model that is developed during this thesis.

Banwell *et al.* (2012b) calibrated the Rye *et al.* (2010) model for use in the Paakitsoq area of West Greenland. They then modelled lake formation by combining this calibrated surface mass balance model with simulated lateral transport, using the catchment algorithm of Arnold (2010) and the flow delay algorithm of Arnold *et al.* (1998). The flow delay algorithm ensures that the flow speed is dependent on the speed that water is able to move either by Darcy's Law for flow through a porous medium or in a supraglacial stream. The 2-D approach here is more sophisticated than the 1-D approach used in this thesis when considering lateral transportation but it is missing certain key processes. For example, the refreezing of meltwater during lateral transport, which as will be shown in Section 4.2.3 can impact on the amount of meltwater that is transported laterally in the

case of the Larsen C Ice Shelf. Development of this model would have been needed for its inclusion here and a simpler approach will be used, based on the data available and computational expense.

Banwell *et al.* (2012b) were able to model the filling rate of a supraglacial lake in Paakitsoq with a high level of accuracy. However, for application to the Larsen C Ice Shelf there are processes not included in this approach that would be important for modelling lakes on Larsen C that are therefore dealt with during this thesis.

1.5.3 Leeson et al. 2012

Leeson *et al.* (2012) model the growth of supraglacial lakes on the western margin of the Greenland Ice Sheet, using runoff estimates from a regional climate model, which are routed across the ice sheet using a 2-D hydrology model which incorporates data from a digital elevation model.

The hydrology model combines Darcy's law for flow through a porous medium with Manning's equation for open channel flow and calculates water displacement based on the ice and water surface level in neighbouring cells.

This modelling approach shows a reasonable level of agreement between the location of modelled and observed lakes and also with the total cumulative area and onset days of lakes.

However, it does not account for excess water created through ablation at the lake bottom, which Lüthje *et al.* (2006a) find to be an important process in enhancing ablation in Greenland.

1.5.4 Clason et al. 2012

Clason *et al.* (2012) developed a model for the delivery of meltwater to the base of ice sheets, an important process as this can promote enhanced basal motion through the lubrication of the glacier bed (Zwally *et al.*, 2002b). This study is relevant here as part of their model involves calculating the total surface summer ablation across the catchment area of the case study area (Devon Ice Cap, Nunavut, Canada). The study is conducted using a degree-day method.

1.5.4.1 The degree day method

The degree day method involves using daily-averaged temperatures, T_t, to calculate a value of melt, M_t, by applying a degree day factor, DDF, for all days with a mean temperature above freezing, such that

$$M_t = (DDF \times T_t) \qquad T_t \geq 0^{\circ}C \tag{1.1}$$

$$M_t = 0 \qquad T_t < 0^{\circ}C \tag{1.2}$$

Separate values for DDF are used depending on if the surface is ice or snow. For the area studied, the situation is more similar to that of Greenland, as described above in Lüthje *et al.* (2006a) where it is expected that the whole seasonal snow cover will melt each year and expose the ice below.

In the Clason *et al.* (2012) study the degree day method was chosen for its simplicity and to accommodate the meteorological data available. Although this type of method would use considerably less computing time than the model developed during this thesis it would not be able to incorporate the diurnal cycle for example, which may be significant in lake formation on the Larsen C Ice Shelf where the overall number of hours that melting can occur is small.

A flow algorithm is used to move the calculated value of meltwater around the study area. This approach does not account for transit time through the snowpack, and instead assumes that melt generated in each cell will reach its final destination in a crevasse on the ice surface within one timestep. This may mean that the level of water calculated in crevasses on the ice shelf is overestimated. This approach would not be valid for the work in this thesis as meltwater may not be able to reach lakes during the time available since there are limitations on the rate that the meltwater can flow by Darcy's Law (see 4.2.3). Furthermore, it will be argued that meltwater will be lost due to refreezing within the snowpack so it cannot be assumed that all water will move from one area to another and remain as water.

Clason *et al.* (2012) use a digital elevation model in order to calculate flow across the ice surface, but also pre-prescribe the areas where supraglacial lakes are present, assigning each lake a maximum volume which, if exceeded, means that all further meltwater will contribute to downstream run off. This approach ensures that the results are likely

to closely follow observations of lakes but allows no room for changes in lake depth that may occur under changing climatic conditions.

Lakes on the Devon Ice Cap are here assumed to drain through to the bed during each melt season, whereas lakes on Larsen C are assumed in this thesis to refreeze in situ between melt seasons, so although the initial part of the Clason *et al.* (2012) study for lake formation is useful for comparison here, the approaches taken after lake formation mean that comparing these two study areas beyond this is not useful.

Sensitivity studies on the Clason *et al.* (2012) model suggest that the value of DDF is not important in delivering meltwater to the bed of the ice cap. However, the DDF for ice and snow are both altered in the same study (one is increased and one is decreased) so it is hard to tell here how sensitive the model is to changes in the value of the DDF.

It is noted by Marshall (2012) that although degree day models provide a simple approach as they only require air temperature data they are far removed from the physics of the melt process and so perform poorly when applied to short timescales such as hourly or daily melt. This would suggest that this approach is not suitable for areas with short melt seasons or those where the daily melt can be very variable.

1.5.5 Sergienko and MacAyeal 2005

The Sergienko and MacAyeal (2005) study investigates surface melt on the Larsen Ice Shelves. They compare a positive degree day method (similar to that described for Clason *et al.* (2012) above) with an energy and mass balance model. They looked at this in the context of the Larsen B breakup as a way of determining if these methods suggest enough water was present for crevasse propagation. This is done using weather station data from an automatic weather station on the Larsen C Ice Shelf.

For the positive degree day method it is noted that observations for use in determining the degree day factor are lacking for Antarctica as a whole and therefore a Northern Hemisphere figure is used and taken to be an upper bound for the Larsen Ice Shelves. This method does not predict enough melt to satisfy the amount calculated in the study that would be necessary to fill crevasses and initiate the collapse of the Larsen B Ice Shelf. However, it should be noted that using data from the Larsen C Ice Shelf is likely to underestimate melt rates as Larsen C is further south than Larsen B.

The energy- and mass-balance model developed during the study consists of thermodynamic, hydrodynamic and snow-compaction components. It models heat transport through the firn, and subsequent meltwater generation, percolation and refreezing. Here the assumption is made that not all energy is absorbed at the surface and instead absorbed radiation is attenuated using Beer's Law. This study does not include meltwater saturation of the firn, ice lensing or lake formation so may underestimate meltwater production as it does not account for the albedo changes associated with these phenomena. However, it does account for the extra energy absorbed due to crevassing as crevasses can absorb more energy than flat surfaces.

The model predicts a greater amount of melting than the positive degree day method, possibly due to it being able to use hourly data instead of a daily average and therefore capture the warmer parts of the diurnal cycle which could be lost in the daily averaging of the positive degree day method. The model predicts a higher ablation level in the years of significant Larsen B breakup and also states that meltwater penetrates deeper into the ice shelf during these years, although exact figures are not given.

1.6 Aim and content of this thesis

This thesis presents the results of a modelling study investigating lake formation on an ice shelf. Chapters 2 and 3 describe the model in detail. Chapter 4 describes the application of this model to the Larsen C Ice Shelf in the Antarctic Peninsula and Chapter 5 then describes the sensitivity tests carried out on this setup for Larsen C. Chapter 6 provides a discussion of the results of these sensitivity tests alongside some calculations of the possible contribution of meltwater to crevasse propagation. Finally, Chapter 7 presents our conclusions.

Chapter 2

A one dimensional model for melting on the surface of an ice shelf

In order to investigate surface melting on ice shelves a one-dimensional model was created that takes into account the melting of snow at the surface of the ice shelf and the percolation and refreezing of this meltwater through the firn (compacted, old snow) at the top of the ice shelf. The formation, development and refreezing of melt lakes are also included in the model; this is covered in Chapter 3.

2.1 Overview of model physics

2.1.1 The transfer of heat through an ice shelf

The initial model setup calculates the surface energy balance and heat transport through the upper ice shelf in one dimension with no melting present but considering firn densification with time.

Heat transfer through the ice shelf is modelled using a heat diffusion equation,

$$\rho c_p^{total} \frac{\partial T}{\partial t} = \frac{\partial}{\partial z}(k^{total} \frac{\partial T}{\partial z}), \tag{2.1}$$

where T is temperature (K), t is time (s) and z is height (m), which here is positive upwards with the ice shelf surface at $z = 0$ m. c_p^{total}, the specific heat capacity, is dependent on density and is taken as a combination of the specific heat capacities of ice and air,

$$c_p^{total} = \phi c_p^{ice} + (1 - \phi) c_p^{air}, \tag{2.2}$$

where ϕ is the solid mass fraction of the firn with density ρ:

$$\phi = \frac{\rho}{\rho_{ice}}. \tag{2.3}$$

Here, ρ_{ice} is the density of solid ice, 917 kgm^{-3}. This approach follows that outlined for bulk properties of two-phase materials in Batchelor (1974), where it was shown that an isotropic distribution of two phase media results in a parallel addition of their conductivities.

Although combining the conductivities in the parallel limit would mean that the values calculated are at the upper limit of those possible (see Sturm *et al.* (1997)), previous measurements have been taken for seasonal snow of densities generally much lower than those dealt with here and the value of k is closer to the parallel than series limit for the higher densities measured in Sturm *et al.* (1997). However, we acknowledge that the method used here will mean that the values calculated for the conductivity may be an overestimate.

Thermal conductivity, k, is set in a similar way:

$$k^{total} = \phi k^{ice} + (1 - \phi)k^{air}. \tag{2.4}$$

Following Alexiades and Solomon (1993) the values used to calculate c_p^{ice} and k_{ice} are dependent on temperature:

$$c_{p_{ice}} = 7.16T + 138 \quad \text{J kg}^{-1}\,\text{K}^{-1} \tag{2.5}$$

$$k_{ice} = 2.24 + 5.975 \times 10^{-3}(273.15 - T)^{1.156} \quad \text{Wm}^{-1}\text{K}^{-1}. \tag{2.6}$$

For air, following Ambaum (2010) and Moaveni (2010), the values used are

$$c_{p_{air}} = 1004 \quad \text{J kg}^{-1}\,\text{K}^{-1} \tag{2.7}$$

$$k_{air} = 0.022 \quad \text{Wm}^{-1}\text{K}^{-1}. \tag{2.8}$$

The surface boundary condition is set such that for surface temperatures of less than 273.15 K,

$$\varepsilon F_{LW} + (1 - \alpha)F_{SW} - \varepsilon\sigma T^4 + F_{Sens} + F_{Lat} = k\frac{\partial T}{\partial z}, \tag{2.9}$$

where F_{LW} and F_{SW} represent the incoming longwave and shortwave radiation (taken as positive downwards), α is the albedo of the surface of the firn, F_{Sens} and F_{Lat} represent the sensible and latent heat fluxes respectively, ε is the surface emissivity and σ is the Steffan-Boltzmann constant (5.67×10^{-8} W m^{-2}K^{-4}). The value of α used in this study is taken as an average for the Larsen C Ice Shelf, calculated from Automatic Weather Station data (see Section 4.2.1).

The sensible and latent heat are calculated using bulk formulae, following Ebert and Curry (1993) so that

$$F_{sens} = \rho_a c_{p_{air}} C_T \nu (T_a - T_0), \tag{2.10}$$

$$F_{lat} = \rho_a \mathcal{L}* C_T \nu (q_a - q_0). \tag{2.11}$$

Here ρ_a is the density of dry air (1.275 kg m^{-3}), c_p^{air} is the specific heat capacity of dry air, T_a and T_0 are the air and surface temperature respectively, ν is the wind speed, q_a and q_0 are the air and surface specific humidities and $\mathcal{L}*$ is the latent heat of vaporisation, equal to 2.501 x 10^6 J kg^{-1}. C_T is a function of atmospheric stability following Ebert and Curry (1993) where

$$C_T = C_{T_0}(1 - \frac{2b'Ri}{1 + c|Ri|^{1/2}}) \qquad Ri < 0, \tag{2.12}$$

$$C_T = C_{T_0}(1 + b'Ri)^{-2} \qquad Ri \geq 0, \tag{2.13}$$

where $C_{T_0} = 1.3x10^{-3}$, $b' = 20$ and $c = 50.986$ are constants and Ri is the bulk Richardson number, equal to

$$Ri = \frac{g(T_a - T_0)\Delta z}{T_a \nu_a^2}, \tag{2.14}$$

where Δz is equal to 10 m.

The assumption is made that all solar energy is absorbed at the surface. This assumption is also made by Lüthje *et al.* (2006a) for a bare ice surface, and as snow will be highly scattering to incoming shortwave energy that assumption is more valid here.

When the surface temperature reaches 273.15 K we have

$$\varepsilon F_{LW} + (1 - \alpha)F_{SW} - \varepsilon\sigma T^4 + F_{Sens} + F_{Lat} = k\frac{\partial T}{\partial z} + \phi\rho_{ice}\mathcal{L}\frac{dH}{dt}. \tag{2.15}$$

Here $\mathcal{L}$ =3.34 x 10^5 J kg^{-1} is the latent heat of fusion due to phase change at the surface and $\frac{dH}{dt}$ is the height change of the surface of the snow due to melting and subsequent percolation of the melt into the snow. Therefore the term $\phi\rho_{ice}\mathcal{L}\frac{dH}{dt}$ is only activated when melting occurs. The value for the albedo, α is changed to a wet snow value of 0.6 once melting has begun (Singh, 2001).

In addition, a bottom boundary condition is imposed such that at 35 m below the surface we have

$$k\frac{\partial T}{\partial z} = 0. \tag{2.16}$$

The assumption that there is no temperature change at the bottom of the area is made based on ice core data suggesting that the ice shelf is isothermal below around 25 m (see Section 5.9).

This model setup is shown in Figure 2.1.

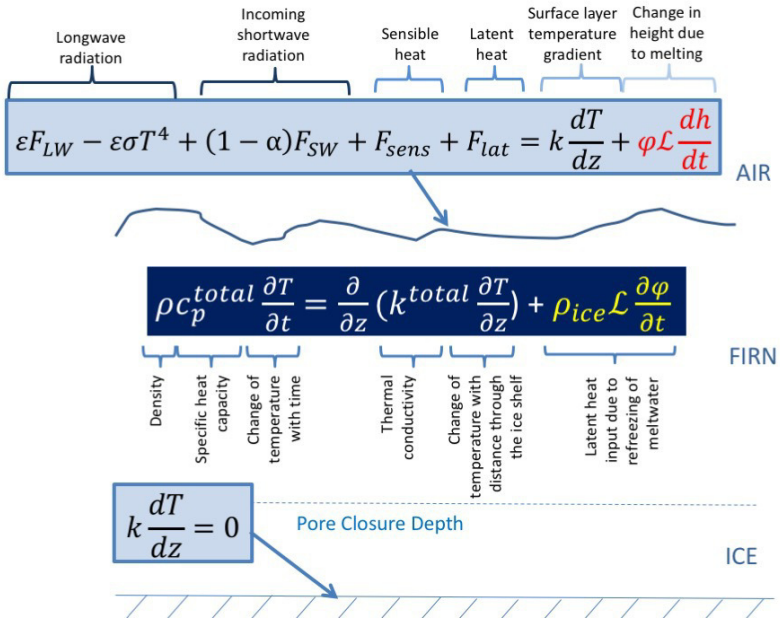

Figure 2.1: The setup of the heat transfer model. The final term of the boundary condition (shown in red) is only activated when the surface temperature is above freezing, 273.15 K. The pore closure depth is defined in Section 2.1.3. The yellow term is the latent heat due to the refreezing of meltwater.

2.1.2 Firn densification

The densification of the firn in the upper layer of an ice shelf is an important consideration due to the dependence of the thermal conductivity, specific heat capacity and

permeability of the firn on density. Furthermore, the pore space available in the snow will need to be known in order to determine at what point the snow becomes saturated with meltwater (see Section 2.1.3).

2.1.2.1 Existing firn densification models

No fully physical model for firn densification is currently available; even those that are physically based tune some parameters. The number of models concerned with firn densification is large so here, as this work is concerned with surface melt, three models with the purpose of calculating surface elevation changes were investigated (Thomas Blunier, personal communication); Cuffey (2001), Zwally and Li (2002a) and Arthern *et al.* (2010).

Cuffey (2001) models the firn densification rate as the addition of the grain boundary sliding rate and vapour flux in the firn pore spaces. However, it is noted that the sliding mechanism used in the topmost few metres of the snow is inadequate and as this is a key area for surface melt this model is not suitable for use here.

The Zwally and Li (2002a) model uses a temperature dependent densification equation. Although the model exhibits seasonal variation the match with observations is not good. Furthermore, when the model is applied to Berkner Island, Antarctica by Li and Zwally (2002), the seasonal density variation contrasts with that from ice core records which suggests that the model is not suitable for use here when seasonal variation is a key factor in melt occurrence.

The Arthern *et al.* (2010) model is also based on a temperature dependent equation. Here, there are issues relating values of its terms to laboratory-based estimates. Ligtenberg *et al.* (2011) use this model to study surface elevation evolution with time and although it produces a seasonal cycle they do not compare this to observations to know if the amplitude of the cycle is realistic.

2.1.2.2 Arthern et al. (2010) model for firn densification

Of the models covered in Section 2.1.2.1, the Arthern *et al.* (2010) model was proposed to be the most suitable for use in this case. It models the change of density in the firn with time, which occurs on the ice shelf due to accumulation and the weight of the firn above the grid cell being examined. It has mostly been used for understanding upper

snowpack dynamics on shorter timescales and calibrated accordingly (Christo Buizert, personal communication) and therefore is appropriate for use in looking at timescales of the length of less than a year, which here is the timescale over which dry firn densification is important. During the melt season the refreezing of meltwater will be a far more important process in densification, see Section 2.1.3.

The model, in a time dependent form as used by Ligtenberg *et al.* (2011), and the form that is implemented here, is as follows:

$$\frac{d\rho}{dt} = C\dot{b}g(\rho_i - \rho)e^{(\frac{-E_c}{RT_s} + \frac{E_g}{RT_s})}, \tag{2.17}$$

where $E_c = 60$ kJ mol^{-1}, $E_g = 42.4$ kJ mol^{-1} and C are constants (E_c being the activation energy for self-diffusion of water molecules through the ice lattice and E_g being the activation energy for grain growth). C varies depending on whether ρ is above or below the critical density, with values of 0.03 and 0.07 ms^{2}kg^{-1} respectively. The critical density, 550 kgm^{-3} is taken to be the level at vertically above which the dominant densification processes are grain settling and the packing of snow grains, whereas below this they are sublimation, diffusion and deformation. $\dot{b}$ is the average annual accumulation (in kgm^{-2}a^{-1}) which is calculated here from reanalysis data. g is the acceleration due to gravity (m s^{-2}), ρ_i is the density of ice (917 kg m^{-3}), T_s (K) is the surface temperature (with $\bar{T_s}$ being the annual average of T_s) and R is the gas constant (8.314 J mol^{-1} K^{-1}).

The equation has been derived by combining an expression for lattice-diffusion (Nabarro-Herring) creep of consolidated ice with one for grain growth. Nabarro-Herring creep changes with the inverse of the square of the grain size, hence the opposite sign of the two terms in the exponential term of the equation.

2.1.3 Meltwater percolation through firn

When melting occurs on an ice shelf the water produced can percolate through the snowpack up until it reaches a point where the temperature is below freezing, or up until the depth at which the density of the firn is greater than the pore closure density (830 kgm^{-3}), which is the depth where any remaining air in the firn gets trapped as bubbles within the ice and the firn is therefore impermeable (Ligtenberg *et al.*, 2011). The refreezing of meltwater can lead to the development of an isothermal layer: this raises the temperature of

the surrounding firn by releasing latent heat (Tseng *et al.*, 1994). The assumptions made in modelling this are discussed in Section 2.1.3.1. As water percolates through the firn a small amount is retained due to capillary forcing (Ligtenberg *et al.*, 2011). This process is described in the algorithm demonstrated in Figure 2.2.

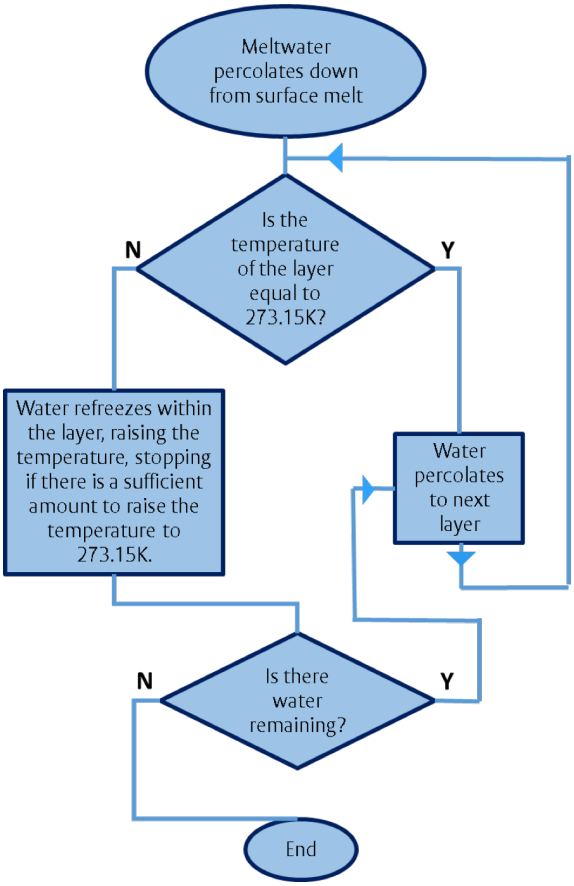

Figure 2.2: The algorithm that deals with the fate of surface melt.

As this work is concerned with the formation of melt lakes, the fate of this meltwater is a key process to consider. Melt can lead to the formation of melt lakes in three possible ways:

1) The meltwater will percolate down from the surface through the snowpack, refreezing and raising the temperature of the local region through the release of latent heat whenever it reaches a depth of the ice shelf that is below the freezing temperature. Further melting will fill any pore space above the pore closure depth, eventually saturating the firn if there is a large enough volume of melt. The snow beneath the surface, from the pore closure depth up, becomes completely saturated with meltwater meaning

that any further melt that occurs will be left to sit directly on top of ice shelf, forming a melt lake.

2) If melt in one region is not sufficient to fully saturate the snow it is possible that the topography of the ice shelf will lead to the accumulation of meltwater in certain regions and that the addition of meltwater from different locations will provide enough liquid to saturate the snow and lead to lake formation.

3) Meltwater will percolate down through the snowpack and reach a point where the temperature is low enough that a large enough volume of meltwater refreezes to increase the density of that layer to the point that the pores close off, forming an impermeable ice lens. Further melt will then saturate the pore space above the ice lens, potentially leading to melt lake formation when this snow is fully saturated.

These three possible mechanisms of melt lake formation are demonstrated in Figure 2.3.

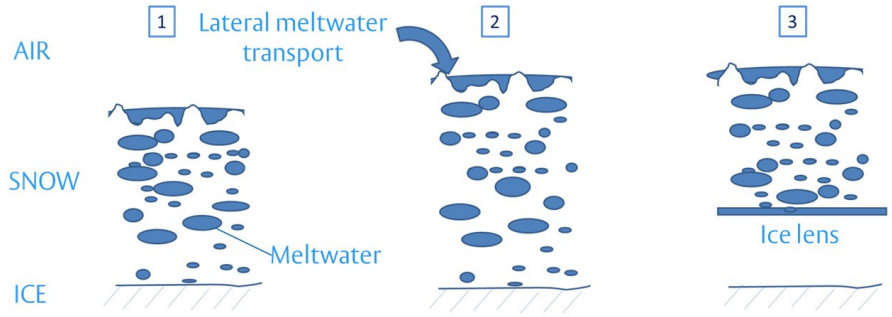

Figure 2.3: The possible mechanisms of melt lake formation. (1) All firn above the pore close-off depth becomes completely saturated with meltwater that percolates down vertically from surface melt. (2) As with (1) but with the addition of meltwater from lateral transport due to the topography of the ice shelf. (3) Meltwater percolates vertically through the ice shelf and refreezes at a point where the temperature is below freezing, forming an impermeable ice lens meaning that all further melt will saturate the firn above this depth.

Following the mechanism set out above, surface melt in the model percolates down through the snowpack and refreezes at the first grid cell it reaches that has a temperature

below freezing. Tseng *et al.* (1994) assume that local heat conduction is an instantaneous process and that thermoequilibrium is reached instantly with snow at the freezing temperature when meltwater is added. Here, this percolation and refreezing is calculated between timesteps of the heat equation as this process occurs at greater speeds than heat transfer. In order to justify this, and the assumption that the water will refreeze faster than it will percolate to the next grid cell the following two calculations were made.

2.1.3.1 Comparison of speeds of water percolation and heat diffusion through the upper layer of firn

The speed, $\mathbf{u}$, at which water can percolate through firn is a combination of the speed at which it can percolate through the permeable air pockets in the firn, $\mathbf{u_p}$, and the solid ice parts of the firn, $\mathbf{u_{imp}}$. So here we have,

$$\mathbf{u} = (1 - \phi)\mathbf{u_p} + \phi\mathbf{u_{imp}}, \tag{2.18}$$

where ϕ is the solid fraction of the firn. But since $\mathbf{u_{imp}}$ is equal to zero, $\mathbf{u}$ is equal to the flow through the porous part of the firn and this can be calculated using Darcy's Law as follows, as shown in Paterson (2000) :

$$\mathbf{u} = -\frac{\Pi}{\eta}(\nabla p - \rho\mathbf{g}). \tag{2.19}$$

Here ∇p is the pressure gradient and η is the viscosity. Π is the specific permeability of the material which, following Shimizu et al., can be calculated as follows:

$$\Pi = 0.077\delta^2 e^{-7.8\rho_s^*}. \tag{2.20}$$

The mean grain size, δ, is taken to be 1 mm. This is larger than the favoured modelled value of 100 μm used in Larsen C Ice Shelf modelling by Kuipers Munneke *et al.* (2012a), but the value that they use is, by their admission, small for melting snowpack so the larger value of 1 mm is used. ρ_s^* is the specific gravity of the firn (calculated as the density of the firn as a proportion of the density of water).

The pressure gradient term of equation 2.19 can be replaced with the following term:

$$\frac{\partial p}{\partial z} = \rho g + \frac{w}{z}. \tag{2.21}$$

The weight of the water in the surface meltlake, w, is spread over the height of the firn under consideration, $z = H$. Thus we have that equation 2.19 in the vertical direction becomes

$$u = -\frac{\Pi_v}{\eta}(\frac{w}{H}). \tag{2.22}$$

Therefore, given that w is equal to $\rho_{liq} g \Delta h$, with Δh being the height of the meltlake and ρ_{liq} being the density of water, the speed of the vertical flow through the firn is:

$$u = -\frac{\Pi_v}{\eta}\frac{\rho g \Delta h}{H}. \tag{2.23}$$

which, using the values in Table 2.1 suggests that u has a value of approximately 1.39x10^{-5}m s^{-1}.

The speed of heat diffusion through this upper layer of firn can be estimated using the heat equation,

$$\rho c_p^{total}\frac{\partial T}{\partial t} = \frac{\partial}{\partial z}(k^{total}\frac{\partial T}{\partial z}) \tag{2.24}$$

which, taking the timestep needed for heat to diffuse through the distance H to be τ we have that τ will be of the order of:

$$\tau = \frac{H^2}{\kappa}, \tag{2.25}$$

where

$$\kappa = \frac{k^{total}}{\rho c_p^{total}}. \tag{2.26}$$

Calculations of τ using the example values given in Table 2.1 compared to the time needed for meltwater to percolate through the firn depth (H/u) estimate that τ is approximately 6 years, which is several orders of magnitude larger than H/u, which is

approximately 17 days and thus we have

$$\frac{H}{u} \ll \tau. \tag{2.27}$$

Here the assumption has been made that the lake is very small in order to look at the case where it just consists of the very top of the firn melting (an increase in Δh will increase the value of u and thus further validate the assumption).

These calculations suggest that the assumption made in running the percolation algorithm between timesteps of heat diffusion that water percolation is a much faster process than heat diffusion is justified.

Π	hydraulic permeability (m^2)	2.53×10^{-10} [1]
η	viscosity (Pa s)	1.787×10^{-3} [2]
ρ	density of ice (kg m^{-3})	917
g	acceleration due to gravity (ms^{-2})	9.8
Δh	lake height (m)	0.05
δ	snow grain size (m)	0.001
H	depth of the firn (m)	35

Table 2.1: Values used in the calculations of speeds of meltwater percolation and refreezing.

2.1.3.2 Comparison of speeds of water percolation through the firn and water refreezing within the firn

In making the assumption that meltwater will refreeze within one timestep in the layer that it currently is in (if the temperature of that layer is below freezing), we are assuming that this refreezing takes place more quickly than the time taken for the water to percolate down to the next layer.

The time taken for meltwater to freeze across one snowgrain can be estimated as follows. For freezing we have that

$$\rho \mathcal{L} \frac{dh}{dt} = k \frac{\partial T}{\partial z}, \tag{2.28}$$

[1] Following the formula given in Shimizu (1970), and obtaining a value in keeping with the values found by Colbeck and Anderson (1982).

[2] Following Paterson (2000).

which for a snowgrain of size δ would give us a time τ for refreezing, with

$$\tau = \frac{\rho \mathcal{L}}{k \Delta T} \delta^2. \tag{2.29}$$

This gives an approximate value of τ as $167 \frac{1}{\Delta T}$s. Using the percolation speed calculated in section 2.1.3.1 it would take approximately one hour for meltwater to percolate through one 5 cm grid cell. So therefore the assumption holds even for small values of ΔT (although given the sharp temperature changes seen in the model between the layers with meltwater and those without it is unlikely that ΔT will ever be very small.

2.1.4 Refreezing of percolating meltwater

For each layer of the firn that is found to be below freezing the algorithm compares the amount of energy input needed to raise the temperature of that layer to the freezing point,

$$Q_{change} = \rho_{ice} \phi \Delta x c_p \Delta T \tag{2.30}$$

to the maximum amount of heat that would be released if all of the available meltwater froze,

$$Q_{max} = V \rho_{liq} \mathcal{L}. \tag{2.31}$$

Here ρ_{ice} and ρ_{liq} are the densities of solid ice and water respectively, ϕ is the solid fraction of the layer, Δx is the height of the layer, ΔT is the temperature change needed to raise the temperature of the layer to 273.15 K, V is the volume of meltwater available and $\mathcal{L}$ is the latent heat of fusion of ice, equal to 3.34 x 10^6 J kg^{-1}.

If Q_{change} exceeds Q_{max}, all of the meltwater is refrozen in its current layer and the layer temperature is adjusted for the subsequent latent heat release. However, if there is sufficient meltwater to raise the temperature of the layer to the freezing point (i.e. Q_{max} exceeds Q_{change}) then the volume of meltwater required to achieve a temperature change of ΔT is refrozen, the layer's temperature is adjusted to 273.15 K. The remaining meltwater is allowed to percolate down to the layer below, except for a small amount of liquid water (equal to 5% of the available pore space) that remains within the isothermal layer in order to mimic capillary forces following Ligtenberg *et al.* (2011). Q_{change} and Q_{max} are then recalculated for this lower layer and the process is repeated until no more

meltwater remains. This process is represented by the yellow term in the firn in Figure 2.1.

This refreezing within the firn can lead to an isothermal temperature profile going downwards into the firn as once melt has heated up a layer, any further melt will percolate through this layer and refreeze in the layer below it, thus raising the temperature of that layer and so on.

Once melting has begun the calculations for the specific heat capacity and thermal conductivity for each layer are adjusted to take into account the proportion of the layer that is liquid water such that Equation 2.4 becomes

$$k^{total} = \phi k^{ice} + (1 - \phi - W)k^{air} + Wk^{liq} \tag{2.32}$$

and similarly for the specific heat capacity. Here W is the mass fraction of a grid cell that is liquid water and the values for the thermal conductivity and specific heat capacity of water are taken from Touloukian *et al.* (1970) and The Engineering ToolBox (2016) respectively.

The choice of using a method that calculates the temperature and subsequent refreezing within the snowpack may be more computationally expensive that other methods such as the P_{max} method, which assumes that there is an upper limit on the proportion of annual snowfall which is retained by refreezing, or the 2 m method (after Oerlemans (1991)), which determines the total energy available for melting as an exponential function of the temperature of the top 2 m of a glacial surface. However, Wright *et al.* (2007) found that a method of the type used here worked well when evaluated against field measurements for the Midre Lovénbreen glacier in Svalbard and recommend this type of model for use. Furthermore, as freezing within the snowpack is essential for ice lens formation (see Section 2.1.5 below) this method is the most appropriate here as this can significantly impact on melt lake formation.

2.1.5 Ice lens formation

The refreezing of meltwater within the firn causes an increase in density. Once the density of a grid cell reaches the impermeable density (830 kgm^{-3}) then meltwater can no longer pass through that grid cell and an impermeable ice lens has been formed. Once this

situation has occurred the model allows all further surface meltwater to only percolate as far as that grid cell, thus saturating the firn from the level of the ice lens upwards, eventually leading to exposed meltwater should sufficient melting occur for the top of the snowpack to become fully saturated.

As the depth of each grid cell in the model is 5 cm it is assumed that once one grid cell of the model reaches the density to form an ice lens (due to refreezing of melt) that this ice lens will then be strong enough to support further saturation of the snow above it. Should the firn become fully saturated and meltwater be exposed at the surface, the model switches to the lake present state as described in Chapter 3.

2.1.6 Accumulation

Accumulation is added using ERA-Interim data for the location available closest to that of the automatic weather station being used to provide the data to force the model, as described in Chapter 4. As the accumulation data is only available in twelve hour timesteps it is assumed that the amount of snow in any one of these timesteps is evenly split between each of the twelve one hour timesteps that the model runs over.

Accumulation is added at a density of 350 kg m^{-3}, following Kuipers Munneke *et al.* (2012a). Although this may be slightly denser than fresh snow, the assumption here is made that initial densification of the snow happens very quickly and will not be significant for the modelling results. This assumption is examined further during the sensitivity studies in Chapter 5.

This new layer of accumulation is added at the air temperature, following Sergienko (2005). However, should the air temperature be above freezing, the accumulation is added at 273.1 K. In Sergienko (2005) the accumulation is added at the freezing temperature of water for these conditions, but here it was added slightly below to prevent the model from switching into a lake state before a lake is present.

Once a lake is formed (see Chapter 3) accumulation into the lake is taken to be negligible as the lake is only exposed for a short while. A future model improvement could be to include this accumulation as meltwater and account for the temperature changes as it melts. Once the lake has started to refreeze, accumulation is added on to the refrozen lid of ice on top of the lake in a similar way to which it is added to the firn.

2.1.7 Refreezing of meltwater stored in the firn

As it is possible for layers that contain meltwater to drop to a temperature below freezing, the meltwater needs to refreeze when this happens. In order to account for this, at the end of each timestep the model checks the temperature and water content of each layer. For those layers that are found to contain water and have a temperature below freezing, some or all of the water is refrozen, following similar calculations to those described in Section 2.1.4, except that here if any water is remaining after enough has been refrozen to bring the layer's temperature up to the freezing point this water remains where it is instead of percolating down through the firn.

This process is important as for lakes to be able to form the firn needs to be impermeable or fully saturated with meltwater. Refreezing will reduce the permeability of the firn for subsequent years, densifying it and reducing the space for meltwater to saturate it, which ultimately can lead to lake formation (Scambos *et al.*, 2003).

2.2 Numerical implementation of the model

Based on the above, the following mathematical system is solved using Matlab:

$$\rho c_p^{total} \frac{\partial T}{\partial t} = \frac{\partial}{\partial z}(k^{total} \frac{\partial T}{\partial z}), \tag{2.33}$$

for $T(0,t)$:

$$F_{LW} + (1-\alpha)F_{SW} - \varepsilon\sigma T^4 - F_{Sens} - F_{Lat} = k\frac{\partial T}{\partial z} + \phi\rho_{ice}\mathcal{L}\frac{dH}{dt}. \tag{2.34}$$

and for $T(H,t)$:

$$k\rho\frac{\partial T}{\partial z} = 0. \tag{2.35}$$

The algorithm shown in Figure 2.2 is run in between timesteps of the solution of the above system.

The surface melt model has been created using Matlab, with all results stated here calculated using Matlab version 2015a. It consists of a main module from which the code can be run, which calls several functions depending on the status of the model. The basic

state is described here, with the lake development and refreezing states being covered in Chapter 3.

For more information about the model structure see Appendix A for a diagram of the relationship between the functions that can be called by the model and Appendix B for a brief description of these functions.

To solve the equation 2.33, Matlab's inbuilt partial differential equation solver *pdepe* is used. This solver uses the method of lines, a finite difference method (MathWorks, 2015) (Skeel and Berzins, 1990).

2.2.1 Coordinate transform

In order to take into account height changes due both to melting and accumulation a front fixing coordinate transform is used (Crank, 1984). This makes it simpler to compare results over time as the domain is always scaled between 0 and 1 with 1 being the surface of the ice shelf.

If s(t) is the ice-air interface at time t, and is initially set to 35 m above the bottom of the model domain then we have that

$$\xi = \frac{\mathbf{z}}{s(t)}, \tag{2.36}$$

(where $\mathbf{z}$ is the vector of values of vertical grid cells within the model) such that the boundary is located at $\xi = 1$ for all t.

Therefore the terms of the equation for heat transfer through the firn can be transformed as follows, firstly the left hand side of equation 2.1:

$$\left.\frac{\partial T}{\partial t}\right|_z = \left.\frac{\partial T}{\partial \xi}\right|_t \left.\frac{\partial \xi}{\partial t}\right|_z + \left.\frac{\partial T}{\partial t}\right|_\xi \left.\frac{\partial t}{\partial t}\right|_z. \tag{2.37}$$

Here we have that

$$\left.\frac{\partial \xi}{\partial t}\right|_z = \frac{1}{s}\left.\frac{\partial z}{\partial t}\right|_z + z\left.\frac{\partial \frac{1}{s}}{\partial t}\right|_z \tag{2.38}$$

which, since z is fixed and by the reciprocal rule, gives us

$$\left.\frac{\partial \xi}{\partial t}\right|_z = -s\xi\frac{1}{s^2}\frac{\partial s}{\partial t} = -\xi\frac{1}{s}\frac{\partial s}{\partial t}, \tag{2.39}$$

and therefore we have that

$$\left.\frac{\partial T}{\partial t}\right|_z = -\xi\frac{1}{s}\frac{\partial s}{\partial t} + \frac{\partial T}{\partial t}. \tag{2.40}$$

Secondly, the right hand side of equation 2.1 becomes:

$$\frac{\partial}{\partial z}(k\frac{\partial T}{\partial z}) = \frac{\partial k}{\partial z}\frac{\partial T}{\partial z} + k\frac{\partial^2 T}{\partial^2 z}. \tag{2.41}$$

Here we have that, since $\frac{\partial \xi}{\partial z}$ is equal to $\frac{1}{s}$,

$$\frac{\partial k}{\partial z} = \frac{\partial k}{\partial \xi}\frac{\partial \xi}{\partial z} = \frac{1}{s}\frac{\partial k}{\partial \xi} \tag{2.42}$$

$$\frac{\partial T}{\partial z} = \frac{\partial T}{\partial \xi}\frac{\partial \xi}{\partial z} = \frac{1}{s}\frac{\partial T}{\partial \xi} \tag{2.43}$$

$$\frac{\partial^2 T}{\partial^2 z} = \frac{1}{s^2}\frac{\partial^2 T}{\partial^2 \xi} \tag{2.44}$$

$$\tag{2.45}$$

which means that equation 2.41 is transformed to

$$\frac{\partial}{\partial z}(k\frac{\partial T}{\partial z}) = \frac{1}{s}\frac{\partial k}{\partial \xi}\frac{1}{s}\frac{\partial T}{\partial \xi} + k\frac{1}{s^2}\frac{\partial^2 T}{\partial^2 \xi} = \frac{1}{s^2}\frac{\partial}{\partial \xi}(k\frac{\partial T}{\partial \xi}) \tag{2.46}$$

and therefore the transformed heat equation becomes

$$c_p\rho(s\xi\frac{\partial s}{\partial t}\frac{\partial T}{\partial \xi} + s^2\frac{\partial T}{\partial t}) = \frac{\partial}{\partial \xi}(k\frac{\partial T}{\partial \xi}). \tag{2.47}$$

Here the first term of the left hand side of equation 2.47 is zero unless melting or accumulation occurs at the top of the firn in which case it is the term that represents the temperature change of a layer of the model due to the domain of the model reducing or increasing.

2.2.2 Model initialisation

Initial conditions for the modelling in this thesis are based on those for the Larsen C Ice Shelf.

The initial density profile used is that given following Paterson (2000), using the formula of Schytt (1958):

$$\rho(z) = \rho_{ice} - (\rho_{ice} - \rho_{sfc})e^{-cz}, \tag{2.48}$$

where ρ_{sfc} is the density at the surface and $c = 1.9z_t$, with z_t being the location of the firn-ice transition. For the Larsen C Ice Shelf, the measured value of 37 m from Jarvis and King (1995) was used.

The suggestion that the firn-ice transition (which is equivalent to the pore closure depth) is at 37 m below the surface does means that full saturation of the firn in the model is not possible using a vertical profile of only the top 35 m. However, during initial testing it was confirmed that an ice lens consistently forms at depths higher than 35 m using this density profile and a range of surface conditions, so full saturation of the firn down to the pore closure depth would not happen in this situation. It is suggested that if the model is used for a different location, then the model domain would need to be extended to below the pore closure depth for that area at least for initial testing.

It was confirmed that full saturation of the firn is possible by running the model with a much lower density profile to prevent ice lens formation and a larger domain. The model did behave as expected in this situation, saturating the firn from the pore closure depth upwards.

An initial surface density of 500 kg m^{-3} was used as this was observed on the ice shelf during the period where much of the weather station data used here was available (Bernd Kulessa, personal communication).

The initial temperature profile is linear, starting at 253 K at the surface and increasing to 263 K at the bottom of the model domain. These values were chosen based on ice core data from a field expedition to Larsen C in 2009-10 (Andrew Shepherd, unpublished data). Here, the temperature was found to reach 264 K between 25 and 30 m in the snow, with a minimum temperature recorded of 263.5 K. Unfortunately there were no ice cores taken deeper than 30 m so a bottom value here of 263 K was chosen as temperature did not change very much below the top 20 m in either profile. Although the ice cores

were taken during the summer and the model is run starting in the Antarctic winter it is expected that these values from deeper in the ice shelf will not vary a great deal seasonally through heat conduction (see Section 2.1.3.1). However, this does mean that the ice cores cannot provide useful information about the winter surface temperature and therefore it is taken to be close to the value for the MAM average given in Kuipers Munneke *et al.* (2012a).

2.3 Model testing

In order to confirm that the model behaves as expected it is first tested using artificial forcing. The total of the net longwave and shortwave radiation, sensible and latent heat is set to be equal to 800 W m^{-2} for every timestep, giving a constant artificially large positive forcing at the surface to ensure that melting and lake formation do take place. This is run for 300 timesteps to allow sufficient melting to take place for ice lens formation. This constant forcing leads to heating of the firn and then surface melting.

Once the surface temperature has reaches 273.15 K the subsequent meltwater that is produced percolates down through the firn and refreezes in the first grid cell that it reaches that has a temperature below freezing, thus raising the temperature of the grid cell. As shown in Figure 2.4, this leads to an isothermal layer that forms vertically down from the surface and the formation of an ice lens at just under 25 m below the surface as enough meltwater freezes, as shown in Figure 2.5.

Subsequent melt then leads to saturation of the firn, starting from the layer above the ice lens and working upwards as each layer becomes fully saturated, until eventually there would be exposed water at the surface should the model continue to be forced with positive forcing. This saturation of the firn is demonstrated in Figure 2.6. Here, Figure 2.6a shows that the firn from the lens level and approximately 6 m upwards from this has a high water content, suggesting that this firn is fully saturated with meltwater. This is in agreement with Figure 2.6b, which shows that this firn has no remaining air space. The firn above this up to the surface has a much lower water content but water is still present, suggesting that this firn is not saturated, but some water has remained due to the capillary effect.

The sharp density variations in Figure 2.5 were confirmed to be due to the percolation

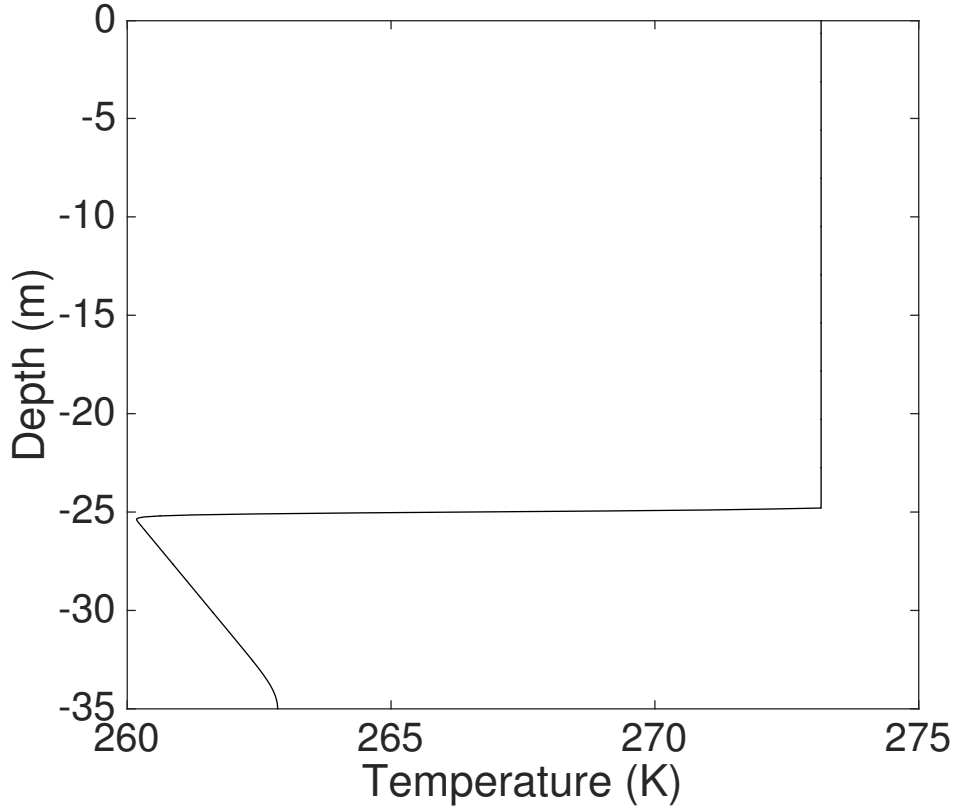

Figure 2.4: Ice shelf temperature profile at lens formation, showing the isothermal layer down to the ice lens level. 0 on the vertical axis is the ice shelf surface and negative numbers go down into the ice shelf.

algorithm rather than the model not solving the heat equation correctly. The model was run without meltwater percolation and the temperature profile was smooth. The model was run at a variety of spatial and temporal resolutions in order to select a resolution to minimize these oscillations. Although the oscillations are non-physical, the small error associated with this numerical noise would not influence the conclusions that we draw from our analysis.

In addition, the percolation algorithm was tested by running the model with a uniform temperature profile of 273.15 K for the top half of the profile and a lower temperature below it. As expected, water percolated through the uniform part of the profile and was seen to refreeze as soon as it reached a level where the temperature was below freezing; this was confirmed by a sharp increase in density and temperature at this level.

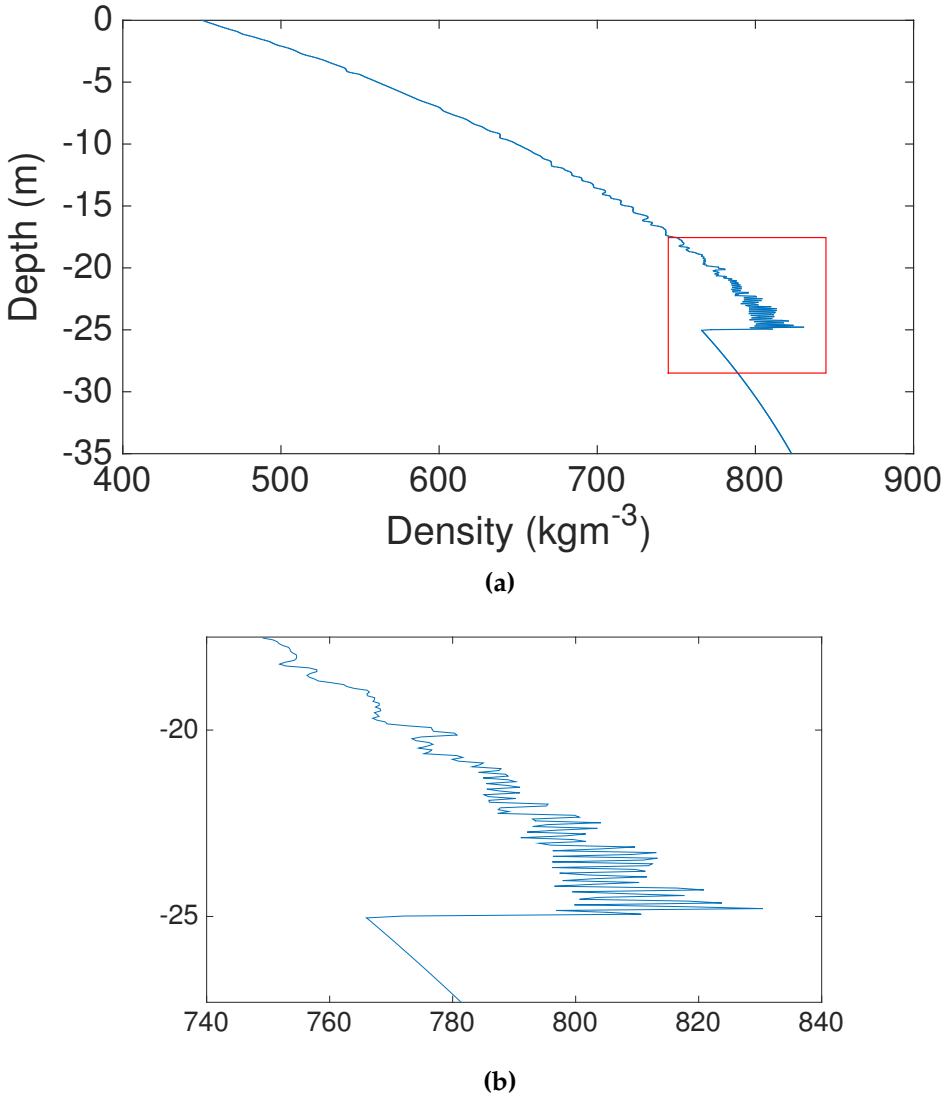

Figure 2.5: Ice shelf density profile at lens formation for (a) the whole model domain and (b) a zoom in to the ice lens level.

2.3.1 Lens depth

As the density of an entire grid cell must be raised to the pore closure density (830 kg m^{-3}) for an ice lens it is important to check that the depth at which the ice lens occurs is not dependent on the grid cell size. Figure 2.7 shows the formation of ice lenses at a range of resolutions and suggests that for the chosen resolution this is not an issue.

2.3.2 Mass conservation

It is important that the model conserves mass, especially as density is a key factor in how far meltwater percolates into the firn. However, the model will be constantly gaining mass due to the addition of precipitation in the form of snow.

Therefore, to ensure that the model is conserving mass a record of the total precipitation added is kept, and also the total mass in the model through calculating the mass in each layer at each timestep. If the model were to conserve mass than the result of subtracting this first value from the second should remain constant. It was found that this was the case and therefore the model was conserving mass within a reasonable error margin. Mass was found to increase by only 0.18% between the initial profile and lake formation. It is expected that this is a result of model resolution; by increasing the resolution to 1 cm the mass increase was reduced to 0.12% although this slight reduction was not felt significant enough to change the resolution used for the model given the extra time needed to run the model at this resolution.

2.3.3 Energy conservation

As above, it is also important that the model does not gain or lose energy during the solution of the heat equation and running of the percolation algorithm. In order to confirm this the amount of energy in each layer of the model was calculated by multiplying the temperature of each layer by the layer's density and its specific heat capacity. This accounts for the sensible heat in each layer. The total energy in the model is the sum of these values for each layer. Although the total energy should consist of this and latent heat, latent heat is not taken into account here (other than at the surface) as the temperature changes caused by the conversion of energy to or from latent heat are included in the temperature changes that take place within the model when melting or freezing occurs. It was found that during model testing the start and final energy did not change significantly during timesteps (the change is of the order of 0.001%).

2.3.4 Model domain

As the model showed no sign of the temperature changes penetrating to the lower half of the model due to conduction over the timescales looked at, a model domain of 35 m

was chosen.

However, this choice of value needs to be justified and a consideration also needs to be made when making this assumption for the fact that the ice shelf will be affected by the interaction between the ocean and the bottom of the ice shelf.

In order to verify this a basic calculation can be done to estimate the timescales that it would take for a temperature change to penetrate either from the top of an ice shelf to 35 m deep, or from the bottom of an ice shelf to the point 35 m below the surface. Example values can be used if we take the heat equation 2.1 and integrate to give us an idea of the time scales involved. Doing this we have

$$\tau = \frac{s^2}{\frac{2k}{\rho c_p}}. \tag{2.49}$$

Here τ is the time taken for a heat change of one degree to transfer a distance of s meters through an ice shelf of density ρ with specific heat capacity c_p and thermal conductivity k. Using typical values for ice shelves we obtain the results that a heat change at the top of the ice shelf would take nearly 10 years to reach the bottom boundary of the model and over 500 years to reach the bottom boundary should the change occur at the bottom of the ice shelf, even using the lower end of the range of figures found by Griggs and Bamber (2009) for the thickness of Larsen C around the areas that lakes have been observed. For the thickness reconstructed by the Bedmap2 consortium of 564 m (Fretwell *et al.*, 2013) for the Cabinet Inlet area where lakes have been observed this figure increases to over 2200 years. Based on this and the timescales that this work has been investigating it was felt that a zero temperature gradient bottom boundary condition was therefore appropriate and heat changes from the ocean would not be significant here.

This calculation also suggests that modelling the top 35 m of the ice shelf is appropriate as the temperature changes over the time scales looked at will not penetrate to the bottom of the model domain.

2.3.5 Model resolution

Ideally the model should not be dependent on either the spatial or temporal resolution chosen. However, when the density of a grid cell is so important to processes such as ice lens formation, it is inevitable that some dependence will occur. In order to ascertain the

level of dependence of the model on spatial resolution the model was run at a range of spatial resolutions, one of the outputs of which are shown in Figure 2.7. As can be seen from this figure, which demonstrates the model being run at a range of resolutions for a prescribed level of melt, results for resolutions of 5 cm and below were identical and therefore 5 cm was chosen as the resolution for the model in order to minimise the time taken for the model to run.

The smallest temporal resolution of the data for the case study of the Larsen C Ice Shelf described in Chapter 4 was used, giving a timestep of one hour.

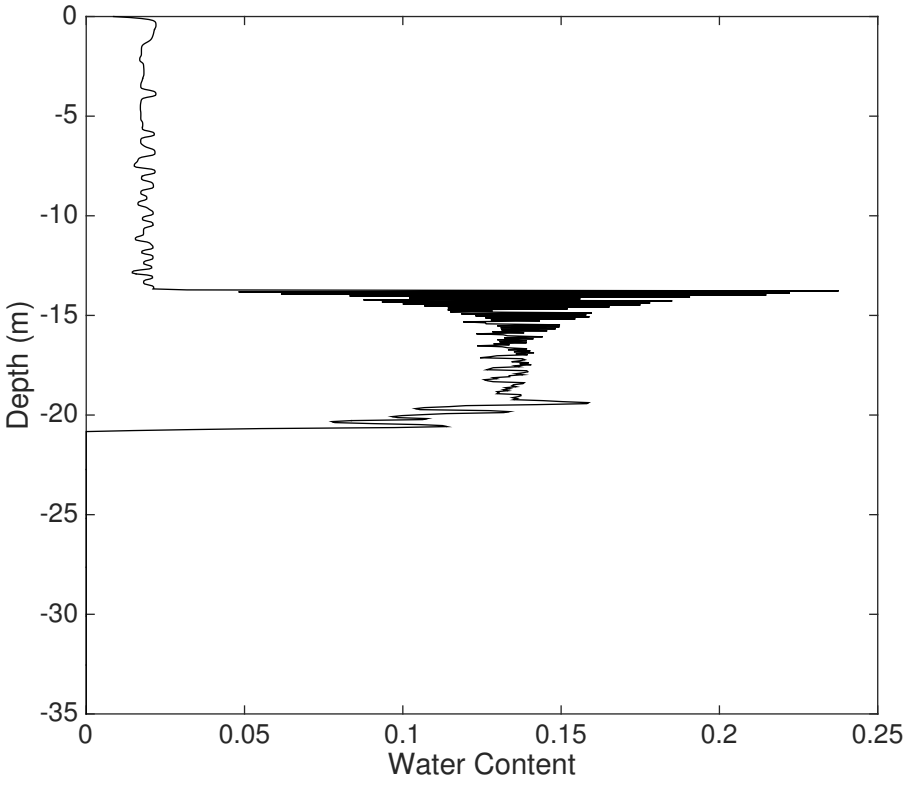

(a)

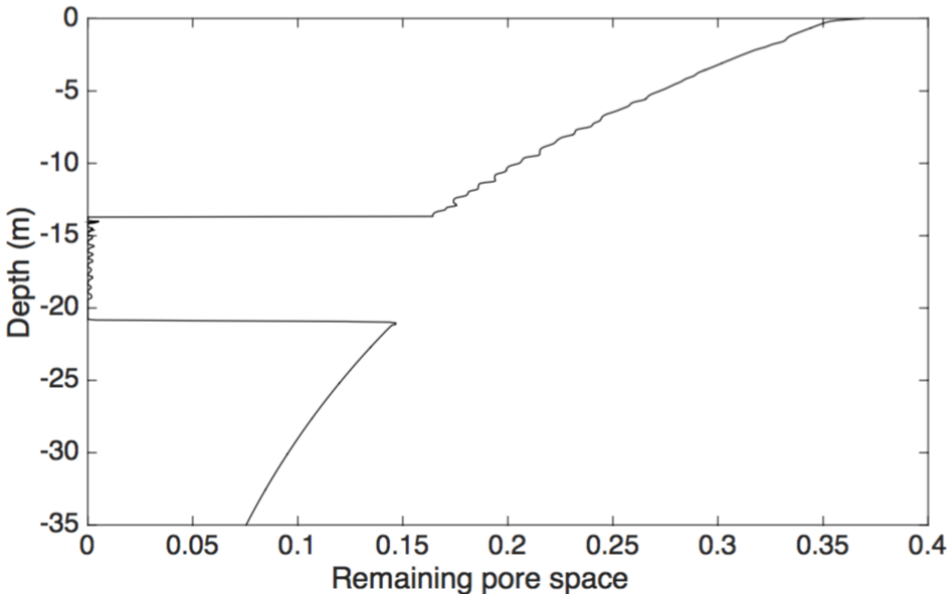

(b)

Figure 2.6: The model tested under constant positive forcing leads to saturation of the firn from the ice lens upwards with (a) an increased water content and (b) resulting reduced pore space. Each of these are shown as a fraction of the total volume of each grid cell. The increased water content in the top 14 m is due to the capillary effect.

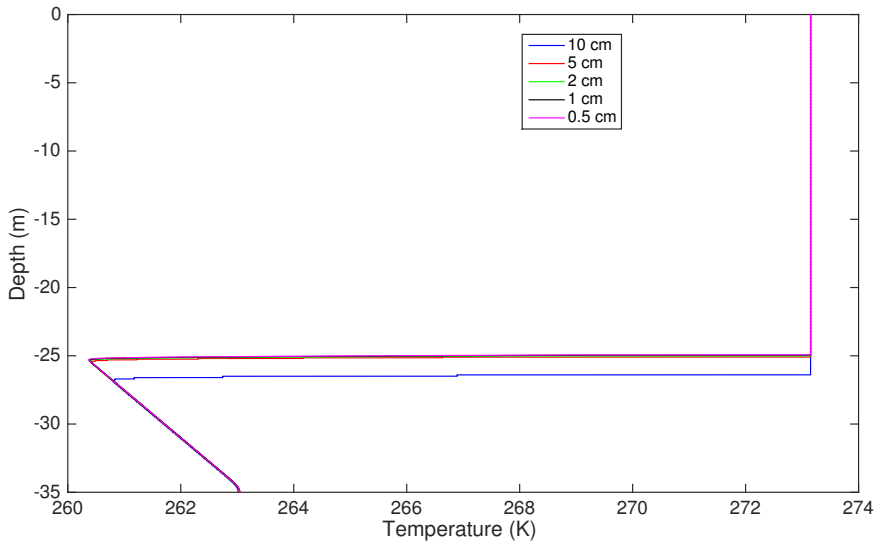

(a)

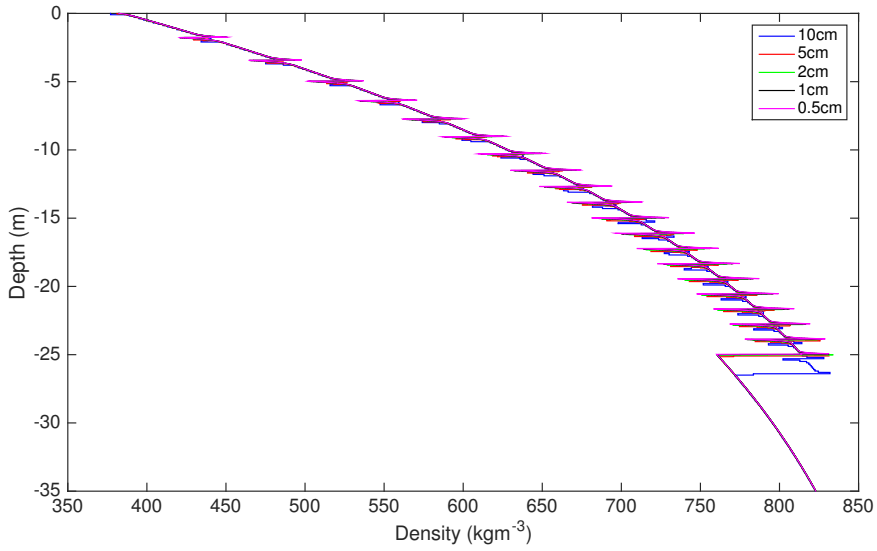

(b)

Figure 2.7: A comparison of the resulting (a) temperature and (b) density profiles when the model is tested at a range of resolutions with a prescribed level of melt.

Chapter 3

A one dimensional model for melt lake development and refreezing on an ice shelf

3.1 Model overview

3.1.1 Melt lake formation

Once the permeable snowpack above the pore closure depth (or ice lens) is fully saturated further melting will lead to the formation of a lake. If the temperature at the surface goes over 273.15 K then the surface energy balance is calculated as in equation 2.15, that is

$$\varepsilon F_{LW} + (1-\alpha)F_{SW} - \epsilon\sigma T^4 + F_{Sens} + F_{Lat} = k\frac{\partial T}{\partial z} + \phi\rho_{ice}\mathcal{L}\frac{\partial H}{\partial t}, \tag{3.1}$$

except that here although the term $\frac{dH}{dt}$ still represents the amount of ice that melts, the height of the surface does not reduce as the melted ice just stays in place as it can no longer percolate vertically.

Since the term ϕ takes into account the fraction of each layer that is solid, the speed at which the surface layer melts depends on how much solid ice there is in it.

This melting is assumed to continue in this way until the lake is 10 cm deep, and then the model switches to a lake development phase, as described in Section 3.1.2. The value of 10 cm was chosen as it is high enough for the lake to become convective (see Section 3.1.2) and large enough that it was not found to often refreeze soon after it has formed which was found to be the case during initial testing of a 5 cm threshold which also guaranteed convection but was found to often refreeze rather than develop into a deeper lake.

During model testing it was observed that having exposed meltwater did not necessarily lead to a lake of over 10 cm being formed, so it cannot be assumed that every time the firn becomes saturated a lake will form and the model will switch to a lake state. Therefore, we decided that should 24 hours of the surface temperature of the model be calculated as being consistently below freezing, the model reverts to the state where it is assumed that a lake is not present, as described in Chapter 2. The refreezing of meltwater due to this decrease in temperature is dealt with by the algorithm described in Section 2.1.7.

3.1.2 Melt lake development

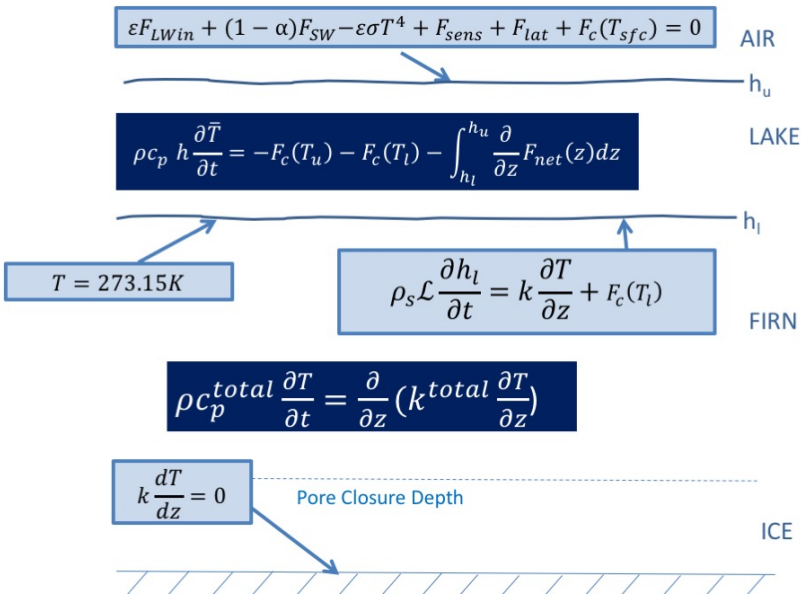

Figure 3.1: The model setup for lake development. Here h is the total depth of the lake, with h_u and h_l being the upper and lower boundaries respectively. $\bar{T}$ is the average temperature of the lake, $\mathcal{L}$ is the latent heat and F_c are the fluxes out of the lake as described in Equation 3.4. The turbulence equation in the lake equates the change in sensible heat in the turbulent core with the heat fluxes in or out of the upper and lower boundaries (second and third terms) and the total heat gain from internal heating due to incoming shortwave radiation (fourth term where F_{net} is calculated using Beer's law).

Once the top 10 cm of the saturated firn has fully melted, a lake is taken to be present and its development is calculated, as shown in Figure 3.1. The surface temperature of the lake is determined as follows:

$$F_{LW} + (1-\alpha)F_{SW} - \epsilon\sigma T^4 - F_{Sens} - F_{Lat} + F_c(T_{sfc}) = 0. \tag{3.2}$$

The value of the albedo for the lake is taken to be equal to

$$\alpha = \frac{9702 + 1000e^{3.6h}}{-539 + 20000e^{3.6h}}, \tag{3.3}$$

where h is the height of the lake, following Lüthje *et al.* (2006a). The change in h with lake depth is shown in Figure 3.2.

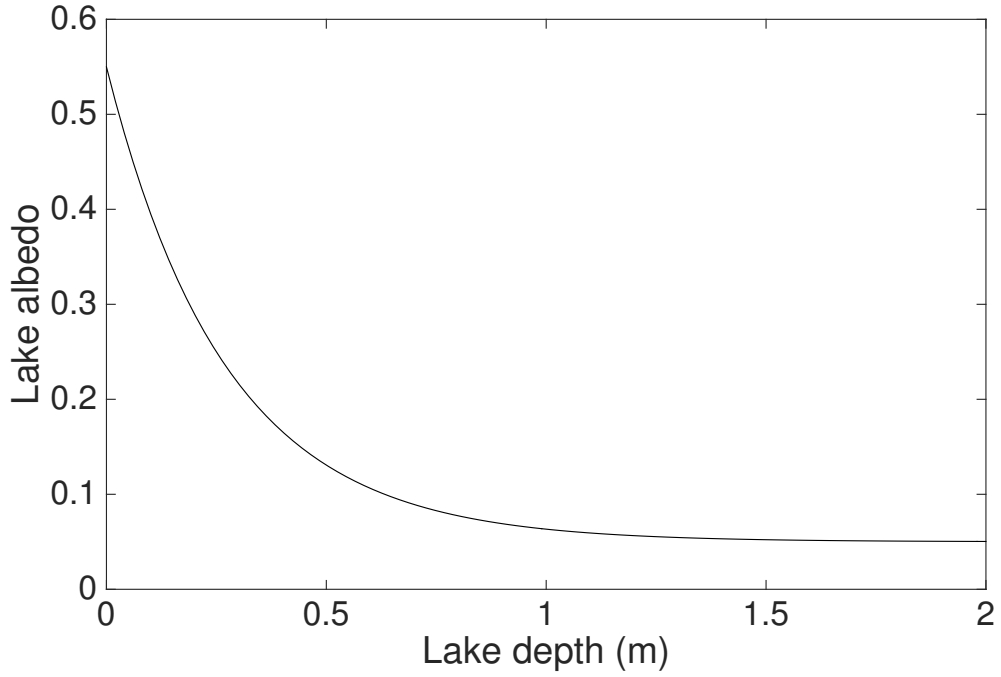

Figure 3.2: The change in lake albedo with lake depth

The convective heat flux $F_c(T_{sfc})$ and later the heat fluxes directed outward at the boundaries of the lake ($F_c(T_l)$ and $F_c(T_u)$)are calculated using the four-thirds law for turbulent convection:

$$F_c(T^*) = sgn(\bar{T} - T^*)(\rho c)_l J|\bar{T} - T^*|^{4/3}, \tag{3.4}$$

where T^* is the boundary temperature, $\bar{T}$ is the average temperature in the lake and J is the turbulent heat flux factor, equal to 1.907 x 10 $^{-5}$m s^{-1} K$^{-1/3}$.

The movement of the boundary between the top of the firn and the bottom of the lake is described by a Stefan equation, as follows:

$$\phi\rho\mathcal{L}\frac{\partial h_l}{\partial t} = k\frac{\partial T}{\partial z} + F_c(T_l). \tag{3.5}$$

Here h_l is the location of the boundary between the lake and the firn and T_l is the temperature at that boundary.

Following Taylor and Feltham (2004) a Rayleigh number of 630 is taken to be the critical value over which the lake becomes turbulent and, since this is exceeded as soon as a 10 cm lake forms, the lake has a well mixed core of constant temperature.

The temperature within the lake is calculated as

$$(\rho c)_l H \frac{\partial \bar{T}}{\partial t} = -F_c(T_l) - F_c(T^u) - \int_{h_l}^{h_u} F_{net}(z)dz, \tag{3.6}$$

where H is the lake height (m), $(\rho c)_l$ is the volumetric specific heat capacity of water and $F_{net}dz$ is calculated using Beer's Law to account for the attenuation of shortwave radiation as it passes through the lake.

The lake and any subsequent lid of ice that forms on top of the lake (see Section 3.1.3) are taken to have 20 grid cells each, spread equally over the height of the lake or lid. The actual size of these grid cells is therefore constantly changing with the growing and shrinking of the lake and lid.

The temperature profile of the firn continues to be calculated as described in Chapter 2, except that now the surface temperature of the firn is held at 273.15 K due to that being the location of the firn-lake boundary.

3.1.3 Lake refreezing

When the surface energy balance becomes negative the lake starts to refreeze. An initial lid of ice is formed on top of the lake, the development of which is treated as a Stefan problem as shown in Figure 3.3.

It is likely that in reality the ice lid may form, melt and reform several times due to temperature oscillations before the lake presents a stable ice cover. However, it is assumed here that once a lid is present it does not melt, but in order to minimize errors, we have assumed that the model only switches from a melting to freezing state when a 'virtual' lid of at least 10 cm forms. This happens when enough consecutive timesteps with freezing conditions occur. The amount of freezing that would take place in each timestep is calculated and the total is recorded and only when this total reaches 10 cm does the model switch to a freezing state. The temperature profile of this virtual lid is also

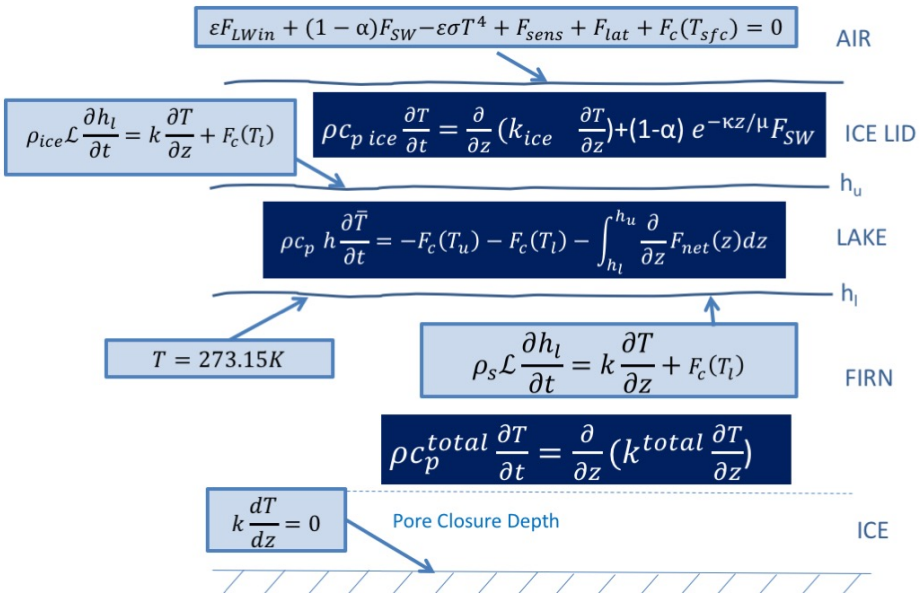

Figure 3.3: The model once the surface of the lake has refrozen and an ice lid develops.

recorded so that should it become a permanent lid it will be assigned this temperature profile. This allows the melting and refreezing of lids to be taken into account without having to build a significantly more complicated model as melting on top of the lid could occur, leading to several layers of the model.

The surface temperature of the lid is calculated to satisfy equation 3.2. The development of the lid-lake boundary is treated as a Stefan problem:

$$\rho_{ice}\mathcal{L}\frac{\partial h_u}{\partial t} = k\frac{\partial T}{\partial z} + F_c(T_u). \tag{3.7}$$

The temperature of the lake, firn below the lake and development of the lake-firn boundary are all calculated as in Section 3.1.2.

While the lid is smaller than 10 cm its temperature profile is taken to be linear. Once a permanent lid is established, the temperature profile through the lid is determined following the equation below:

$$\rho c_p^{ice}\frac{\partial T}{\partial t} = \frac{\partial}{\partial z}(k^{ice}\frac{\partial T}{\partial z}) + (1-\alpha)e^{\frac{-\kappa^* Z}{\mu}}F_{SW}. \tag{3.8}$$

Here, κ^* is the extinction coefficient, set equal to 1 m^{-1} and μ is the cosine for the effective angle for incident sunlight, taken to be 0.5 following McKay *et al.* (1994). The value of α

is taken to be 0.431, following the upper end of the measurements taken by Henneman and Stefan (1999) as the lakes considered here are shallower than that measured in their study.

This heat equation is again solved using *pdepe* and the coordinate transform described in Section 2.2.1 is used, with the heating due to short wave energy that penetrates the lid included as a source term. The rate of solar energy absorption at a distance Z into the lid is calculated through the

$$(1-\alpha)e^{\frac{-\kappa^* Z}{\mu}} F_{SW} \tag{3.9}$$

term of equation 3.8, so this part is also transformed and thus the transformed heat equation for the lid has an additional source term to that for the firn.

3.1.4 Extending the model to multiple year runs

The formation and refreezing of meltwater within the firn has a clear effect on its density (e.g. Figure 2.5). This change in density may have consequences for the formation of future lakes. For the case in Chapter 2 where a lake does not form this is reasonably straight forward; the model can just continue to run as it is if exposed water does not become present as everything is contained within a single layer of the model.

However, there are two other possible cases that must also be accounted for to allow multiple year runs. Firstly, there is the case where enough melt occurs in one melt season that exposed water is present but an established lake does not form (as stated above in Section 3.1.1, a lake is taken to be established once it is 10 cm deep or greater). In order to allow the model to return from the state of initial lake development to the state that exposed water is not present, it is assumed that exposed water is no longer present after 24 hours of the surface temperature being below freezing. The actual refreezing of the exposed water is taken care of by the process described in Section 2.1.7. This then allows the model to continue to run into subsequent years.

Secondly, there is the case that a lake has formed and has refrozen. By this point the model contains three separate layers: the firn, the lake and the frozen lid. These layers are recombined to form one layer of ice and air, with the solid fraction set to unity in the refrozen lake. This leaves one single vertical profile for each of density, temperature, water

content and solid fraction and allows the model to return to its initial state of modelling heat transfer through firn over the new melt season.

Should a lake not completely freeze over during one year then the model can continue to run and the combining of the layer can just take place after a new year has begun. The model did not initially account for the more complex case where surface melting begins again before a lake has completely refrozen as this would need the model to have multiple lake layers. It was not found during testing that this case occurred for current Larsen C conditions but this would be a possible extension for future model development if, for example, the model was used to investigate warmer climates where water in firn can persist annually. However, it was found during some of the sensitivity testing that altering some parameters could lead to lakes not freezing over completely within one year. This is discussed in more detail along with the adjustments made to account for this in Chapters 5 and 6.

3.2 Model testing

In order to test the model a constant positive forcing of 800 W m^{-2} is applied in a similar way to Chapter 2, but this time for 800 timesteps. This is immediately followed by a further 1700 timesteps of a forcing of 100 W m^{-2}. This allows lake formation and development, before switching to conditions that initiate complete refreezing of this lake until all the meltwater has been refrozen and the model can switch back to its original state of a single column of firn and ice. This whole process in demonstrated in Figure 3.4. Here the surface of the firn (in blue) can be seen to decrease in height as melting occurs. A lake forms shortly after 500 timesteps (shown in red) and the firn surface is seen to continue to decrease in height as this change in surface albedo causes more ablation from the lake bottom. The green line shows the surface of the refrozen lid above the lake.

Figure 3.5 shows this saturation of the firn column during melting and the way that it changes the firn density profile. The fully saturated firn begins to refreeze from the top downwards once the lake has refrozen, meaning that there is a solid layer of dense ice near the ice shelf surface. This means that in subsequent melt seasons formation of an ice lens may not occur as the meltwater from the surface will only have to percolate a short distance into the ice shelf before it hits the impermeable ice layer of the previous year's

lake and a new melt lake may be able to subsequently form more quickly.

The effects of the lake formation process on the the firn and lake depths are shown in Figure 3.6. Here it can be seen that the lake depth increases due to ablation from the lake bottom (shown in the top of the four figures as the change in the firn-lake boundary) then the lake depth reduces as it refreezes.

This effect of this full lake lifecycle on the firn column is demonstrated in Figures 3.7 and 3.8. In Figure 3.7 the initial increase in water content is due to water percolating down into the firn and small amounts being left behind due to the capillary effect. Following on from this the increase in water content from the ice lens up is then shown as the firn begins to be saturated as more meltwater accumulates. As this figure only shows the firn profile the lake is not shown until it has completely refrozen and there is a single column of ice and air once more. This is shown in the rightmost panel of the figure, where the small amount of zero water content at the top of the profile is the refrozen lake. This zero water area increases in depth as time continues as the saturated firn begins to refreeze from the top down. This is also shown in Figure 3.8 where the decrease in temperature at the top of the profile in the leftmost panel matches the area where the meltwater has refrozen.

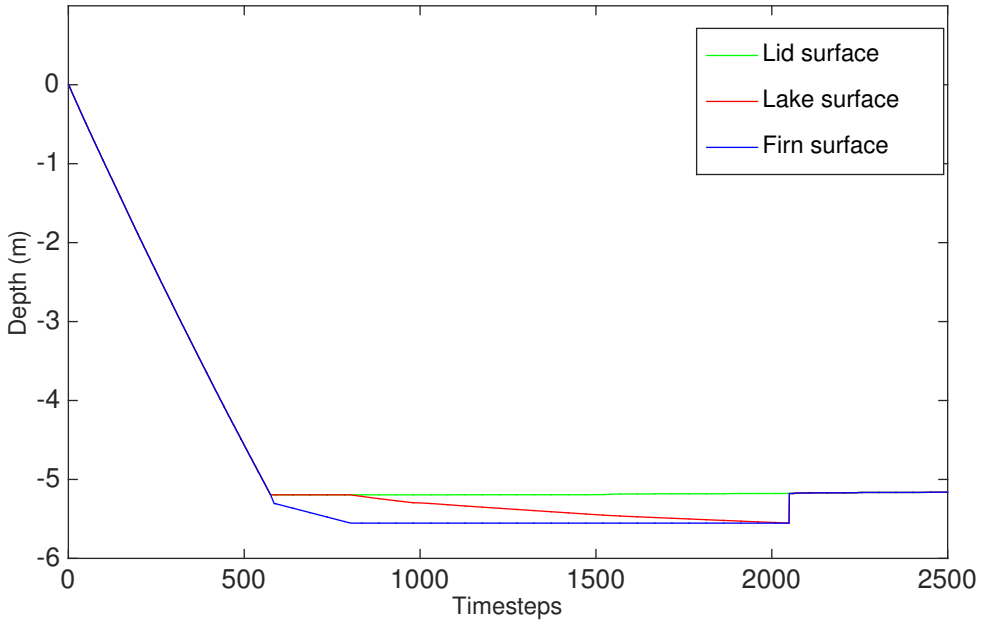

Figure 3.4: The complete lake lifecycle as modelled using imposed forcing. The switch to a lower forcing at timestep 800 is clear as the lake-firn boundary stops moving and an ice lid starts to form.

Figure 3.5 shows the final density profile in this test case. Here it can be seen that the addition and subsequent refreezing of meltwater had caused a large increase in the density of the model domain above the ice lens level. If we compare this to the water content it can be seen that at the top of the model domain there is solid ice where the lake has refrozen but below this is a combination of retained meltwater and ice causing the increase in density.

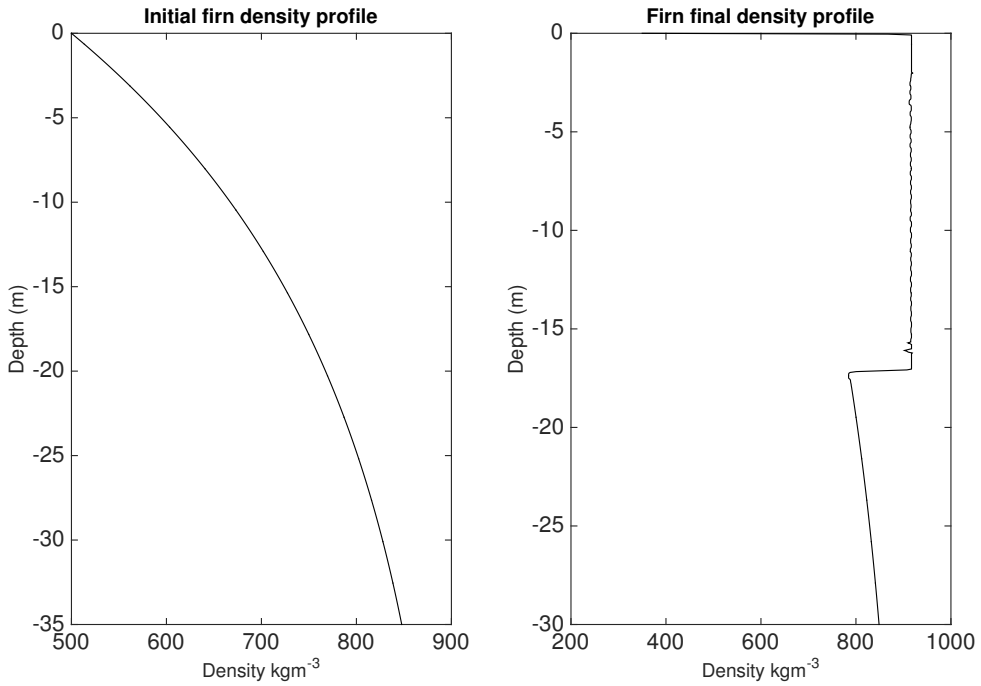

Figure 3.5: The initial and final density profiles of the test run. Note that the vertical axes are different due to surface melting having caused a decrease in height.

3.2.1 Mass and energy conservation

In order to confirm that the model was not losing or gaining mass or energy in error tests similar to those in Sections 2.3.2 and 2.3.3 were performed for the whole lake lifecycle. It was found that under test conditions there was a 0.31% mass gain over the whole cycle and energy changes of a similar magnitude to those found in Chapter 2 so neither of these were thought to be of concern here.

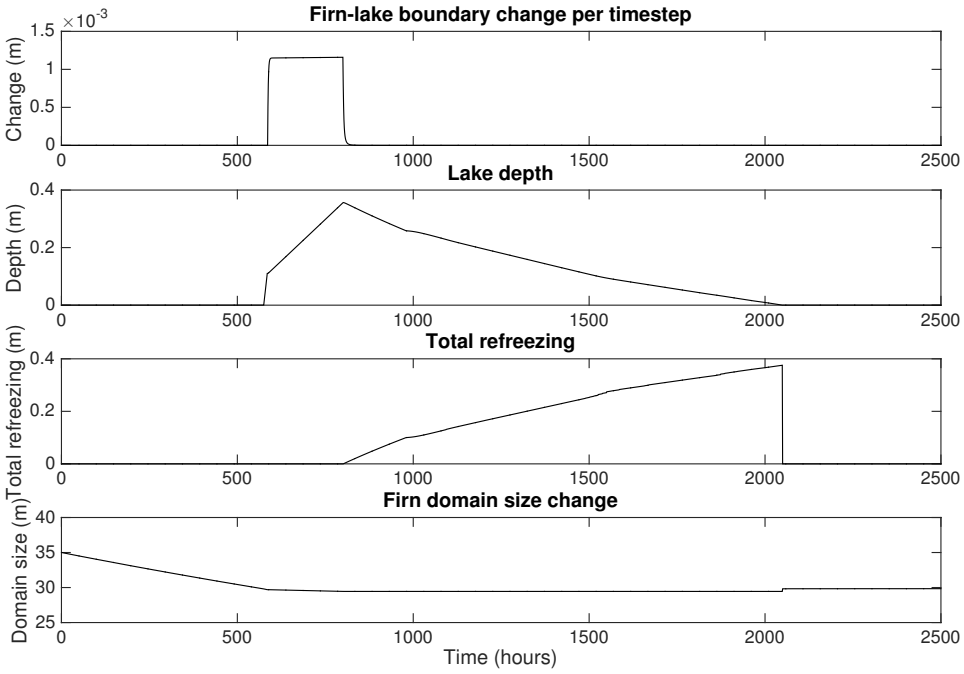

Figure 3.6: Changes in depths within the model during a test run with imposed forcing. The sudden increase in the lower image just after timestep 2000 shows the recombining of the firn layer with the refrozen lake layer such that following on from this the model is once again considered a single column of firn, ice and air.

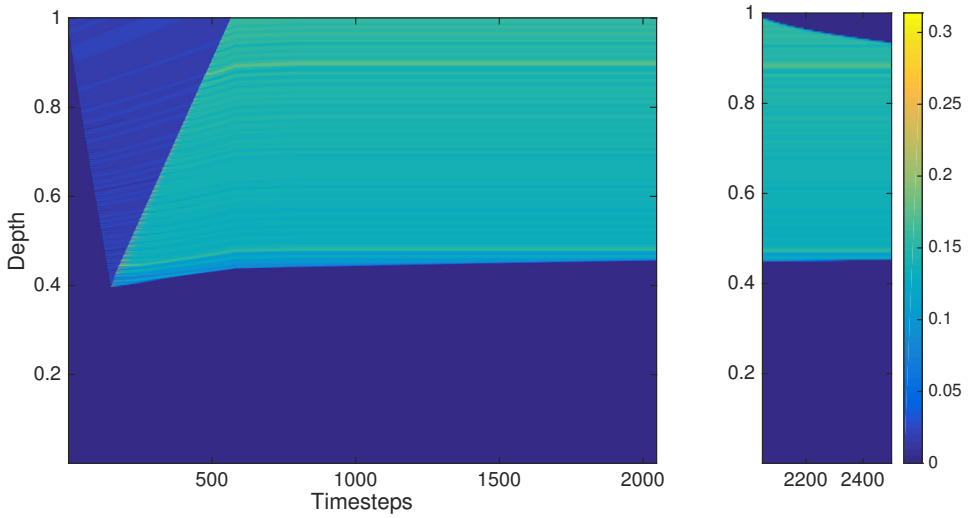

Figure 3.7: The evolution of the water content profile (as a percentage of how much of each layer is water) through the firn for the test model run with imposed high then low forcing. The initial increase in water from top to bottom is due to the capillary effect. Meltwater is percolating down into the firn and most of it is refreezing; the amount which is left behind in the layers that are at the freezing temperature is the change shown here. Subsequent to ice lens formation (at just before 200 timesteps) the water content then increases from the ice lens level up, as the firn begins to become saturated from top to bottom. Depth scaling is from 0 to 1 as with the coordinate transform to allow direct comparison of the profiles. The change and splitting of the plot at just after 2000 timesteps is due to the recombining of the firn layer with the now refrozen lake layer. The size of the initial profile is 35 m, and this reduces to 29.45 m by the end of the left hand image. The right hand image shows the profile after the lid has completely refrozen and has been added to the firn column to form one single profile of depth 29.82 m. The refrozen lid is visible as the darker blue area of solid ice at the top of this right hand plot. After this recombining of the frozen lake and firn profiles the water content then reduces from the top of the firn downwards as this water starts to refreeze in the colder conditions.

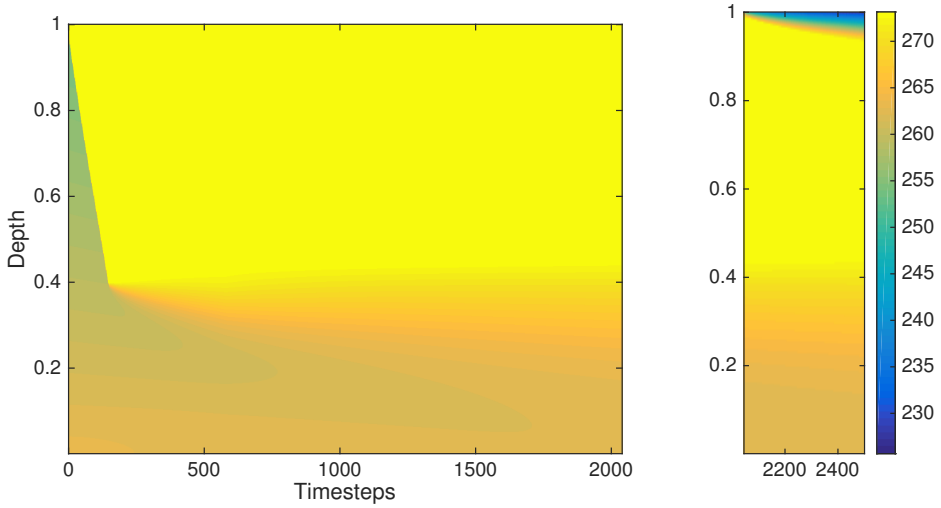

Figure 3.8: The evolution of the temperature profile (in Kelvin) through the firn for the test model run with imposed high then low forcing. The increase of the upper firn surface up to the freezing temperature is shown as meltwater percolates down deeper into the firn with time and refreezes. The temperatures at the lower boundary for the model do not change, further validating the use of the bottom boundary condition. Depth scaling is from 0 to 1 as with the coordinate transform to allow direct comparison of the profiles. Again as with Figure 3.7 the plot has been split at the point of the lake being completely refrozen and the ice lid and firn being combined again to form one profile. Once the switch is made to a lower forcing the top of the firn begins to cool as can be seen in the right hand panel.

Chapter 4

Melt on the Larsen C Ice Shelf

4.1 Evidence of melt lakes on the Larsen C Ice Shelf

Surface melt lakes are visible on the Larsen C Ice Shelf in NASA's MODIS (Moderate Resolution Imaging Spectroradiometer) imagery for multiple years during the period from 2001-mid 2016. The lakes show clearly as dark features, as demonstrated in Figure 4.1.

Although MODIS imagery is temporally irregular and often obscured by cloud, it is possible to obtain an approximate idea of lake presence over the last 16 years. Figure 4.2 shows the periods that lakes can be identified using MODIS imagery. Here it can be seen that lakes do not appear every melt season, but they have been observed in this imagery as far back as the year 2000.

Furthermore, although exact lake onset and refreeze dates are difficult to obtain, the imagery shows how quickly the lakes can refreeze enough to no longer be observable by satellites. For example, they are present on the 14th March 2000 but have disappeared from view by 20th March 2000. This may be due to their frozen lids having formed and grown to a sufficient depth that lakes are no longer visible or due to snowfall on the refrozen lids, but either way this suggests a reasonably quick rate of refreezing for the lid to be deep enough to obscure the lake or strong enough to support snow cover.

It can also be seen from this data that lakes appeared, disappeared and reappeared in 2005. This suggests that it is possible for lakes to partially refreeze but then be subjected to melt again in the same melt season. It was for this reason that the 'virtual' lid was introduced in Chapter 3.

In addition to MODIS imagery, ice lenses have been observed in the firn on the Larsen C Ice Shelf, as demonstrated in Figure 4.3. It was found that ice lenses were present in the firn in Cabinet Inlet during the 2014-15 field season in a distribution that appears to resemble annual layering. This suggests that even if lakes were not forming in the

years immediately previous to this (as implied by the data shown in Figure 4.2), melting and refreezing within the firn was still occurring. Similar annual layering was observed during a separate field expedition on Larsen C by Gourmelen *et al.* (2009).

Near to the grounding line (and the location of lake formation) the flow speed of the ice shelf is low (approximately 200 m/yr for the Cabinet Inlet flow line for example). This flow speed increases further down the ice shelf, with the Cabinet Inlet flow line reaching between four and five hundred m/yr at 160 km away from the grounding line (Bevan *et al.*, 2017). Glasser *et al.* (2009) suggest that there has been little change in the flow speed or direction of the ice flow over at least the last 560 years due to the persistence of surface features down-flow. This suggests that density changes that occur during one melt season will remain in areas of high surface melt for some years and will affect future lake formation.

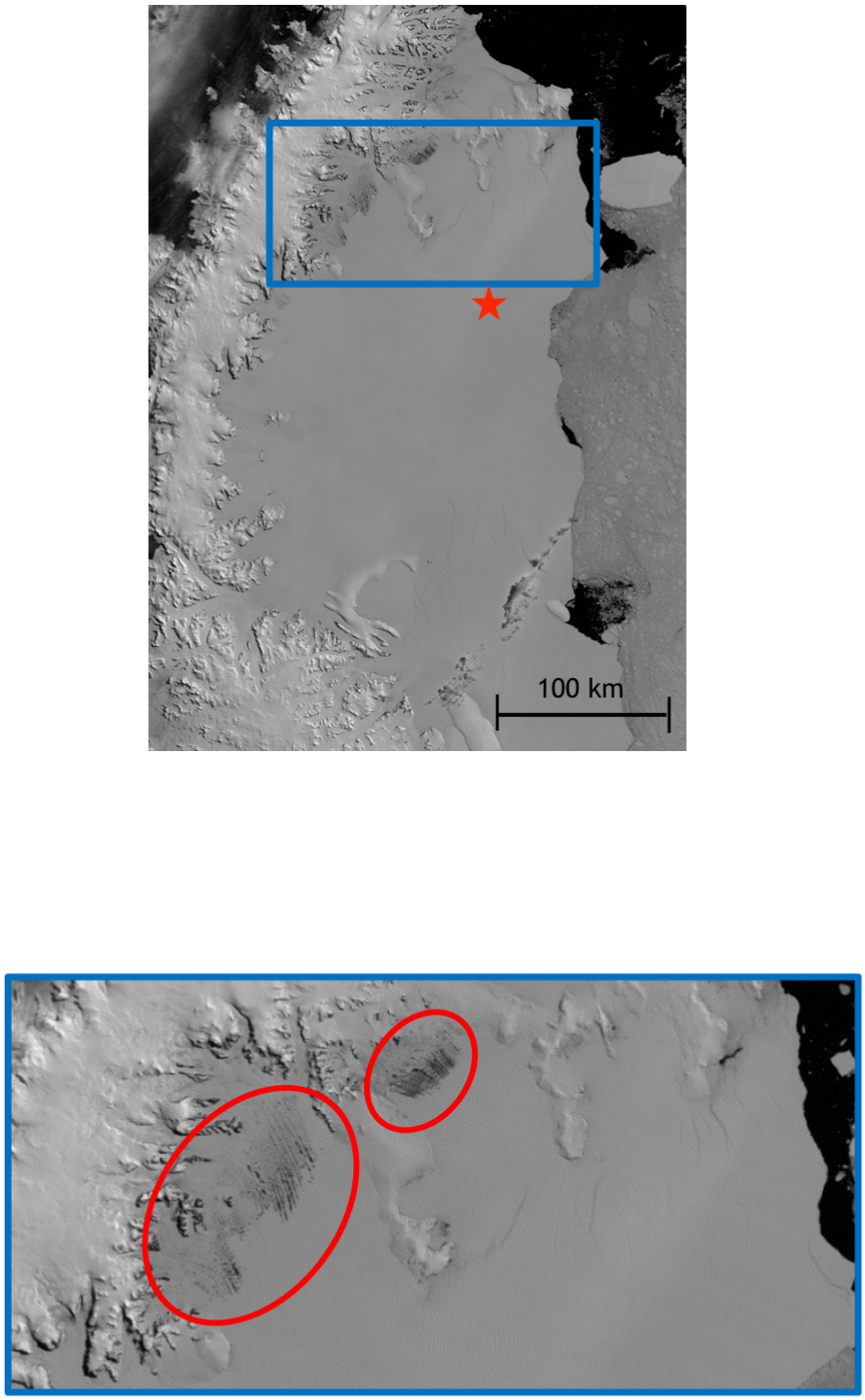

Figure 4.1: (a) NASA MODIS imagery of the Larsen C Ice Shelf. The location of the BAS automatic weather station is shown with a red star. (b) A zoomed in image of the northern part of Larsen C, as shown in figure (a), with visible melt lakes highlighted in red. The image was captured on 07 Jan 2007 at 1315.

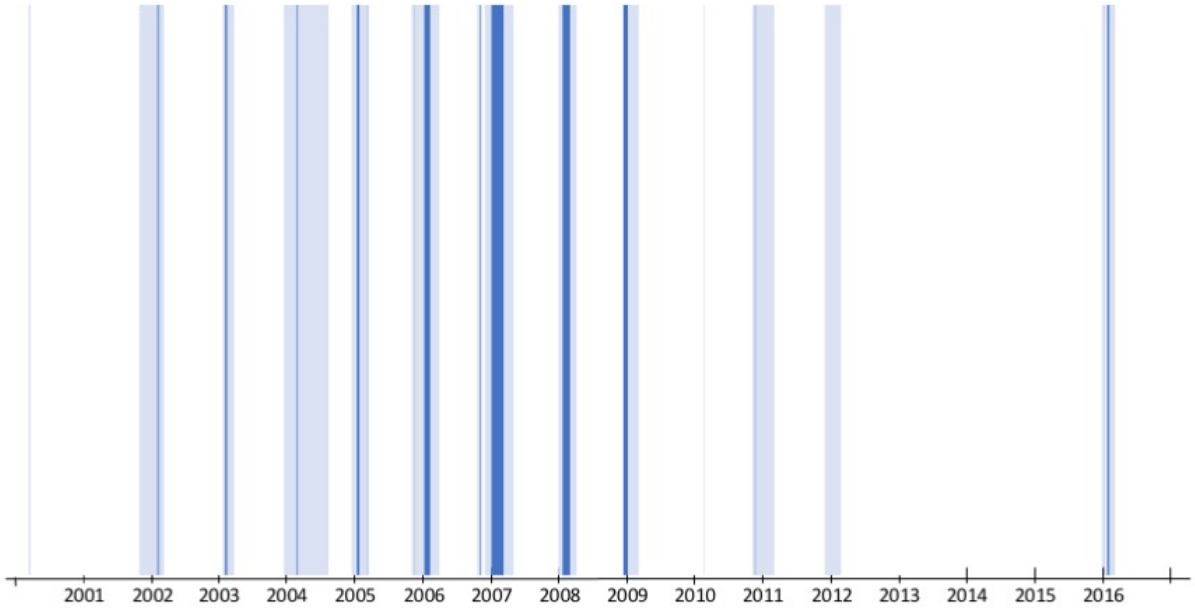

Figure 4.2: Lakes visible in MODIS satellite imagery. Here dark blue dates are those with clear images of lakes and light blue dates cover those periods where the images are unclear but it is possible that lakes are present (this is taken to be the period between an image with clear lakes and one with a clear absence of lakes.

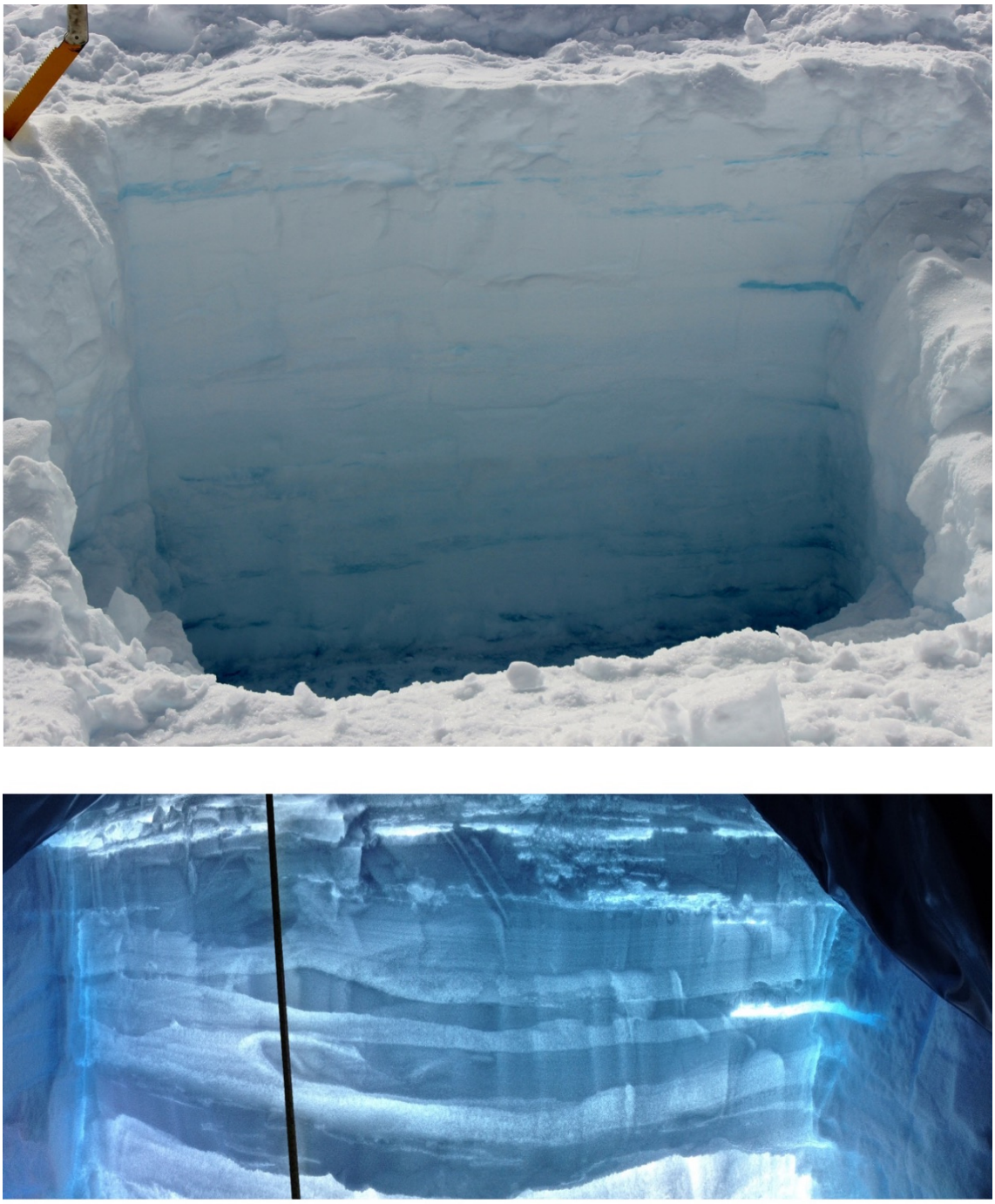

Figure 4.3: A snow pit dug on the Larsen C Ice Shelf during the 2014-15 field season in Cabinet Inlet. The upper image shows the snow pit and the lower image shows the firn with light shone through it in order to demonstrate the structure of the firn. Ice lenses are clearly visible here. Image Adrian Luckmann and Bryn Hubbard (MIDAS Project -Swansea and Aberystwyth Universities).

4.2 Simulating melt lakes on the Larsen C Ice Shelf

4.2.1 Forcing the model with Larsen C conditions

In order to simulate lake formation on the Larsen C Ice Shelf, the model described in Chapters 2 and 3 was forced using automatic weather station (AWS) data provided by the British Antarctic Survey (BAS). The location of this AWS on the ice shelf is shown in Figure 4.2. We chose to use AWS data rather than reanalysis data as the spatial resolution of reanalysis products is too course for melt lake formation as the conditions for this are highly spatially heterogeneous.

The forcing data for the year spanning May 2010 into April 2011 is shown in Figure 4.4. The only information not available that is needed for the model was humidity. For this values were taken from Kuipers Munneke *et al.* (2012a), where the average value for each season is used.

Missing values were set equal to the previous value available, except for a case in the wind speed where the previous value was anomalously high in which case the value from the previous timestep was used, and a long period in the shortwave radiation with missing values where several hours of previous forcing were repeated in order to not lose diurnal variation at a time where this can be significant.

The data are interpolated using a piecewise cubic interpolation. This is due to some of the data being hourly (radiation data) and others being three hourly (wind, air temperature and pressure) and allows the data to be smoothed without losing the diurnal cycle. Matlab's 'pchip' function was chosen for this purpose. The initial conditions for the model were kept the same as specified in Chapter 2. In order to investigate the effect of multiple years of melt the model is set up to loop over the 2010-11 data so that the model experiences multiple melt seasons with the same forcing conditions.

Figure 4.5 shows that after 3 years of continuously applying this forcing, although melt occurs it is not sufficient for lake formation. Figure 4.6 shows the surface temperature over the first two years of this model run, and the density profile after these two years. Again, it is clear that melt is occurring and density does increase from the initial profile, but beyond these two years the changes are no longer significant and do not lead to lake formation.

However, it can be seen in the MODIS imagery that lakes were present on the Larsen

C Ice Shelf during the period of this forcing and therefore there must be some processes not included in the model that lead to lake formation. These processes are investigated in the following two sections.

4.2.2 Inclusion of foehn winds

As can be seen from Figure 4.1, the location of the AWS data available does not match that of the lakes that are visible in the MODIS imagery. One key issue with this is that the areas where the lakes are present are close to the Peninsula mountains and are particularly affected by foehn winds. These are warm, dry downslope winds that bring warm air down to near to the surface of the ice shelf, flushing away cool air that may be present. Foehn winds have been found to be associated with exceptionally high melt rates on the Larsen C Ice Shelf (Kuipers Munneke *et al.*, 2012a) and therefore are an important process that needs to be considered when modelling surface melt on the ice shelf.

Running the model using only the AWS information available did not lead to lake formation. As is shown in Figure 4.6, the firn surface does reach the melting temperature and some densification of the upper part of the firn does occur, but this is far from an amount sufficient for ice lensing or saturation of the firn. This suggests that the model is replicating the conditions on the ice shelf where the forcing originated from and where lakes have not been observed on the ice shelf, and means that further processes need to be included in order to be able to use the model to study lake development on the Larsen C Ice Shelf with the data available.

Therefore, in order to replicate the conditions found closer to the grounding line of the ice shelf where the lakes are found, a foehn wind effect was added in to the data. Following the modelled values found in Luckmann *et al.* (2015), it was estimated that the areas where lakes were formed had an average temperature of up to 7 K higher than the AWS location during foehn wind events, and an average wind speed of up 10 m s^{-1} greater that the AWS location. For the 2010-11 melt season, foehn conditions were seen for around 30% of the time between January and March 2011 (Luckmann *et al.*, 2015). However, foehn events that were measure directly on the Larsen C Ice Shelf were found to be cooler and with a lower wind speed (J. Turton, personal communication). Therefore, based on this information a foehn effect is added into the model by increasing the air temperature by 5 K and the wind speed by 5 m s^{-1} for 18 hours in each 52 between

the months of January to March. The importance of these values is tested during the sensitivity studies in Chapter 5.

Figure 4.7 shows the model run with the inclusion of foehn winds. It can be seen that the addition of the winds has caused the formation of lakes, but only very shallow ones.

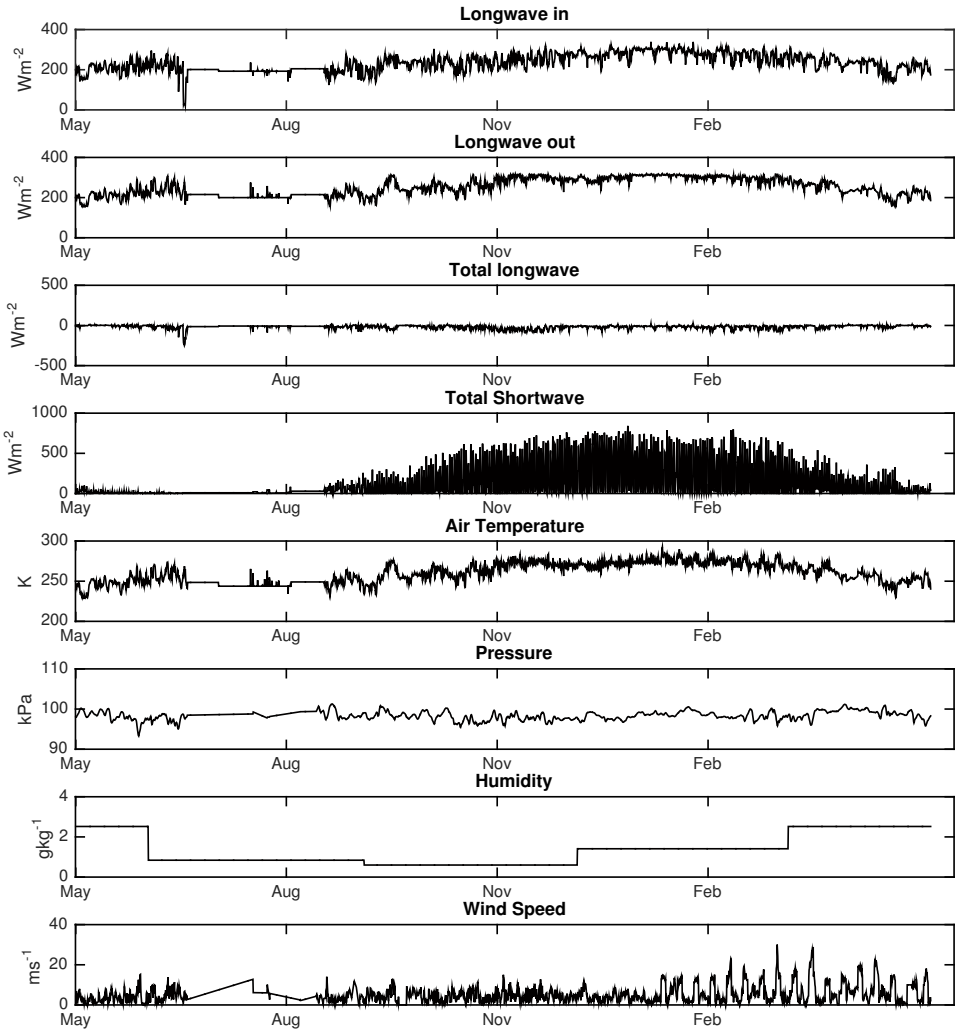

Figure 4.4: The forcing data for 2010-11 used to run the model.

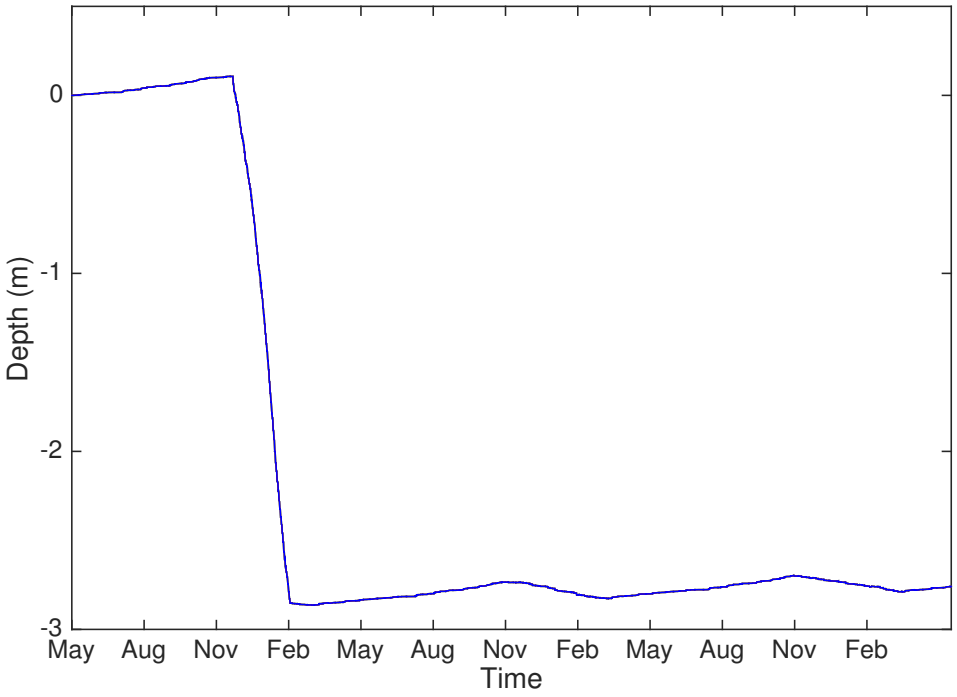

Figure 4.5: The surface of the firn during two years of applying the 2010-11 forcing. It can be seen the surface height decreases as melt occurs but no lake is formed.

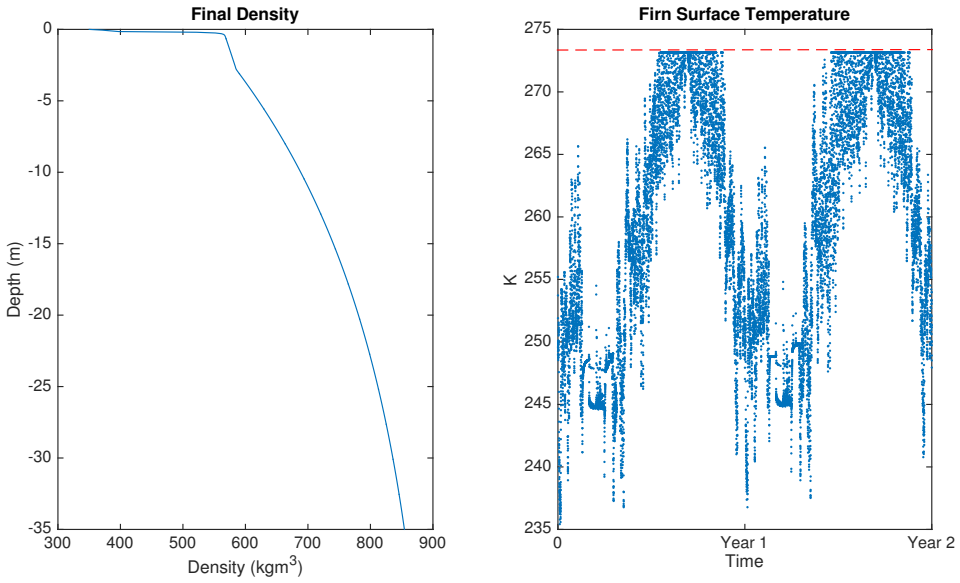

Figure 4.6: The final density profile (left) and developing surface temperature (right) over a two year model run. The red dashed line on the right hand figure shows the freezing temperature for water. It can be seen here that although surface temperatures become high enough for melt to occur, the amount is small enough that its retention in the firn does not have a noticeable effect on the density.

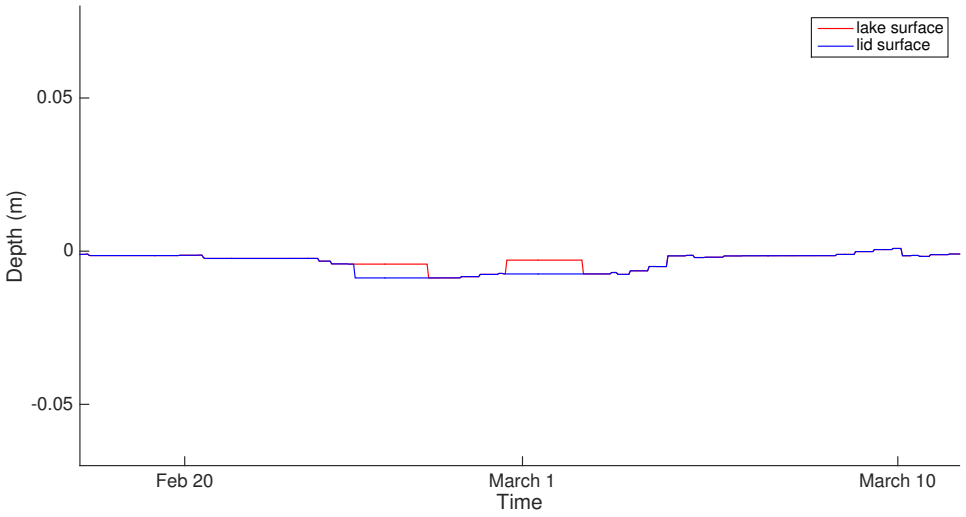

Figure 4.7: The appearance of very shallow lakes occurs when foehn winds are included within the model.

4.2.3 Estimating the catchment area for a single lake

Even with the addition of the foehn wind effect the model does not simulate lakes from only in situ melt. However, this is not unexpected as lakes do not appear over the entire area of the ice shelf that experiences similar weather conditions, but pool in certain locations. It is therefore likely that the topography of the ice shelf is playing a role in determining where the lakes are formed and that lateral transport of meltwater is taking place. The topography of the ice shelf will determine which areas of the ice shelf are sources of meltwater for lateral transport and which are acting as sinks and are locations of lakes. Luckmann *et al.* (2015) suggest that one of the reasons for the rapid filling of lakes they observed is flow of water across the ice shelf in periods of intense melt.

In order to simulate this lateral transport the model allows the addition of meltwater on top of that which is already created by in situ melting. To do this, the amount of available meltwater in a catchment area around the lake is calculated. As all the surrounding firn is assumed to melt at the same rate this is equivalent to multiplying the 1-D firn melt rate (with no exposed lake) by a given factor, the value of which is determined below.

Here, we make the assumption that water will not reach the lake from the catchment area until an ice lens is formed. This is because during the period of meltwater percolation refreezing in the model domain, refreezing will occur in the surrounding firn too. Although some of the meltwater will travel in a diagonal direction down the topographical gradient towards the lake the majority of it will not be able to travel far as it will be refreezing and making the surrounding firn isothermal, leading to ice lens formation in the catchment area too. It is only once an ice lens has formed that water will be able to flow through the isothermal catchment area and accumulate in the lake basin.

However, the catchment area will not remain completely isothermal and there will be some diurnal variation in temperature so it is possible that some meltwater may be lost to refreezing after ice lens formation. This is investigated below.

Initial calculations were carried out to see how much water could reach the lake through lateral transport. Assuming a gradient, $\frac{\partial H}{\partial z}$, of 5% incline (the choice of this value will be explained in the context of equation 4.5) ending in the lake basin the speed of meltwater flow through the firn, u m s^{-1}, as calculated by Darcy's Law, will be as

follows:

$$u = \frac{\Pi}{\eta}\rho g \frac{\partial H}{\partial z}. \tag{4.1}$$

This means that for a given depth of firn, Δz, the energy from latent heat, Q, available to that layer (should enough meltwater be available to refreeze and bring the layer's temperature up to the freezing temperature, T_{frz}) is equal to

$$Q = u(T_{frz} - T_{firn})\rho c_p \Delta z, \tag{4.2}$$

where T_{firn} is the local firn temperature.

The volume of meltwater, V, needed to refreeze to achieve this temperature change is therefore

$$V = \frac{u(T_{frz} - T_{firn})\rho c_p \Delta z}{\rho_{liq}\mathcal{L}}. \tag{4.3}$$

The quantity of the total incoming meltwater volume that is then available to leave a given layer, once sufficient meltwater has refrozen, can be described using a fractional freezing rate, f, which is calculated as follows

$$f = \frac{\Delta T c_p \rho}{\rho_{liq}\mathcal{L}}, \tag{4.4}$$

which, unsurprisingly, is very close to the Stefan number, which gives the ratio of sensible to latent heat.

Assuming a temperature change of 1 Kelvin and using example values used previously (see Table 2.1) we estimate u to be of the order of 10^{-5} and f to be of the order of 10^{-3}. This value of f suggests that the loss of meltwater due to refreezing in the catchment area is not going to significantly change the level of meltwater available through lateral transport through the catchment area as in reality if the surrounding firn has already reached the isothermal stage any diurnal variation that may lead to temperature changes subsequent to this is going to be much less than 1 K over the period of one timestep once the firn surface is warm enough to melt.

Initial modelling efforts shown in Figure 4.7 suggested that melt occurred on approximately 50 days during the 2010-11 melt season, which agrees well with the values given by the Envisat data shown in Luckmann *et al.* (2015). However, given the above suggestion that lateral melt should only occur after ice lens formation, the number of hours

where lateral melt would occur is reduced to 231 and therefore the size of the catchment area will be limited by how far meltwater can travel during this period.

The size of the catchment area can therefore be calculated using Darcy's Law for fluid flow through a porous medium which is this case will be

$$u_l = \frac{\Pi}{\eta} \rho g \Delta H_u \tag{4.5}$$

where ΔH_u is the surface gradient, which is estimated using information from a digital elevation model (DEM)[3]. Various values of ΔH_u were experimented with, with a value of 0.05 being chosen. This gives a speed of 9 x 10^{-4} m s^{-1} which gives a distance of 735 m that meltwater can travel during the given period. The average gradient of the surface over a distance of 735 m on the ice shelf was calculated to be 0.025 using the DEM, so for lake formation it was felt that a doubling of this value would be sufficient (given that not all areas will have lakes present) and this was well within the range of gradients found using the DEM data. Although the spatial resolution of the DEM was not sufficient to provide detailed information about lake catchment areas it is nevertheless useful to see that our chosen value is reasonable in comparison to the DEM values.

Lüthje *et al.* (2006a) use a surface gradient of 0.009 for their calculations of lateral transport on the Greenland ice sheet although unlike the surface in the Lüthje *et al.* (2006a) study we cannot here assume that the ice is snow free and therefore it is likely that a much larger gradient will be needed for water to percolate through snow rather than run off of bare ice. Therefore the higher value suggested by the DEM here seems justified given that a value of 0.01 was not large enough for lakes to form when tested and it is known that lakes are present on Larsen C.

A lake size of 3150 m x 390 m was chosen with these values calculated from a larger lake as found in Landsat imagery (see Section 4.4). A large lake was chosen so that subsequent calculations for crevasse propagation (see section 6.6) could be carried out with the largest volume of water likely to be present on the ice shelf .These values agree with the lake sizes suggested by Luckmann *et al.* (2015). Combining this lake size with the possible meltwater travel distance of 735 m into the lake basin we have a final 'melt multiple' value of 6. This is demonstrated diagrammatically in Figure 4.8.

[3]Thank you to Susan Bevan of the University of Swansea for providing the data for these calculations.

Calculating a separate surface energy balance for the surrounding firn should give a reasonable interpretation of how firn surrounding a melt lake should behave, as the weather conditions will be similar but there will be no change in albedo from lake formation. In order to account for the different density changes and albedo in the catchment area, a separate firn column is modelled to represent this. Therefore the model consists of two separate profiles; one for the lake basin and one for the catchment area.

Initially the two columns will start off with the same conditions. However, once an ice lens is formed in the catchment area column it is assumed that all subsequent melt will runoff into the lake. Therefore, all melt that is calculated as occurring in the firn surrounding the model domain subsequent to ice lens formation will be will be removed from the catchment area firn column. This volume of meltwater will then be multiplied by 6 and added to the incipient lake.

Inclusion of the extra melt from the surrounding firn in this way allowed lake formation, the results of which are discussed in Section 4.3. The sensitivity of the model to the parameters discussed in this section is investigated in Chapter 5 through the variation of the melt multiple value.

In order to determine that the inclusion of the foehn winds and lateral melt were both necessary for lake formation (as oppose to just including lateral melt) a model run without the addition of foehn winds but with lateral melt included was carried out and it was confirmed that in this case lakes did not form. This is shown in Figure 4.9. Here the firn gains some water from the surface down from Mid-November to January as meltwater percolates through the firn and some is retained due to the capillary effect. Then during January the firn is saturated from the ice lens up to the surface. However, once February is reached the saturated firn begins to refreeze from the surface downwards, as shown by the area of zero water content that increases with depth over time and thus a lake is not formed.

4.3 Model results

The model is run with the inclusion of the foehn wind effect and lateral melting. Inclusion of both of these effects was found to lead to consistent lake development in each year. The development of these lakes over ten years is shown in Figure 4.10. Over the ten years

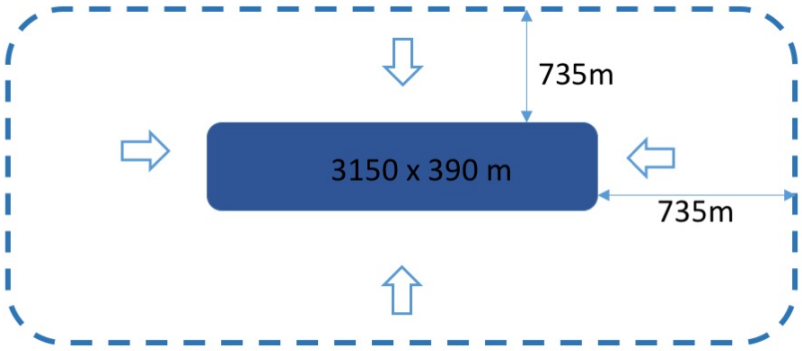

Figure 4.8: The catchment area of an idealised melt lake. Here the melt lake is shown in blue and the maximum distance that the firn can travel is shown by the dashed line surrounding it. The ratio of the white area enclosed by the dashed line to the area of the lake is 6:1, hence the melt multiplier used being 6.

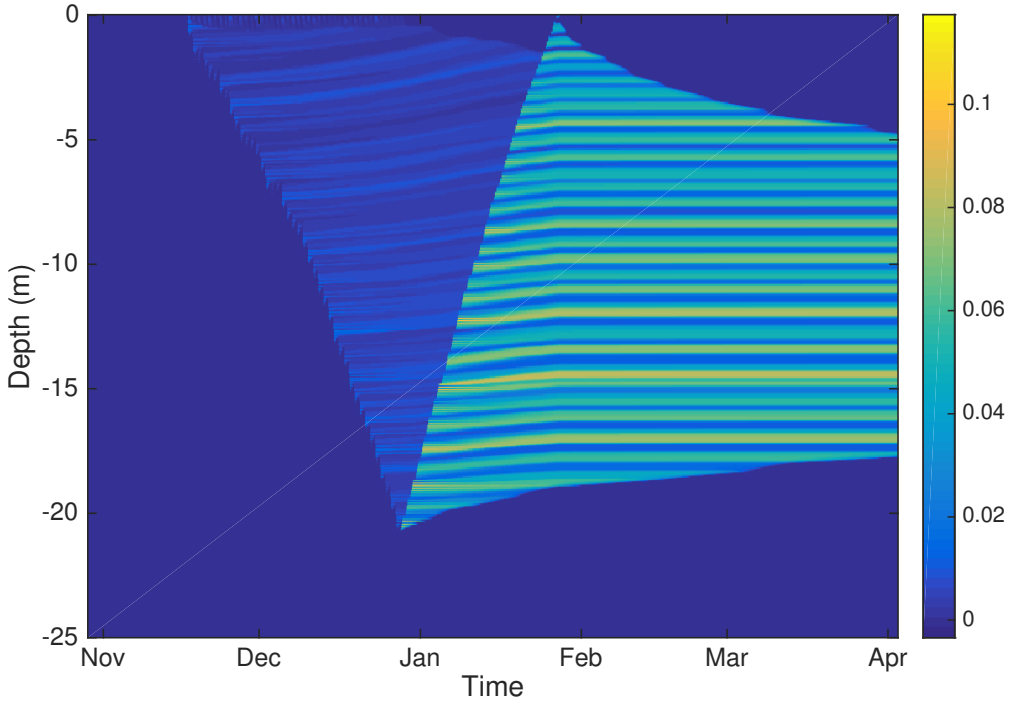

Figure 4.9: The water content of the model when run with lateral transport but not foehn winds included. Content is measured from 0 to 1 with 0 being no liquid present and 1 being purely liquid. Although meltwater accumulates within the firn full saturation is not achieved and therefore a lake does not start to form.

shown here there was a total of 6.09 m of water equivalent firn melt. If we take the spin up period to be five years we have for the final five years an average lake depth of 1.24 m and a maximum lake depth of 1.29 m. It was found that the lake height begins to stabilise after 3 years, with very similar profiles present in subsequent years as the model appears to reach a steady state. This is to be expected as the model is run using the same forcing each year, and once deeper lakes have developed lakes in subsequent years do not melt all the way through the solid ice of the previous year's refrozen lake so the conditions during each year are very similar.

The sharp increases in surface height of the lakes are due to lateral transport of meltwater. The amount with which lateral transport of melt from the catchment area contributes both to firn saturation and to the increase in depth of the lake shown here demonstrates that it is a key process in both lake formation and development.

The surface height initially decreases and firn is melted and saturated with meltwater. However, beyond the spin up period the surface height increases each year due to the addition of meltwater from the catchment area that refreezes in the lake area. This would be expected from constantly adding meltwater and the repeated use of forcing data from a warm year, so this increase of height would not be expected under present day conditions as warmer years do not always immediately follow each other for an extended period. However, this does have implications for the surface gradient used for the calculations of meltwater transport from the catchment area. This is investigated further in Chapter 6.

We can examine the development of the firn profile as a result of the lake formation by looking at the changes in the density, temperature and water content profiles of the firn. In this section all plots have been labelled with the initial depth on the left hand size. In reality, these depth values will change from left to right along the plot with time but due to the coordinate transform used, as each profile is scaled from one to zero, we can directly compare the profiles. However, it was felt that including the initial depth on the left hand axis instead of a scale from 0 to 1 was helpful to give a sense of scale.

Figure 4.11 shows the density profile of the firn for the first year. The initial small increase in density from the surface down beginning towards the end of November is due to the freezing of meltwater percolating down into the firn and the small fraction of meltwater that is retained due to capillary forcing as the meltwater passes through the

upper snow layers.

An ice lens forms at 20.23 m below the surface and subsequent to this there is a small amount of increase in density due to firn densification and refreezing of meltwater which reaches firn that is below the freezing temperature. The density then starts to sharply increase from the lens level upwards as the firn above the ice lens becomes saturated with meltwater. This large block of high density (shown as the yellow area in Figure 4.11) persists for the remainder of the simulation. Small areas of low density appear at the surface as fresh snow falls, but each year they are melted and incorporated into a new lake.

These processes can also be observed in Figure 4.12, which shows the first two years of this simulation. It can be seen here that up to the point of ice lens formation the majority of the meltwater is refrozen. The water retained due to the capillary effect is 5% of the remaining pore space so the volume of water is very small and does not show up clearly in comparison with the greater water content values of the saturated firn in this figure. However, to confirm that the capillary effect was indeed occurring, Figure 4.13 was created to show the firn during the time that only water due to capillary retention was present, allowing the presence of this water to be clearly identified.

The saturation of the firn is shown in the leftmost panel of Figure 4.12. The lake develops above this saturated firn but as the figure shows only the firn the lake is not shown here. The rightmost panel shows the point where the lake has refrozen completely and the firn column has been combined with the solid ice from the frozen lake; this is the area of nil water content at the surface of the firn. The area of saturated firn then decreases with time as the meltwater refreezes from both the top and bottom as the firn column cools.

The development of this profile in later years is shown in Figure 4.14. Here we can see that the saturated firn does not completely refreeze between melt seasons, it is insulated from surface temperature fluctuations by the layer of solid ice from previous lake formation above it and refreezes very slowly, suggesting that a portion of the ice shelf remains isothermal. It is clear from this figure that once a lake has formed and refrozen it acts as an ice lens for the subsequent melt season as only a very small amount of water appears at the top of the firn profile as the current year's snow is saturated but water is not able to percolate any further into the ice shelf due to this layer of solid ice.

We can see that the isothermal layer created by the initial meltwater percolation does persist from Figure 4.15. Each year the surface top 5 m of the firn experience the most temperature changes between melt seasons, but these temperature changes do not penetrate very deep into the ice shelf as meltwater can no longer percolate deep into the firn and the only method of heat transfer is then through conduction which occurs much more slowly.

We can also examine the changes that happen to the lakes and their refrozen ice lids over the period modelled. Figure 4.16 shows the development of the lake core temperature over the simulation. It can be seen here that once the lake forms it begins to heat up and the temperature fluctuates within a small range of less than 2 K. The maximum temperature reached during this simulation is 274.88 K.

Figure 4.17 shows the change in temperature of the surface of the refrozen lid of ice on top of the lake. Unsurprisingly, the temperature of this lid has a general negative trend as each melt season ends and the conditions head towards that of the Austral winter.

The total volume of in situ melt that is produced during the sixth melt season (taking the spin up period to be 5 years) is 497 mm of water equivalent. This is slightly higher than the 260 mm annual average found by Kuipers Munneke *et al.* (2014), although not unreasonable given that the year modelled here is both warmer than average and has the effect of albedo change due to lake formation which is not the case for every year on Larsen C.

In order to further investigate the effect of annual variations in climate on lake formation the model was run alternating data from 2009-10 and 2010-11. As can be seen from Figure 4.18, lakes form during both years but are significantly smaller during the 2009-10 melt season (odd years) than the 2010-11 melt season (even years). Regardless, the model again reaches a steady state but with a period of two years. This is again occurring as the lakes in each year do not manage to melt through the previous year's refrozen lake so each new year experiences similar initial conditions. It is unclear from MODIS data if lakes formed in the 2009-10 melt season; although they cannot be seen in imagery they may not be large or deep enough to show up and there are periods where the images are unclear. However, these results do suggest the previous lake formation will make subsequent lake formation easier even in cooler years.

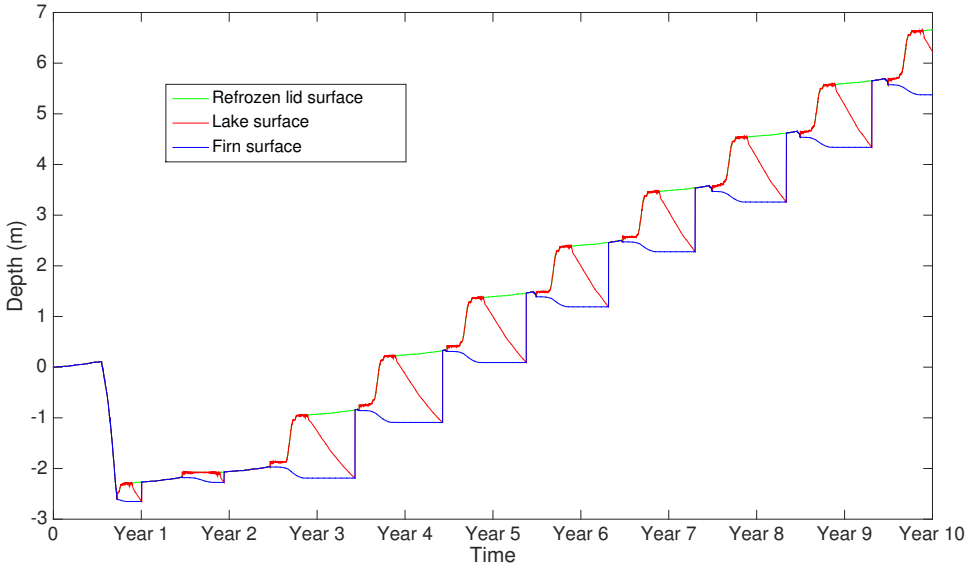

Figure 4.10: The development of surface melt lakes over a 10 year model run using 2010-11 data. Here, the blue line shows the firn surface, the red line the lake surface, and the green the refrozen lid.

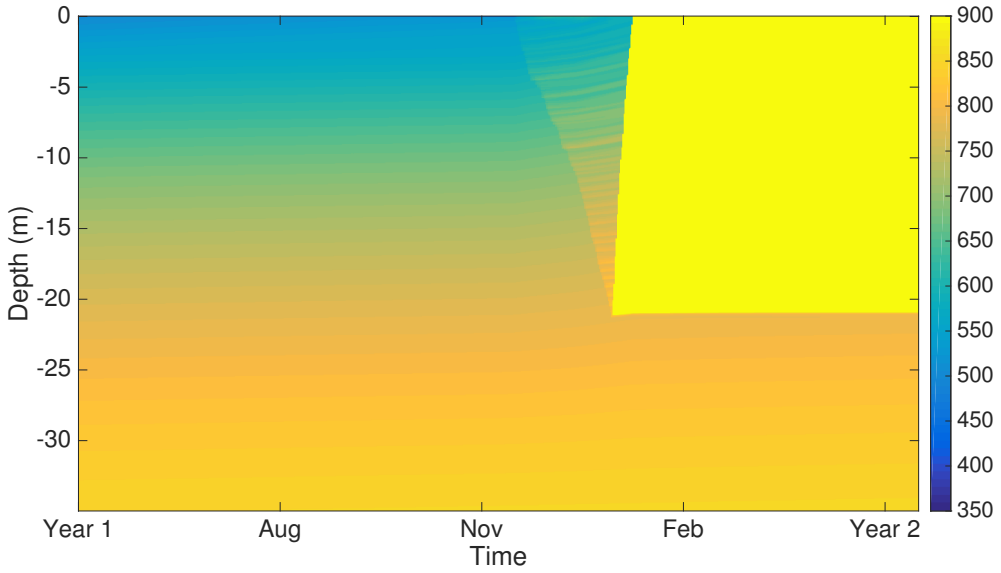

Figure 4.11: The development of the density profile of the firn over the first year of the model simulation. The colour bar shows the density in kg m^{-3}

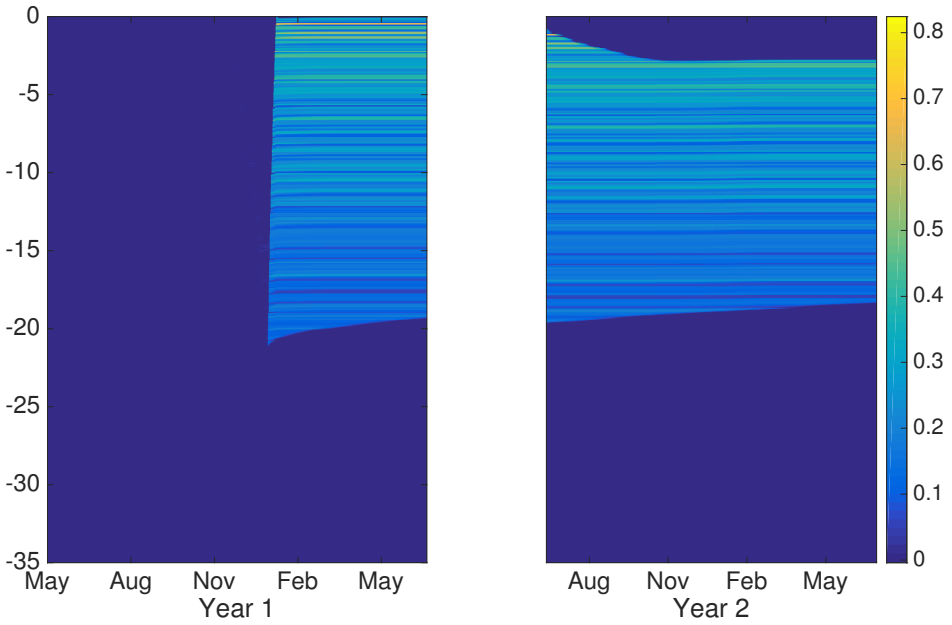

Figure 4.12: The development of the water content profile over the first two years of the model simulation. The split in the figure occurs when the lake from the first year has fully refrozen and this solid ice is added to the firm profile.The colour bar shows the water content as a fraction of each grid cell.

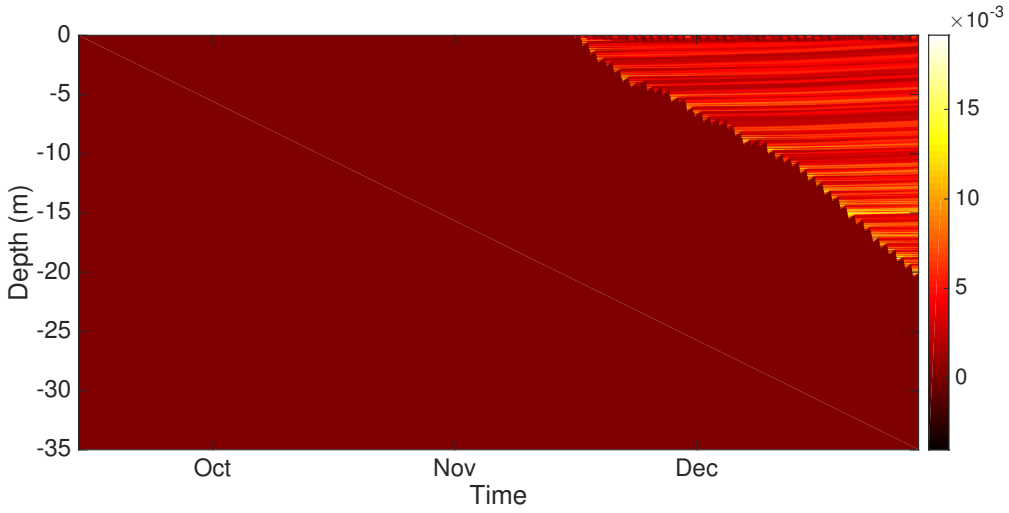

Figure 4.13: The water content of the firn during the period in the first year of the simulation before ice lens formation where the only liquid water present has been retained due to capillary forcing. The colour bar shows the fraction of each grid cell that consists of liquid water.

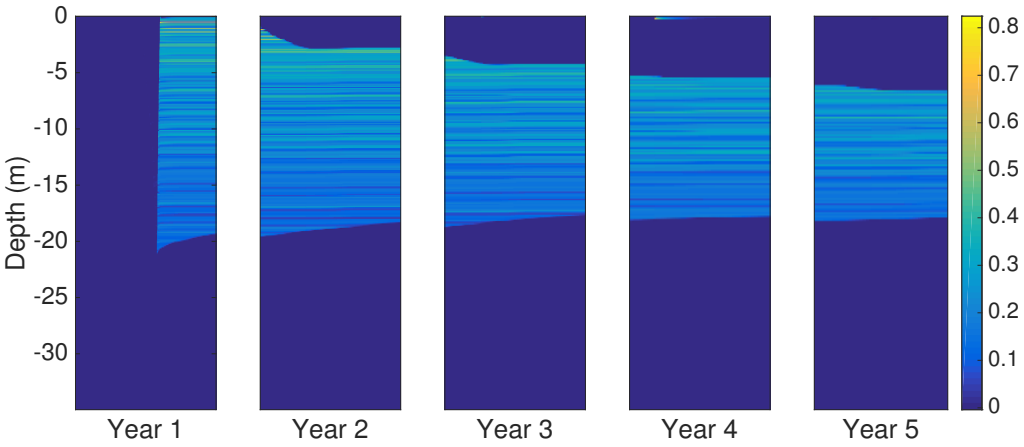

Figure 4.14: The development of the water content profile over five years of the model simulation. A new pane in the figure is created each time a lake has fully refrozen and this solid ice is added to the firm profile. The colour bar shows the water content as a fraction of each grid cell.

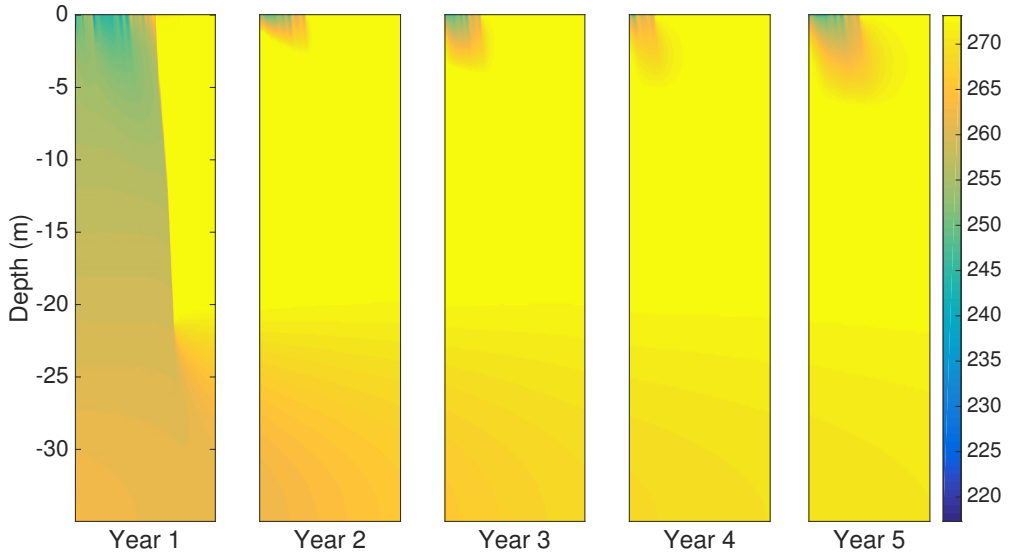

Figure 4.15: The development of the temperature profile over five years of the model simulation. A new pane in the figure is created each time a lake has fully refrozen and this solid ice is added to the firn profile. The colour bar shows the temperature range in Kelvin.

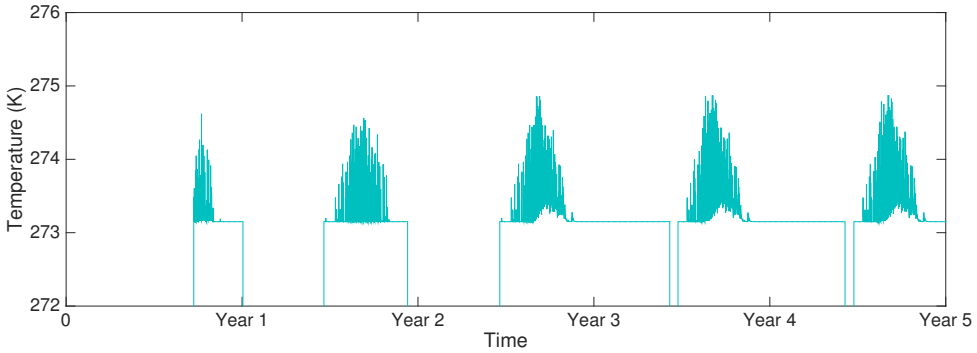

Figure 4.16: The development of the lake core temperature over a five year model simulation.

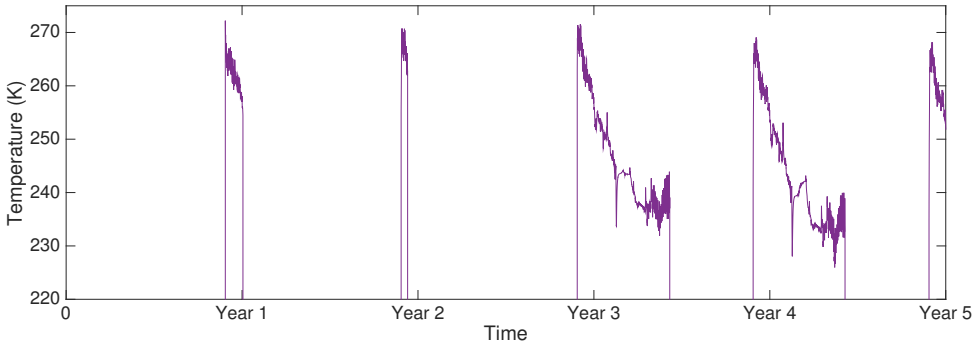

Figure 4.17: The development of the temperature of the surface of the lid of frozen ice on top of the lake over a five year model simulation.

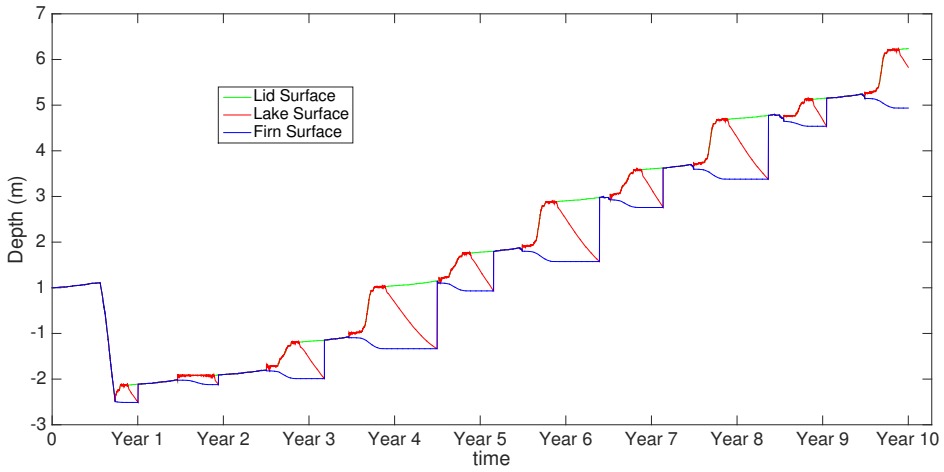

Figure 4.18: The firn, lake and refrozen lid surface heights over 10 years with the forcing alternating each year between 2009-10 (odd years) and 2010-11 (even years) forcing data.

4.4 Model verification

4.4.1 Verification using Landsat data

NASA's Landsat program[4] has acquired data that can be used to look at both the distribution and the depth of lakes on the Larsen C Ice Shelf. In order to verify that the availability of lake free areas surrounding lakes matches or exceeds that needed for a catchment area of the size suggested in Section 4.2.3, data from Landsat can be used. Here a comparison of the ratio of 'lake' pixels to 'ice' pixels is calculated from a small area shown in Figure 4.19 where multiple lake forms are present. Even in this area (which was chosen due to it being densely populated with lakes and therefore can be taken to be a minimum value of this ratio) we have a ratio of approximately 1:40, suggesting that the melt multiplier used above is well within the bounds of the available catchment area and that it is the distance water can travel rather than the volume of available water that constrains lateral transport.

In addition, lake depths can be calculated from Landsat 8 imagery (Pope *et al.*, 2016). Here the depth of a lake is approximated based on the following equation,

$$h = [ln(A_d - R_\infty) - ln(R_{lake} - R_\infty)]/g* \tag{4.6}$$

where A_d is the lake bottom albedo, R_∞ is the reflectance of optically deep water, R_{lake} is the reflectance of a lake pixel and g* is related to the losses in upward and downward travel through the water column (with units of m^{-1}).

Pope *et al.* (2016) compare this method with an empirically based formula and found it to be as or more accurate for lakes tested in Greenland. However, they estimate the accuracy of this method to be ± 1.6 m when compared with digital elevation model derived lake depths, which are created using imagery of lakes both before and after drainage. As can be seen from Figure 4.20, this level of accuracy is not sufficient for individual lakes on the Larsen C Ice Shelf. However, it is noted by Pope *et al.* (2016) that the mean depth derived from this method shows good agreement with digital elevation models and therefore this is still of use here where a specific lake is not being considered.

The data from the scene shown in Figure 4.19 was used to create Figure 4.20. The

[4]Thank you to Allen Pope of the NSIDC/ University of Washington for providing these images and the Landsat data used here.

average lake depth from this area was 0.52 m and it can be seen from Figure 4.20 that the spread of lake depths is also concentrated around the 0.1-1.3 m range, suggesting that the lake depths found by the model are, given the level of accuracy of this method, within realistic bounds, especially given that they are created by repeatedly forcing the model with data from an unusually warm melt season.

For the time period of data available used to force the model the Landsat 7 satellite would have been in use rather than Landsat 8 which was used for the Pope *et al.* (2016) study and for the data shown in Figures 4.19 and 4.20. However, further work has been done to use this method for Landsat 7 data which gave average lake depths ranging from 0.34 to 0.47 m for various scenes analysed for the period 2007-2009 and similar ranges of values to those from Figure 4.20. Although this method is less tested than the use of this technique for Landsat 8 data it is nevertheless useful to see here that the lake depths calculated during this modelling study again match reasonably well with the ranges and averages calculated from the Landsat data.

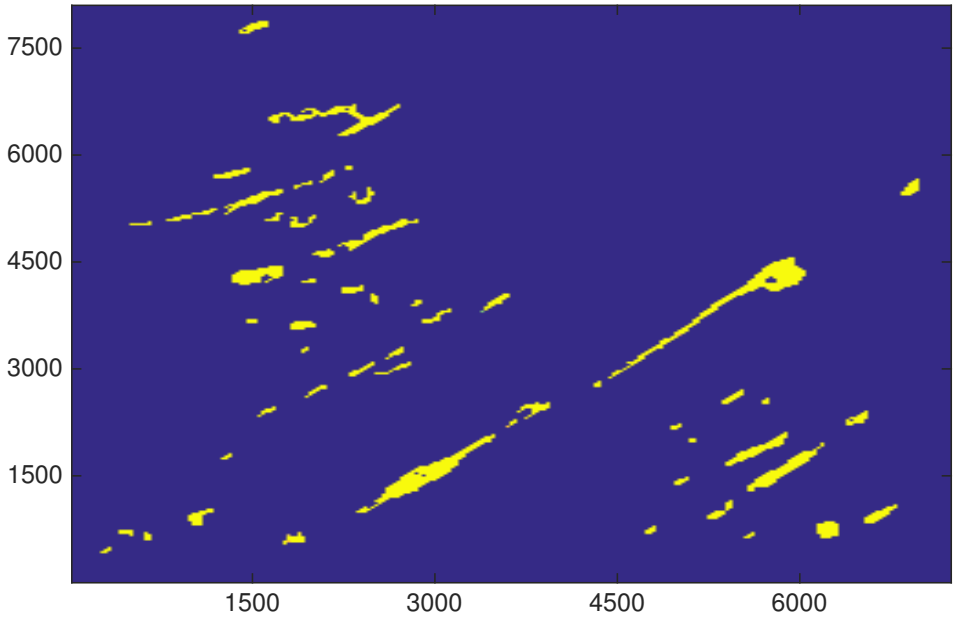

Figure 4.19: Landsat image of a section of the Larsen C ice shelf where melt lakes were present on 06/01/2016. Both axes have units of meters. Here the lakes are coloured yellow and areas where lakes were not present are coloured blue. Although this data was taken from the Landsat 8 mission so is from a later time than the lakes examined using the 2010-11 melt season, it is likely that the lakes will be similar in many aspects due to the role of topography in the location of lake basins.

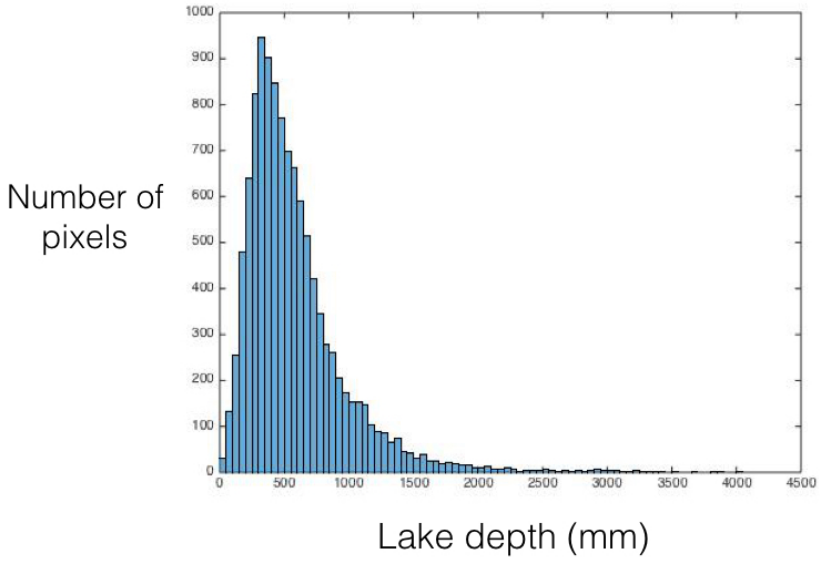

Figure 4.20: Lake depths on the Larsen C Ice Shelf as calculated from Landsat data from 06/01/2016. The horizontal axis gives lake depths in mm and the vertical axis gives the numbers of pixels for each depth.

4.4.2 Verification using MODIS imagery

As stated above, the number of melt days that occur in the model simulation presented here matches well with those from Envisat data (Luckmann *et al.*, 2015). Ensuring that these days match the onset times of lake formation could be possible using MODIS imagery but is difficult due to the sparse temporal availability of clear MODIS imagery. For the year examined (the 2010-2011 melt season) there is no clear evidence of lake onset day, although there is a clear image of lakes in mid-November. The lake onset days given by the model are towards the beginning of November each year and this corresponds well with the evidence available for lakes from 2005-2009 where lakes often form in November or December.

Chapter 5

Sensitivity Testing

In order to determine the sensitivity of modelling results to various parameters the model was run many times changing one parameter each time, and these runs compared with the base case simulation described in Chapter 4. Ten years was deemed an appropriate length of time to carry out sensitivity simulations as it was found in Chapter 4 that the lake volume quickly becomes quite consistent in the base case simulation (see Figure 4.10), and ten years allows for a five year spin up period plus five years of simulations to compare after this spin up period.

Our initial testing involved running the model beyond this 10 year period in order to determine if the model would reach a stationary state. These longer runs determined that, due to the non-linear dynamics of the model, a stationary state is not reached but a steady limit cycle does exist. After the first five years this limit cycle was consistently observed and therefore five years was chosen as an adequate spin up period.

In order to account for this spin up period, the calculations and comparisons below are carried out using the final five years of data from each simulation, unless specified otherwise.

The results of the sensitivity tests for each parameter are discussed below. Here the average lake depth is taken as the average annual maximum value.

5.1 Air temperature

Both the average and maximum lake depth were found to vary with the air temperature. Increasing the air temperature by 0.5 K was found to increase the maximum lake depth by 0.1 m to 1.34 m and the average lake depth was found to increase by 8.1%. As expected, in the opposite case, decreasing the average air temperature by 0.5 K was found to reduce the maximum lake depth over 5 years by 0.16 m and the average lake depth was reduced by 13.9%. The maximum lake depths for each year of the simulations, including the spin

up period, are shown in Figure 5.1.

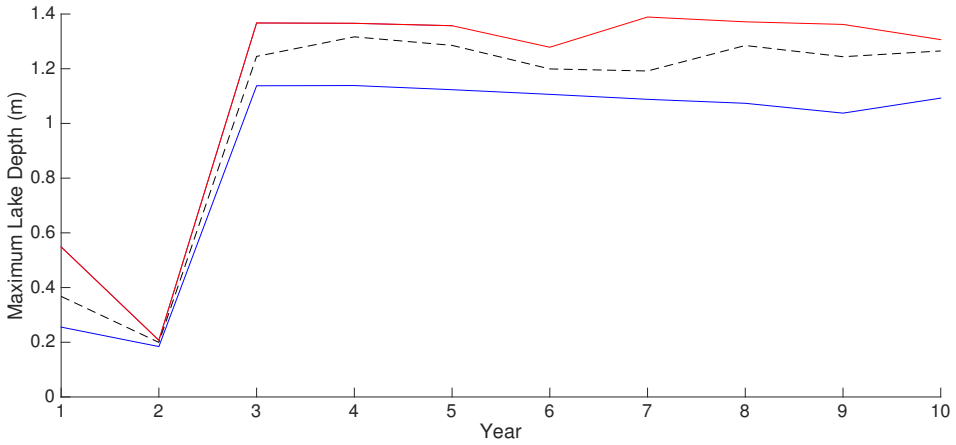

Figure 5.1: The maximum lake depth each year for the base simulation (black dashed line), a reduction in air temperature of 0.5 K (blue line) and an increase in air temperature of 0.5 K (red line).

Decreasing the air temperature will affect the sensible heat term of the surface energy balance. As stated in equation 2.10, the sensible heat flux is calculated as

$$F_{sens} = \rho_a c_p^{air} C_T \nu (T_a - T_0). \tag{5.1}$$

Therefore, the effect of changing the air temperature on the sensible heat is dependent on whether the firn surface is at a higher or lower temperature than the air. During times of melting when the air temperature is often higher than the surface temperature, reducing the air temperature will therefore decrease the value of the sensible heat and reduce the overall energy input at the surface and vice versa with increasing the temperature. Similarly, during times of refreezing of the lake when the air temperature may be lower than the surface temperature, reducing the air temperature further will make the value of the sensible heat more negative and increase the speed of refreezing of the lake.

A further effect of changing air temperatures that is not captured by the model here is the effect on the latent heat flux. As shown in equation 2.11, the latent heat flux is dependent on the humidity. Warmer air is able to hold more water vapour and thus can have a higher humidity. Increasing the difference between the air and surface specific humidity increases the latent heat flux, but as humidity is forced here this will not be shown in these results.

The effect of increasing the air temperature further than the values given here is in-

vestigated in Chapter 6.

5.2 Lateral melt catchment area

It would be expected that increasing the lateral melt water available would increase the average lake depth and vice versa. In order to test this, the model was run with both melt multiples of 3 and 9, the results of which are shown in Table 5.1.

As expected, it is clearly demonstrated that meltwater from the catchment area plays a significant role in determining lake depth as well as in overall lake formation; there is an 85.2% increase in average lake depth between the 3x and 6x simulations, and further 35.8% increase from the 6x to the 9x value.

Melt Multiple	x3	x6	x9
Maximum Lake Depth (m)	0.78	1.28	1.77
Average Lake Depth (m)	0.67	1.24	1.68

Table 5.1: The maximum and average lake depths for the final five years of simulations for melt multiple values of 3, 6 (base case simulation) and 9.

5.3 Accumulation

In order to determine the model's sensitivity to the addition of accumulation in the form of snow, tests were performed where the accumulation was halved and doubled compared to the base case level of accumulation.

The level of accumulation can have three competing effects on the formation of lakes on an ice shelf. These all occur due to the density of fresh snow being less than that of compacted, older firn.

First of all, adding more accumulation will mean that there is a larger region of high pore fraction at the surface of the ice shelf. This means that a longer time is needed for the pore space to be saturated with meltwater and a lake created. Based on this it would be expected that a greater level of accumulation would lead to shallower lakes, or no lakes at all.

However, as the fresh snow is less dense than compacted, older firn the second possibility is that more accumulation could lead to melting of a greater vertical distance into

the firn for the same energy input. This can lead to quicker exposure of melt lakes and therefore to deeper lakes forming due to the change in albedo.

Finally, less dense snow will have a lower thermal conductivity than denser firn meaning that surface temperature fluctuations do not propagate as far into the ice shelf. Heat will be gained or lost from a smaller surface layer, which will lead to a greater amplitude in surface temperature fluctuations. It is unclear what the result of this particular effect will be as this could both increase melting due to temperature increases at the surface, but also cause quicker refreezing as heat may be lost to the surroundings more quickly.

The interplay of these effects means that the response of the melt lakes to changes in accumulation can be complicated and is neither monotonic nor linear. Here we compare two cases for a sensitivity study, 0.5 and 2 times the base level of accumulation, but in Chapter 6 we investigate further the response of greater increases in snowfall.

In these cases it seems that the second situation described above is occurring; an increase in the amount of snow leads to an increase in lake depth. The results of this are shown in Table 5.2. It appears that for this range of accumulation levels, the amount of snow available to melt is acting as a limiting factor for lake depth. It will be shown in Chapter 6 that this trend in fact continues for up to five times the base case level of accumulation, but the situation changes for greater amounts of snowfall than this.

	Base	x0.5 snow	x2 snow	300 kg m^{-3}	400 kg m^{-3}
Average lake depth (m)	1.24	1.11	1.30	1.24	1.11
Max lake depth (m)	1.28	1.33	1.35	1.29	1.14

Table 5.2: The results of testing the sensitivity of the model to snowfall, by varying the total snowfall (columns 3 and 4) and the density of the snowfall (columns 5 and 6).

In addition to the above, the sensitivity of the model to the density of the accumulation was investigated. Once again there will be competing effects of less dense snow meaning more pore space needs to be filled to saturate the firn, but less dense firn also requiring less energy to melt through the total snowfall if the snow depth remains the same.

It appears that here, in a similar way to adding greater amounts of less dense snow to the denser firn, decreasing the density of the snow also leads to deeper lakes. As shown in Table 5.2, both the average and maximum lake depths were increased through

a reduction of the snow density to 300 kg m^{-3} (from the base case value of 350 kg m^{-3}) and decreased through an increase of the snow density to 400 kg m^{-3}.

5.4 Dry snow densification

Section 2.1.2 describes the dry snow densification that is simulated by the model. Figure 5.2 shows the effect of this process alone on the firn density profile. In order to test the sensitivity of the model to this process the model was run with the dry snow densification turned off. It was found that this meant that the initial ice lens formed 0.92 m further down in the firn and also that 5.1% more in situ melting was required for lens formation. Furthermore, the initial lake formed in the first year was less deep without dry snow densification than that of the base case simulation. This would be expected given that without dry snow densification there would be a greater amount of pore space to fill for saturation of the firn and a greater amount of refreezing of meltwater needed within any given level of the model for ice lens formation.

However, once the initial lake had formed and the amount of saturation of the firn needed for subsequent lake formation is much decreased (due to the previous year's refrozen lake acting as an impermeable layer meaning that only new snowfall needs to be melted or saturated) the lakes in the simulation with no dry snow densification become deeper than equivalent lakes in the base case simulation, with the average lake depth being 2.4% deeper in the case with no dry snow densification.

If we look at Figure 5.3 we can see that turning off the dry snow densification does not have a large impact on lake onset time. Furthermore, the melting of the lake base in both cases is similar. It is the meltwater that is added from the catchment area that makes a difference here; the catchment area with no dry snow densification will have a lower density than that of the base case, meaning that less energy is needed to raise the surface temperature to the melting point and more melting occurs in the catchment area (and is subsequently added to the lake) as a result.

Nevertheless, these differences are small and the importance of dry snow densification is far outweighed by that of the densification due to refreezing of meltwater; not only are the changes in density far greater due to the meltwater refreezing, but without the formation of ice lenses then a great deal more saturation of the firn would be needed

for lakes to form.

There are other processes that play a role in the densification of snow that are not taken into account here but may also play a significant role in the densification of Antarctic firn and therefore in lake formation. For example, the densification of snow and the formation of density strata in snow due to wind packing has been observed on Greenland (e.g. Fujitai *et al.* (2014)) so is very likely to play a role in the firn structure on Antarctic ice shelves too. Fujitai *et al.* (2014) note that density strata are mainly formed due to wind packing in winter and require less refreezing of meltwater to reach the pore closure density. This could be a possible mechanism for ice lenses forming higher up in the firn than suggested by the results here, in addition to less meltwater being required to saturate this denser firn. This may lead to the formation of deeper lakes as melt lakes will be exposed sooner.

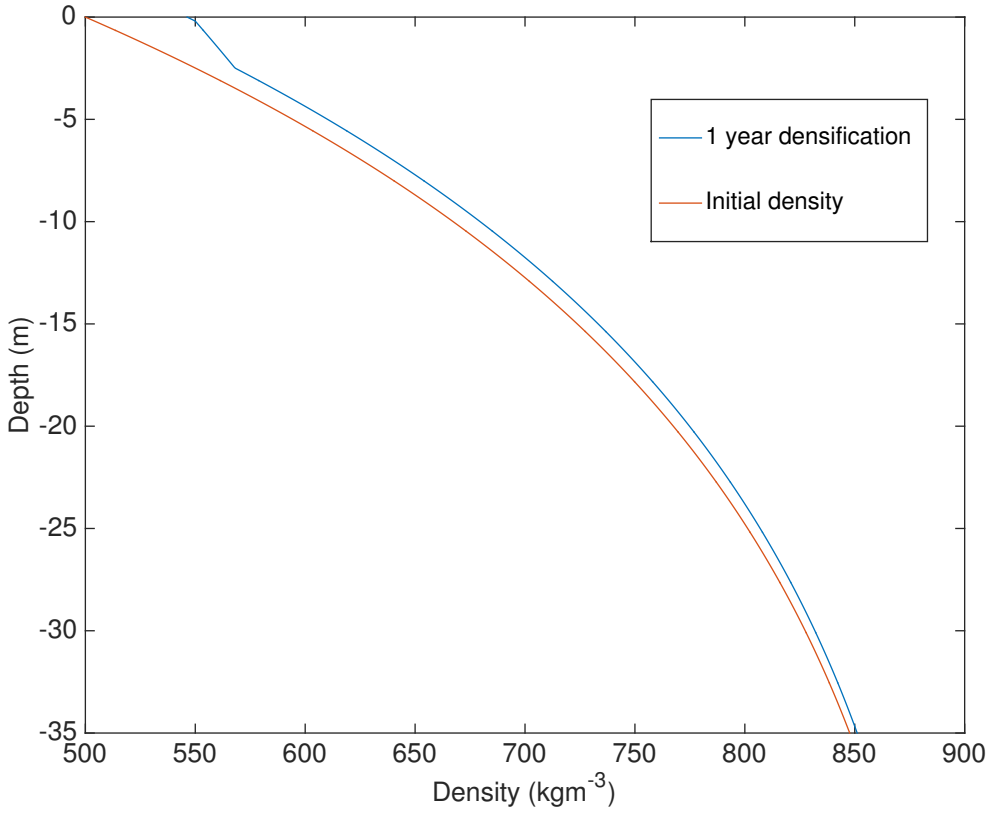

Figure 5.2: The initial firn density profile and the effect of one year of dry snow densification on this profile (no other forcing is included here).

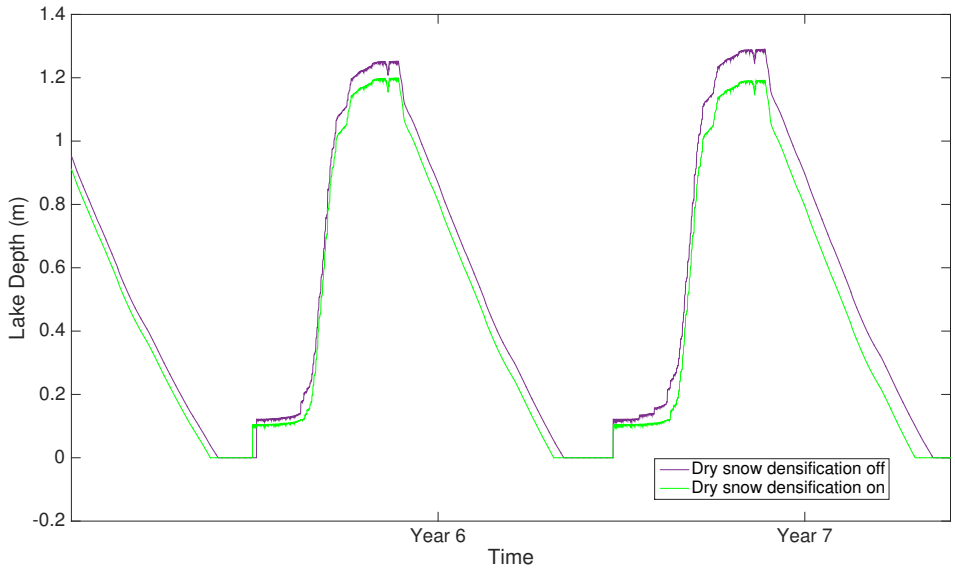

Figure 5.3: Two years of the lake depths found in the base case run and the sensitivity study with the dry snow densification turned off.

5.5 Foehn winds

The foehn wind effect added to the model alters both the air temperature and the wind speed during the designated foehn wind events. Therefore sensitivity tests were carried out on both of these values independently.

The modelled foehn wind events add 5 K to the observed AWS air temperature during their period of occurrence. Therefore the change in temperature was examined by changing this value to both 3 K and 7 K.

As would be expected an increase in foehn wind temperature led to an increase in the average lake depth and vice versa, with an increase of 10.9% for a 2 K increase of temperature and a decrease of 3.5% for a 2 K decrease in temperature.

The situation with the foehn wind speed is less straight forward as the wind speed affects both the sensible and latent heat. For the sensible heat the sign of this effect is dependent on the air and surface temperature so, for example, an increase in wind speed could either increase or decrease the sensible heat. Likewise with the latent heat the sign of the change can be positive or negative.

This leads to a non-monotonic relationship between average lake size and wind speed. It was found that reducing the foehn wind speed below the base case level by

5 m s^{-1} (to 0 m s^{-1}) causes a decrease of 4.3 cm in the average lake depth size, but increasing the wind speed by 5 m s^{-1} (to 10 m s^{-1}) causes a decrease in lake depth too, this time of 4.4 cm.

In order to determine the cause of this response of average lake depth to changes in wind speed we can examine the sensible and latent heat fluxes separately. As can be seen in Figure 5.4 an increase in the foehn wind speed amplifies the latent heat for both positive and negative values. The increased positive values are around the time of lake formation so it could be expected that increased wind speed would increase lake depth based on the latent heat.

However, when we examine the sensible heat flux as shown in Figure 5.5 we can see that in comparison to the base case, the addition of an extra 5 m s^{-1} of foehn wind speed on top of the base case value causes an increase in the magnitude mostly of the negative sensible heat values and this will be negating the positive influence of the latent heat flux that the wind is having during the time of lake formation somewhat, which would account for the reduced lake depths overall.

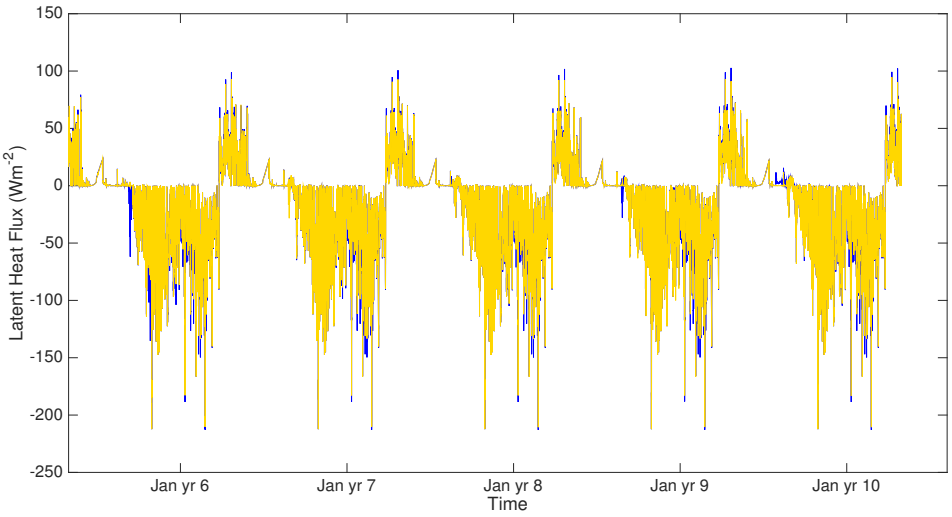

Figure 5.4: A comparison of the latent heat flux for the base case (shown in yellow) plotted on top of the case where the foehn wind speed is increased by an extra 5 m s^{-1} up to 10 m s^{-1} (shown in blue). Here the flux is shown as positive upwards, so a negative flux during the austral summer represents the flux going into the ice shelf.

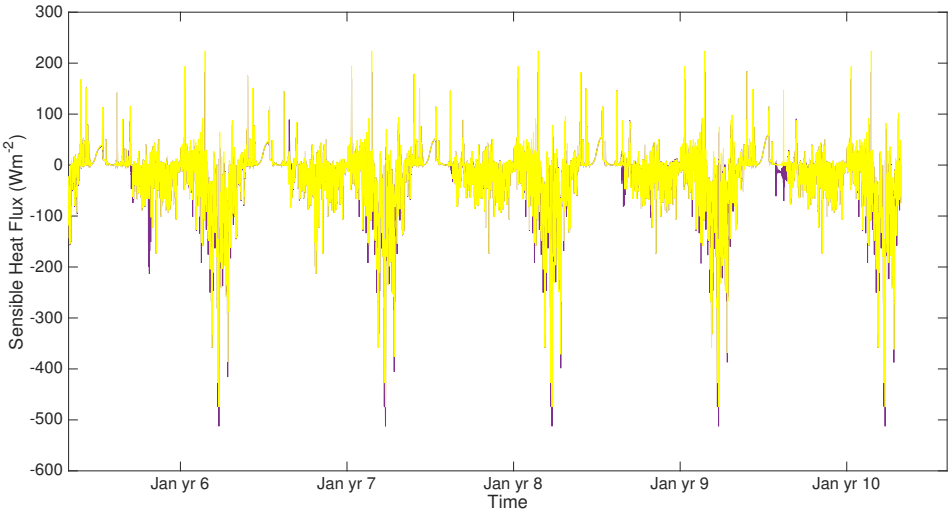

Figure 5.5: A comparison of the sensible heat flux for the base case (shown in yellow) plotted on top of the case where the foehn wind speed is increased by an extra 5 m s^{-1} up to 10 m s^{-1} (shown in purple).Here the flux is shown as positive upwards, so a negative flux during the austral summer represents the flux going into the ice shelf

5.6 Wet snow albedo

The value of the wet snow albedo in the model is set as a constant which is used for the surface albedo once melting has begun, until the point that a lake is formed or the wet snow has refrozen. The sensitivity of the model to this parameter is tested by both reducing and increasing the chosen value for the wet snow albedo by 0.1 from the base case value of 0.6 to 0.5 and 0.7 respectively.

Increasing the value of the albedo should mean that more shortwave radiation is reflected by the surface and therefore less energy is available for melting and smaller lakes would be expected. In contrast it would be expected that reducing the value of the wet snow albedo would mean that less shortwave radiation is reflected and therefore more energy is absorbed and available for melting and deeper lakes would occur.

The sensitivity studies suggest that this is indeed the case, although the effect of the change in wet snow albedo did not lead to a large change in the lake depths. For an increase in the wet snow albedo value the average lake depth is reduced by 1 cm, a reduction of less than 1% from the base case simulation, and for the decrease in wet snow albedo the average lake depth is increased by 0.1 cm, an increase of 0.1 %. It was found that the overall melt was increased by reducing the wet snow albedo, especially during

the spin up period, but in the final 5 years of the simulation the difference was very little.

5.7 Melt lake albedo

Similarly to changing the wet snow albedo, it would be expected that increasing the melt lake albedo would reduce the lake depth and decreasing the albedo would increase the lake depth.

The melt lake albedo is calculated from the formula given in equation 3.3 which is dependent on the lake depth. Here the albedo is varied by adding or subtracting 0.05 from the value calculated from this formula. This is a smaller variation than that made for the study of the wet snow albedo due to the fact that for deep lakes this could lead to the albedo becoming negative.

Results of this variation in albedo are presented in Table 5.3. Here it can be seen that, as expected, increasing the lake albedo leads to a reduction in both the average and maximum lake depths, and reducing the lake albedo has the opposite effect.

Lake Albedo	+0.05	Base Case	-0.05
Average lake depth (m)	1.23	1.24	1.33
Maximum lake depth (m)	1.27	1.29	1.34

Table 5.3: The change in average and maximum lake depths when the wet snow albedo is varied.

5.8 Initial density profile

For the initial density profile input into the model the empirical equation used (equation 2.48) requires two choices of value: that for the surface density and that of the firn-ice transition, or pore closure depth. Therefore both of these choices are examined here.

For the case of the pore closure depth there are two conflicting possible effects on melt lake size from changing this variable. First of all, a pore closure depth closer to the surface will mean a denser initial firn profile overall which will require less meltwater to saturate it fully. Therefore there is the potential for lakes to form more quickly. However, a denser profile means more ice which will require more energy to melt than a smaller amount of less dense ice, which may delay lake formation. The difference in initial density of

these profiles is shown in Figure 5.6. It can be seen that the formula used here means that the input value of the firn-ice transition depth does not match exactly to the pore closure depth, although the pore closure depth does increase or decrease as would be expected from changing this input value. This suggests that the results could potentially be improved by using a real firn density profile for the ice shelf should this information become available, rather than an empirical formula.

From reducing and increasing the firn-ice transition depth by 10 m it was found that of the possible effects the former was the one that was initially having the greater influence; the shallower the pore closure depth was (and therefore the denser the overall profile was) the deeper the lakes were, with the opposite being true for the deeper pore closure depth. This is shown in Figure 5.7.

Despite an initial large effect on lake depth, with time the effect of changing the pore closure depth is much reduced. For the final five years of the simulations there is a maximum of 3.1% difference between these simulations and the base case for the average lake depth and a maximum of 1.4 % difference for the maximum lake depth.

Secondly, the initial surface density is varied by increasing and decreasing the base case value by 100 kg m^{-3}. The results from these two variations were as would be expected from the results of varying the pore closure depth; the higher density case resulted in a deeper average lake depth than the base case and the lower density case resulted in shallower lakes. The denser the initial profile the less melt water would be required to saturate the firn and therefore deeper lakes are possible with a less dense initial profile with the same amount of meltwater present.

Again, this effect is reduced with time. As shown in Figure 5.7, despite large initial differences in lake depth, both simulations tend towards similar values after the spin up period. Examining the final 5 years we see that there is a maximum of 2.7 % difference between these simulations and the base case for the average lake depth and a maximum of 3.4 % difference for the maximum lake depth.

5.9 Bottom boundary condition

The assumption that the temperature gradient is zero at the bottom of the firn is tested by setting the gradient equal to a non-zero constant instead. The zero gradient condition

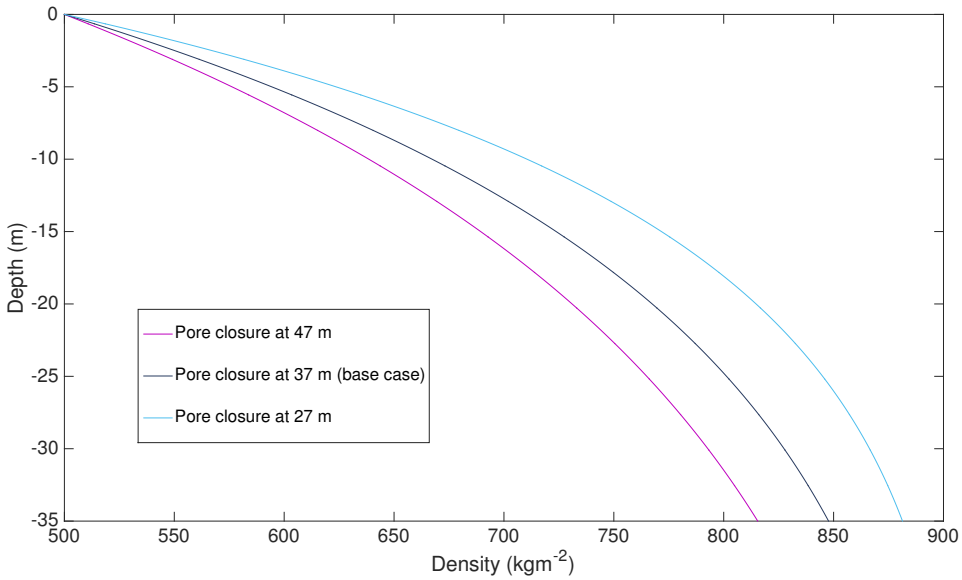

Figure 5.6: The initial density profiles for the base case and the two sensitivity studies where the firn-ice transition depth was increased and decreased by 10 m.

was implemented as it was found during initial testing that temperature changes did not penetrate very far into the ice shelf on time scales of a few years (excluding the changes due to meltwater refreezing) so it is expected that if there is a temperature gradient within the middle of the ice shelf it is very small. This seems to be the case for the ice core profiles mentioned in Section 2.2.2 which, as shown in Figure 5.8, have sharp gradients near the surface but then fluctuate around a range of approximately 2 K below 20 m.

Here the values chosen to test the sensitivity of the model to this bottom boundary condition were 0.5 K m^{-1} and -0.5 K m^{-1}. These values were chosen as values that could be physically realistic; the temperature gradients below 20 m in Figure 5.8 rarely exceed 1 K m^{-1} and the most negative temperature gradient used at any point in the ice shelf in the modelling study of Holland and Jenkins (1999) is -0.125 K m^{-1}.

It was found that setting the bottom boundary condition equal to a constant gradient had no significant effect on the average lake depth. For the bottom boundary condition set to 0.5 K m^{-1} the maximum and average lake depths did not vary from the base case values (up to 4 decimal places). For the bottom boundary condition set to -0.5 K m^{-1} the average lake depth varied by 3.1% from the base case value and the maximum lake depth varied by only 0.4% from the base case.

If we look at the initial 5 years of the model run we can see that the influence of the

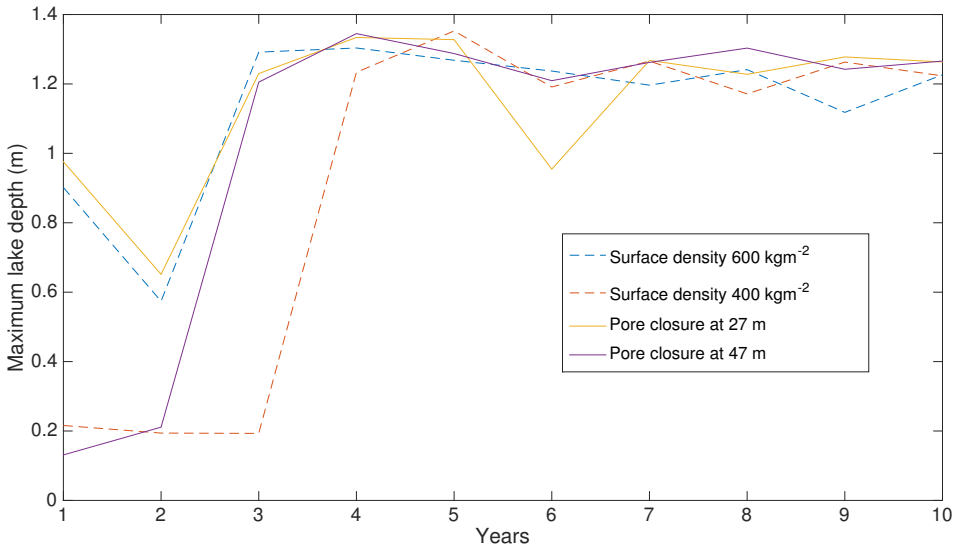

Figure 5.7: The maximum lake depth for each year of the simulation for the four sensitivity studies varying the initial density.

bottom boundary condition is even less; for the average lake depth over those 5 years the -0.5 K m^{-1} case only varies by 0.32% from the base case. This suggests that the influence of the bottom boundary condition, although weak, increases with time. This is likely to be due to the meltwater penetrating deep into the top of the ice shelf in early years as the temperature change from this will take a long time to reach the bottom boundary of the model domain as heat is being transferred by conduction below the pore closure depth. This does suggest that for more accurate results a larger model domain could be used, but as the difference was only a small percentage here the 35 m profile was maintained for model efficiency.

5.10 Initial temperature profile

The initial temperature profile input into the model was examined by increasing and decreasing the initial surface temperature by 5 K. As the initial profile is based on a linear equation this will change the whole initial temperature profile. For the final 5 years of the simulation there was less than a 4.5% difference between average lake depth and the base case for either simulation and a maximum difference of 1.2% for the maximum lake depth.

The results of changing the initial firn temperature on the evolving maximum lake

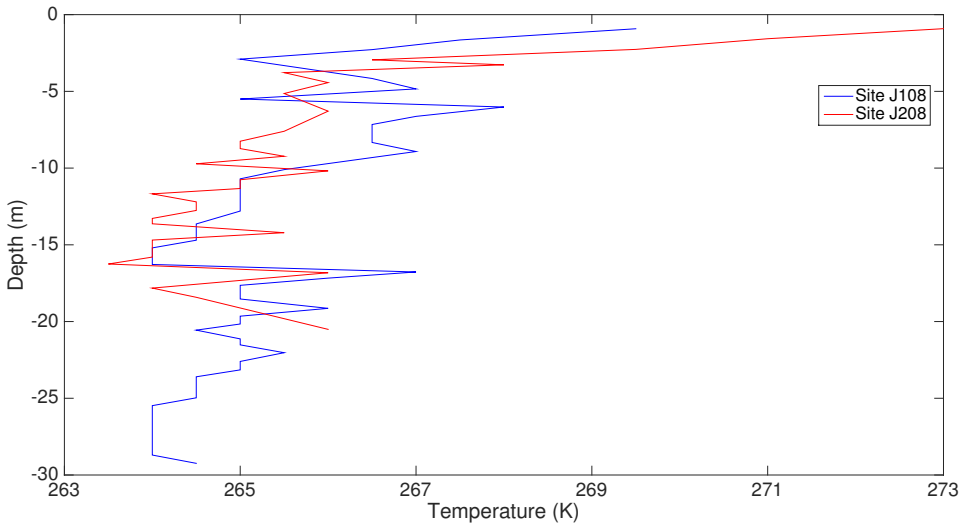

Figure 5.8: Two ice core temperature profiles from the Larsen C Ice Shelf.

depths for the first 5 years of these two simulations are shown in Figure 5.9. Here it can be seen that although the initial lake depth is strongly influenced by the initial temperature profile, this quickly levels off and in later years the difference between the lake depths in these two cases is much reduced as the model loses memory of the initial temperature profile. However, there are still small differences between the base case and these two simulations throughout the 10 years of the simulations. This suggests that although most of the effect of the initial temperature profile will be lost as long as an adequate spin up period is applied, the lower grid cells of the model may still retain memory of the initial conditions as changes to them occur much more slowly.

5.11 Incoming shortwave radiation

The lake depth is expected to increase with increasing incoming shortwave radiation and this was found to be the case; multiplying the incoming shortwave radiation by a factor of 1.1 gave a 24.1% increase in the average lake depth (to a depth of 1.54 m) and a 25.6% increase in the maximum lake depth (to a depth of 1.61 m) when compared with the base case simulation.

Similarly, a decrease in the incoming shortwave radiation showed a corresponding decrease in the average and maximum lake depths, but by a smaller percentage. When multiplying the incoming shortwave radiation by 0.9 we see a 1.6% decrease in the aver-

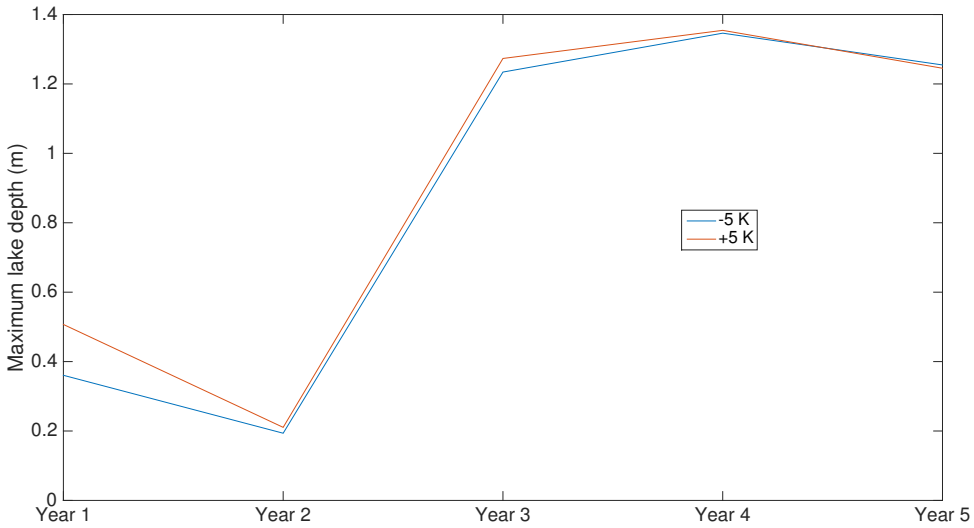

Figure 5.9: The maximum lake depth each year for the cases of a 5 K increase (red) and 5 K decrease (blue) in the initial surface temperature profile.

age lake depth and a 1.5 % decrease in the maximum lake depth.

5.12 Comparison of sensitivity

In order to directly compare the sensitivity of the model to some of the parameters tested above we use a measure of model sensitivity as defined in Taylor and Feltham (2004). Here, a non-dimensional value, d(x), is assigned as a measure of model sensitivity and is calculated as follows:

$$d(x) = \frac{\langle x \rangle}{\langle B \rangle} \frac{\partial(B)}{\partial(x)}. \tag{5.2}$$

Here, $\langle x \rangle$ is a typical range of the parameter being examined, $\langle B \rangle$ is the typical value for the output of which the sensitivity is being tested, $\partial(B)$ is the range in that output value for the sensitivity studies and $\partial(x)$ is the range of the parameter during the sensitivity studies.

For this study two values for B are examined for each parameter, the maximum lake depth and the mean lake depth.

The typical range of a parameter is taken from the base case simulation (for example the minimum to maximum air temperature from the base case is used in the calculation for the air temperature simulation). Where a range of values is not available for the base

case (for example for the melt multiple which is set equal to a constant) then the total range of values used during the sensitivity studies is used here.

Table 5.4 shows the calculated values of this parameter for the sensitivity studies presented above for both the mean and maximum lake depths.

Parameter	Max lake depth sensitivity	Mean lake depth sensitivity
Accumulation amount	0.016	0.149
Accumulation density	-0.117	-0.106
Air temperature	0.214	0.205
Melt multiple	0.770	0.818
Wet snow albedo	-0.012	-0.010
Foehn wind temperature	0.089	0.100
Foehn wind speed	-0.031	0.001
Lake albedo	0.041	0.060
Shortwave radiation	0.233	0.246
Initial surface density	-0.019	-0.011
Initial firn-ice transition depth	0.020	0.047
Initial surface temperature	0.009	0.033
Bottom boundary condition	-0.004	0.031

Table 5.4: Values of the sensitivity parameter given to three decimal places.

Given the size of the catchment area of the lakes it is not surprising that the melt multiple value seems to be by far the most important parameter, demonstrating that topography is not only important in determining where lakes form, but is a key factor in determining the depth of the lakes that form too.

From the values of the sensitivity parameter it is clear that air temperature and shortwave radiation are also key parameters in determining lake depth, as is the snowfall and its density. The sensitivity of the lake depths to further increases in air temperature and snowfall are investigated further in Chapter 6.

These results suggest that although foehn winds are key in lake formation (as is shown in Chapter 4), it seems from this study that the lake depths are more sensitive to the foehn wind temperature than the foehn wind speed. However, the lakes are less sensitive to foehn wind temperature than the overall air temperature suggesting that although foehn events are important in lake formation, an increase in air temperature would have a greater influence in lake depth.

The initial conditions do not seem to have a large influence on the lakes beyond the first year, suggesting that once a lake has formed it alters the temperature and density

profile of the ice shelf enough that conditions before this become insignificant in comparison to several other parameters, and that the spin up period used here is adequate.

Chapter 6

Discussion

Models such as the one presented here can be used to provide insights into both the current and possible future states of an ice shelf. The sensitivity studies described in Chapter 5 illustrated some interesting non-linear behaviour that warranted investigation in more detail. Here we present further analysis of some aspects of the Larsen C Ice Shelf that are pertinent to lake formation and the effect of lakes on the ice shelf, as well as examining some possible responses of the lakes to changing climate conditions.

6.1 The effect of lakes on the surface energy balance of an ice shelf

As melt lakes have a lower albedo than snow they will alter the surface energy balance of the ice shelf such that more melting takes place. The importance of this can be examined by running the model with all meltwater removed from the lake area once an ice lens has formed and comparing this with the base case simulation. This can be achieved by setting the melt multiplier value to zero, which has the consequence that all meltwater produced subsequent to ice lens formation is treated as if it percolates straight out of the model domain.

Carrying out this simulation we can see that it is indeed the case that a lake being present leads to more melting in the lake basin. The total lake basin melting for this zero melt multiplier simulation is 0.76 m of water equivalent firn melt over the final five years of a ten year simulation; this is 69.7% less melt than the base case simulation shown in Chapter 4, where 2.50 m of water equivalent melt occurs in the final five years.

This decrease in melting also means that the density profile for the zero melt multiplier case is different to that of the base case. Figure 6.1 compares the change in density after a five year spin up period for the base case and for the zero melt multiplier simulation, where it can be seen that the saturation of the firn and refreezing of the lake impact the density significantly in the base case in comparison to the zero melt multiplier case.

As the simulations continue the zero melt multiplier simulation continues to densify but no lakes are formed.

This density change has implications for future ice shelf stability. The loss of pore space has been suggested as a precursor for ice shelf collapse by Kuipers Munneke *et al.* (2014) and the more widespread the sinks of meltwater are on the ice shelf the more pore space will be lost.

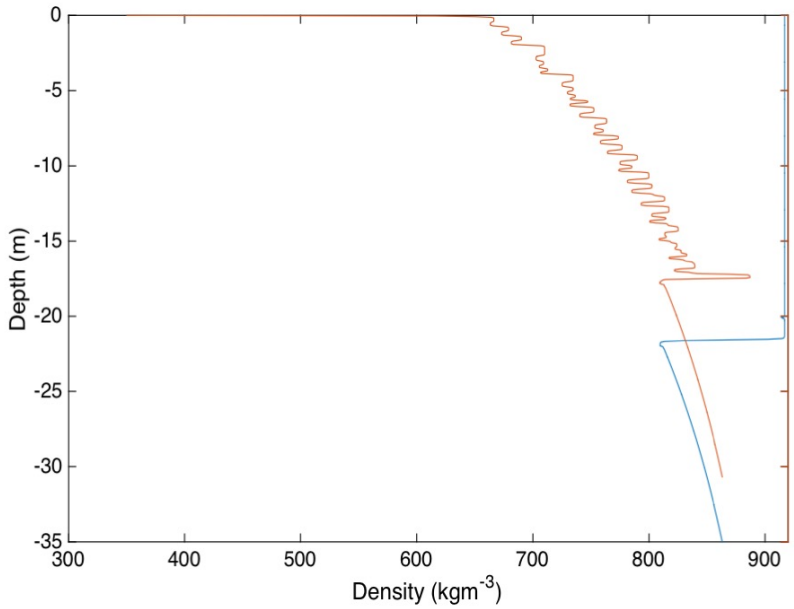

Figure 6.1: The density changes at the end of the spin up period (so after 5 years) for the base case (blue) and the case where all meltwater subsequent to ice lens formation leaves the model domain upon formation (red). Both profiles are shown to scale, hence the red line being shorter as the profile is less deep due to growth from the addition of meltwater from the catchment area not having occurred as it does in the base case.

6.2 The contribution of topography to melt lake formation

In order for water to travel from a catchment area into a lake we have made the assumption that there is a topographical gradient on the ice shelf and that this gradient is maintained from year to year. Here we examine the implications of that assumption and suggest further improvements to the model that could be made.

In reality, if meltwater is constantly pooling in the lake area then the gradient downwards from the catchment area to the lake is unlikely to be maintained in the long term, even given the greater melt and densification in the lake area due to the albedo change

caused by the lake. We can see in the simulations presented in this thesis that the ice shelf surface height increases with time in the lake basin (see Figure 4.10), whereas the catchment area of the lake will be losing some height. This would suggest that the overall surface area of the catchment will decrease with time as the catchment area decreases in height and the lake expands outwards.

This suggests that the model results here may be overestimating the lake depth if the extra melt in this expanded lake area (which will be due to the albedo change of any area that the lake reaches) would not outweigh the reduced contribution from the decreased catchment area and the larger lake area that the melt from the catchment area must be spread over.

However, even using the conservative topographical gradient used here (0.05) if we look at the final five years of the base case simulation the total difference in the height change between the lake basin and the catchment area is 6.28 m, which equates to a maximum of 125.58 m of catchment area lost in each direction around the lake basin. This would give a minimum value of the melt multiple by the end of the five years of 3.62 for this new catchment area and lake basin which, as shown in Section 5.2, would reduce the overall lake depth but would still not prevent lakes from forming.

Furthermore, in years where lakes do not form there will be less accumulation of water in the lake basement and loss of water in the catchment area. Therefore the final difference between the lake basin and catchment area would be much less if lakes only formed in some years, suggesting that the results here may exaggerate this difference in height as the AWS data used was intentionally from a year of high melt.

Although this is clearly an area that the model could be improved in, possibly by having a melt multiplier value that evolves with time, even from looking at the most extreme scenario as discussed above it does not seem that having a constant melt multiplier is causing lakes to develop erroneously. In reality if the topography of a lake basin becomes too elevated it is likely that meltwater will accumulate in new lows; the possibility of modelling this is discussed further in Chapter 7.

6.3 Liquid water remaining on the ice shelf between melt seasons

During the initial running of the model for an increased melt multiple (see Section 5.2) it was found that due to the model condition that was initially set that once a refrozen lid had formed melting would not occur again until the lake had completely refrozen, the model was being forced to stay in the refreezing state for too long and this was impacting on the subsequent year's melting time available. Therefore the decision was made to allow liquid water to remain in the firn between melt seasons and that the reset algorithm could also be run based on a number of consecutive melt days occurring once the lid has formed even if the lake had not fully refrozen at this stage.

The decision to follow this approach was due to the need to avoid having multiple lake, firn and lid layers within the model as this level of complexity would add significantly to the running time of the model. Furthermore, this is not something that has been observed on the Larsen C Ice Shelf, although it is something that would be worthy of consideration for inclusion within the model in future work if the effect of much warmer conditions or higher melt accumulation were being considered.

Figure 6.2 shows the presence of layers of high liquid content within the firn outside of the melt season for 250 days during the simulation with a melt multiple value of 9. Here there are two clear bands of high water content within the firn that remain from lakes that have formed in the previous two years. It can be seen that with time these slowly refreeze as they decrease in width but this is a slow process as they are deep enough within the firn that the colder temperatures at the surface do not affect them quickly. It is for similar reasoning that some meltwater also remains below these two bands; this is from the initial saturation of the firn and although it is much reduced it has not completely refrozen.

As the case where melt lakes not completely freezing over in one year occurred most consistently with the increased melt multiplication value this was examined in more detail. Initially, as the sensitivity study of a melt multiplier of 9 was found to cause water to remain on the ice shelf between melt seasons we also examined cases of a melt multiplier of 7 and 8 (the base case value is 6). It was found that even with an increased melt multiplier of 7, meltwater was being retained between melt seasons after a few years.

If we calculate the maximum depth that the refrozen lid has reached at the point that

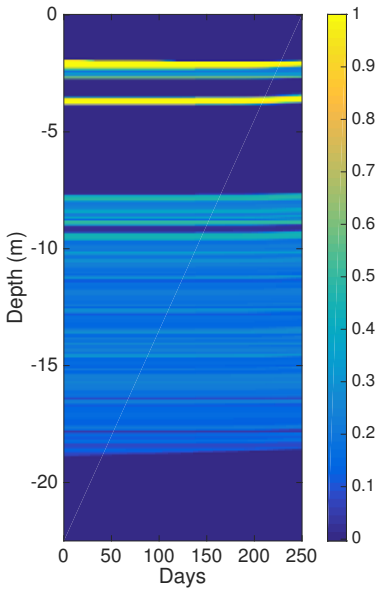

Figure 6.2: The evolution of the water content profile for 250 days, starting from February of the sixth year of the simulation. This period was chosen to allow for a five year spin up period and 250 days was found to be a sufficiently long time period to show the evolution of the water content outside of times when surface melt is occurring, without any melt days occurring. The colour scale shows the proportion of each grid cell that contains water.

melt begins again on the lid surface then this gives us an approximation of the maximum lake depth that can refreeze before a new lake begins to develop. This calculation was made for the first year that a lake does not refreeze completely for the cases of melt multiplier values of 7, 8 and 9. This was found to be fairly consistent between the three simulations: there were values of 1.43, 1.45 and 1.45 m respectively for the lake depth.

Comparing these values of maximum lake depth that could refreeze with the volume of meltwater that is transported in from the catchment area we can calculate the maximum melt multiple value that would allow a lake to completely refreeze within one melt season. We can do this by separating the in-situ melting from the overall lake depth which allows us to calculate the amount of meltwater travelling in from the catchment area that contributes to the lake depth. This gives us a maximum value of 6.33 for a melt multiple value that will keep the lake at a depth where it will refreeze completely between melt seasons. It is likely that the actual value will be slightly higher than this as this does not take into account the earlier onset time of the lake due to the firn being able to saturate more quickly with higher melt multiplier values. However, it does give a good indication that to create lakes deep enough that they will not completely refreeze between melt seasons would not require a much larger catchment area or topographical

gradient than we are currently modelling.

These calculations suggest that the treatment of liquid water persisting between melt seasons may become increasingly important should average temperatures continue to rise; Church *et al.* (2013) suggest that future temperature rises on the Antarctic Peninsula will lead to an increase in surface melting. This is examined further in Section 6.5.

Furthermore, should the model be used for locations outside of Antarctica it may be important to consider in more detail the case of lakes not refreezing between melt seasons. For example, meltwater has been observed to persist in firn between melt seasons in Greenland (Forster *et al.*, 2014).

6.4 The response of lake formation to increases in snowfall

Due to there being several possible ways that increased snowfall could affect melt lake depth, the model was run with larger increases in snowfall than those investigated in the sensitivity study in Chapter 5 in order to determine if the relationship between snowfall and lake depth continues.

Initially increases of 5 and 10 times the base case value of accumulation were tested. It was found for the 5 times case the pattern found in Section 5.3 continues: both the average and maximum lake depths are increased compared to the smaller accumulation values. This can be seen in Figure 6.3.

However, when examining the 10 times case it appears that this upwards trend in average lake depths does not continue; although lakes form they are far smaller with an average depth of 0.17 m. In order to examine this change more clearly an additional simulation of 8 times the base case accumulation was also run. The results of this are plotted in Figure 6.4.

We can see from Figure 6.4 that the lakes in the 8 times accumulation case are also shallow similarly to the 10 times accumulation case for the first two years, but then they become deeper in the final three years of the simulation. In fact, if we look at the 5 times accumulation case we can see that this period of initially shallow but then deeper lakes also occurs at the start of this simulation, but as this occurs during the spin up period it is not noticeable in the analysis shown in Figure 6.3. Figure 6.5 shows this occurring in the first five years of the five times snow simulation.

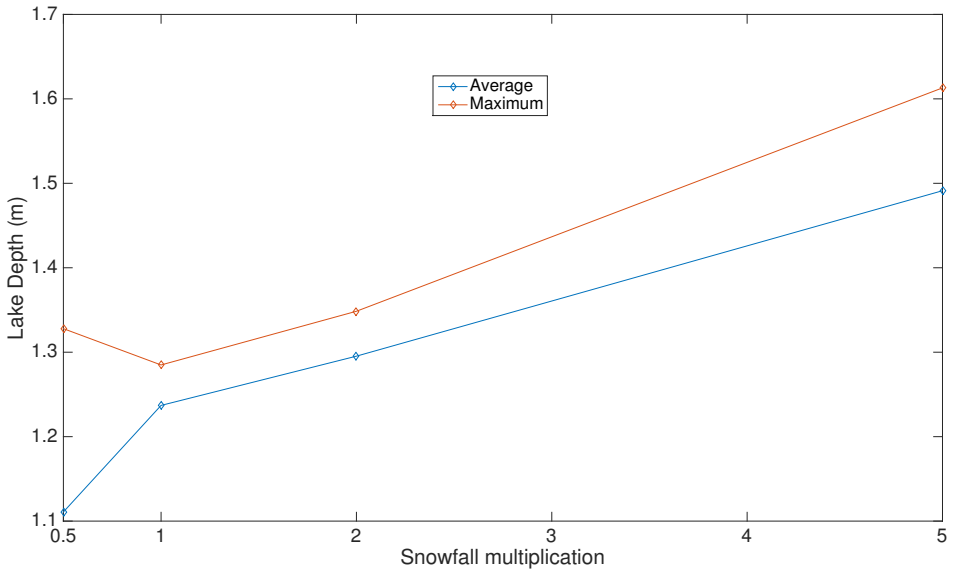

Figure 6.3: The maximum and average lake depth for accumulation values of 0.5, 1, 2 and 5 times the base case level.

If we look at the density and water content of the 10 times accumulation case it becomes clear why the lakes do not reach the depth that they do in the other cases; the accumulation level is high enough that each year's lake does not melt through the new snow. This means that each year the density profile near the surface loses memory of the previous year's lake and a completely new layer of low density snow needs to be densified and saturated and a new ice lens formed for a lake to develop. This can be seen from the lake depths shown in Figure 6.6.

The lakes in the 8 times accumulation case occur after several years of steady densification of the firn profile. However, they are still shallower than those of the cases with lower accumulation levels. This is partly due to there being a greater amount of snow to saturate each year. This can be seen in the later onset time of the lake with increasing snowfall as shown in Figure 6.7.

However, there is also a possibility that the thermal conductivity of the ice of previous years' lakes can be playing a role in the cause of the deeper lakes in the lower accumulation cases. This is because for the lower accumulation cases the solid ice of the previous year's refrozen lake will be exposed as the snow above it melts much more quickly than cases with higher accumulation (if it is exposed at all) meaning that the ice with a higher thermal conductivity is given longer exposure to the warmer temperatures at the surface

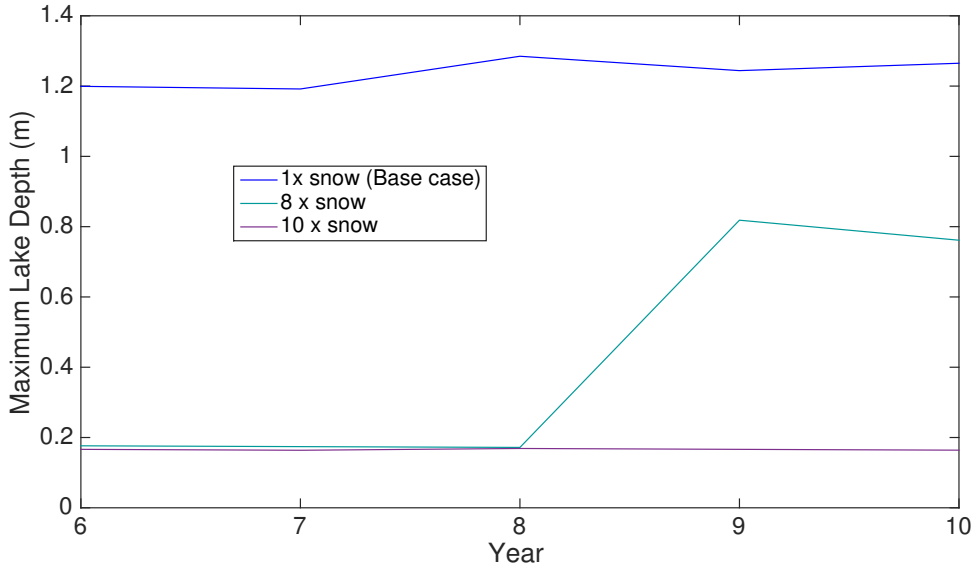

Figure 6.4: The maximum lake depth each year for the 8 and 10 times accumulation values, as well as the base case.

than in the other cases, allowing the upper part of the ice shelf to heat up more quickly. This was confirmed by running the model as a slab of solid ice with constant positive forcing with two different values of thermal conductivity; in this case the higher thermal conductivity case had the greater value of melting. Therefore it can be concluded that the time of exposure of dense ice could also play a role in lake depth.

It is expected that under a future warming climate snowfall will increase over the Antarctic Peninsula (Krinner *et al.*, 2007). However, the rate of increase is far less than those values tested here so for the case of Larsen C it is more likely that changes in lake depth would follow those determined during initial sensitivity testing. However, it is useful to know how the model would respond to greater levels of snowfall should it be used for other regions.

6.5 The response of lake formation to increases in air temperature

The sensitivity studies in Chapter 5 examined the effect of increasing and decreasing the air temperature by 0.5 K. However, it is possible that under some future climate scenarios the air temperature may increase further than this, so here we examine the case where the air temperature is increased by greater amounts.

It would be expected from the sensitivity study results that a further increase in tem-

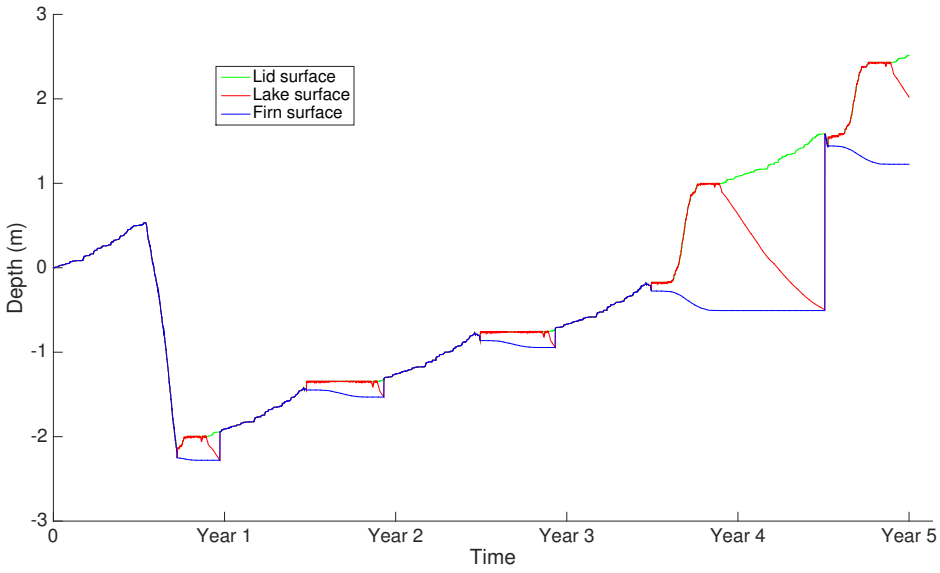

Figure 6.5: The evolution of lakes in the 5 times snow simulation. Here it can be seen that deeper lakes do not form until the fourth year of the simulation.

perature would lead to an increase in lake depths. However, this was not found to be the case when the temperature was increased by 1 K. Although the lakes in the +1 K simulation were deeper than the base case simulation, they were shallower than the +0.5 K simulation. The average and maximum lake depths are shown in Table 6.1.

Temperature	Base Case	+0.5 K	+1 K
Maximum Lake Depth (m)	1.2849	1.3890	1.3131
Average Lake Depth (m)	1.2370	1.3415	1.2552

Table 6.1: The maximum and average lake depths for the final five years of simulations for the base case, and the cases of increased air temperatures on 0.5 and 1 K.

We can begin to explain this result if we look at the times that lakes are exposed for in these simulations. For the +0.5 K simulation the lakes are exposed (so no ice lid is present) for an average of 83.6 days a year whereas in the +1 K simulation they are exposed for 85.7. Yet the lakes are not as deep in the 1 K simulation. This appears to be because the raised air temperatures are enough to prevent a permanent ice lid forming for an extended period when compared to the +0.5 K simulation but not enough that the lake is warming to cause further basal melting. This then leads to a situation where, as a lid is not forming as early, less snowfall is able to accumulate on the lid when it does form. Then, as demonstrated in Section 6.4, the reduced snowfall will limit the depth

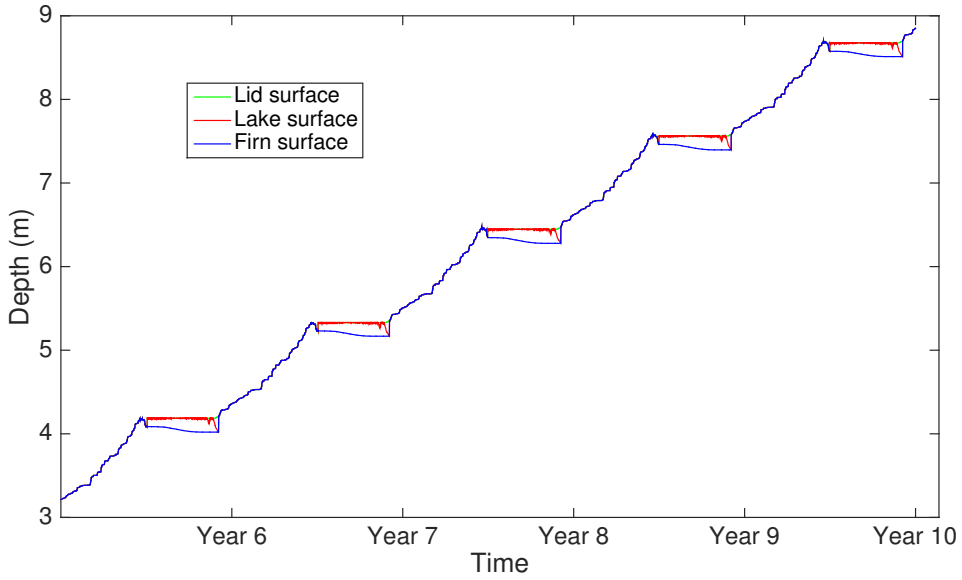

Figure 6.6: The evolution of lakes in the 10 times snowfall simulation. It is clear here that each year's lake is not melting through the new snow from that year so each year the density profile near the surface loses memory of the previous year's lake.

of lakes that can form and this will go some way to counteract the increased melting that would occur as a result of the increased air temperature and its effect on the surface energy balance.

This effect continues to be observed with temperatures increased to 1.5 and 2 K higher than the base case simulation. Although more melting occurs with the increased temperatures and the lakes become deeper than in the +1 K simulation, the lakes do not become as deep as those in the +0.5 K simulation; once spun up the average lake depths are 1.28 and 1.29 m in the +1.5 and +2 K cases respectively.

However, increased snowfall would be predicted with increased temperatures so it may well be that a combination of these factors would actually lead to deeper lakes. Increasing the air temperature alone is not an accurate prediction of a future climate although testing this parameter alone still provides an interesting insight into one of the possible factors that may come into play in the response of ice shelves to changing climate.

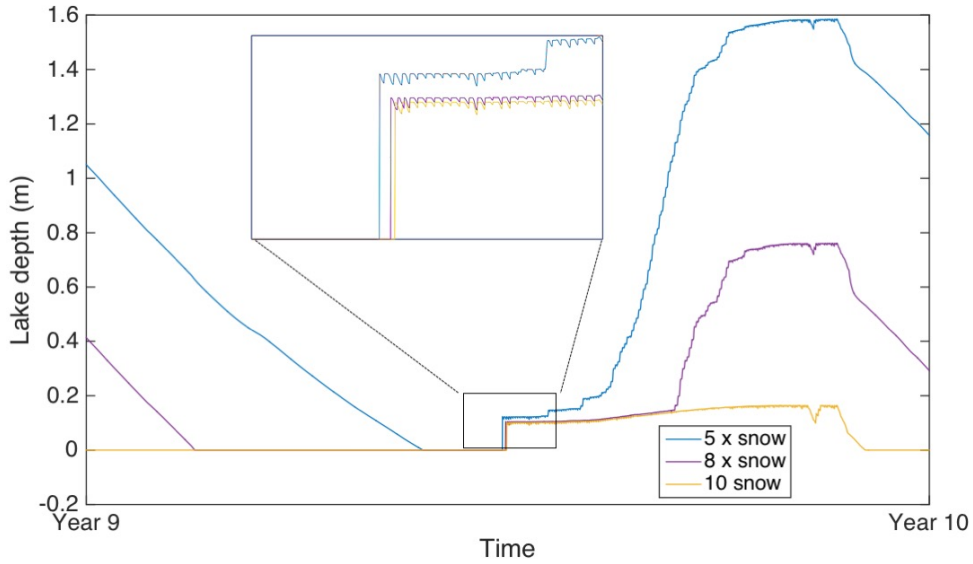

Figure 6.7: The evolution of lake depth of the final year of each of the simulations for 5, 8, and 10 times the base case level of accumulation. The zoomed in area shows that the time of onset is different for each case.

6.6 The contribution of meltwater to crevasse propagation through an ice shelf

Crevasse propagation caused by meltwater infiltration has been suggested as a possible mechanism for ice shelf disintegration (Scambos *et al.*, 2000). The pressure of the water in the crevasses can cause them to expand both laterally and vertically and this may cause them to propagate through the ice shelf.

Scambos *et al.* (2000) state that crevasses that are more than 90% filled with water will tend to propagate through the ice shelf, whereas those that have a lower water content than this will tend to close. For this to occur the crevasses need to be of a critical initial depth, which depends on the surface density (the higher the density the larger the critical depth). The deeper the crevasse the greater the water pressure; the critical depth is defined as the depth at which the hydrostatic pressure of the water exceeds the glaciostatic pressure and full penetration of the ice shelf will occur. Scambos *et al.* (2000) found that this critical depth varied between 10-30 m although for surface densities similar to those found in the modelling efforts here crevasses can initially be as small as 6-10 m.

Using the results of Scambos *et al.* (2000) it is possible to use the modelled values of

meltwater availability on the Larsen C Ice Shelf calculated in this study to infer whether or not this ice shelf may be at risk of crevasses propagating through the ice shelf either now or in the future.

Here we follow the crevasse sizes used by Sergienko and MacAyeal (2005) of 30 m wide and 20 m deep crevasse. In order to be 90% filled with water these crevasses must therefore be filled to within 2 m of the surface. Basic geometrical calculations allow us to determine that the cross-sectional area of this crevasse that needs to be filled with meltwater would be 243 m^2 should the crevasse be triangular. However, should the crevasse be more rectangular with a triangular tip then the area would be much larger, 540 m^2 if we assume that the triangular tip is very small relative to the overall crevasse depth. These two cases are shown in in Figure 6.8. In reality the crevasse shape would be likely be somewhere between these two extremes.

If we assume that a lake such as that modelled in Chapter 4 forms in the location of a pre-existing crevasse we can use the volumes of water that are output by the model run described in Chapter 4 in order to estimate if the lake modelled could contain enough water to cause propagation of that existing crevasse.

If we assume that the crevasse is aligned with the lake along the direction of the lake's length (i.e. the crevasse runs 3150 m along the lake shown in in Figure 4.8) then there will not be enough water to cause this crevasse to propagate through the ice shelf for either the average or maximum lake depth found in the base case run for the case of a rectangular crevasse, but there will be for the triangular crevasse geometry.

However, were the crevasse to run along the lake's width (so running for 390 m) there is ample water available in the lake to cause the crevasse to fill to more than 90% of its depth for either geometry.

For the lake depths and catchment area calculated the minimum width of a lake with a crevasse running down its length is 189 m for the triangular crevasse geometry and the maximum lake depth (196 m for the average lake depth) and 420 m for the rectangular crevasse geometry and maximum lake depth (437 m for the average lake depth). Therefore some of the long, thin lakes observed on Larsen C may be candidates for causing crevasse propagation but many will not be wide enough.

However, this is only a very rough estimate. The existence of a crevasse is likely to change the amount of meltwater produced, both due to the radiative effects of a

crevasse and the albedo change due to lake formation being altered by water pooling in the crevasse. Crevasses can substantially alter the amount of heat absorbed by the ice shelf as radiation is able to be absorbed at depth (rather than having to be transferred from the surface by conduction) and the surface is exposed to different angles of incidence of the radiation (Pfeffer and Bretherton, 1987).

Crevasses have been observed perpendicular to the ice flow (e.g. (Jansen *et al.*, 2015)) whereas lakes are often parallel to the flow, an orientation which may be favourable for crevasse propagation based on the calculations above.

One future adaptation of the model that could be implemented would be to follow work such as that of Sergienko and MacAyeal (2005) and have an effective albedo that is based on a formula calculated by Pfeffer and Bretherton (1987) and takes into account factors such as the solar zenith angle.

Here just a single crevasse and lake has been considered; for the ice shelf to be at risk there needs to be a significant amount of crevasse propagation. For example, Sergienko and MacAyeal (2005) based their calculations of crevasses filling on the Larsen B Ice Shelf on a 5% crevasse density, all of which were assumed to fill with meltwater. Currently, as lakes have only been observed on Larsen C close to its grounding line it seems unlikely that this ice shelf would be a candidate for collapse due to crevasse propagation by meltwater infiltration occurring over a large area of its surface.

It is assumed by Scambos *et al.* (2000) that this penetration will happen within one melt season as meltwater remaining on the ice shelf over the winter will refreeze. For this to happen the crevasse penetration needs to be sufficiently fast that the overburden pressue of the ice will not be able to act to close it in time. However, as noted in Section 1.3, crevasse propagation can still lead to a weakening of the ice shelf through the warming (and softening) of the ice deep within the ice shelf and the infiltration of sea water into the base of the ice shelf (Scambos *et al.*, 2003).

6.7 Using reanalysis data to look at the recent melt seasons on the Larsen C Ice Shelf

In order to examine more recent melt seasons on Larsen C the model was run using reanalysis data. As stated in Section 4.2.1, reanalysis data was thought to be less suitable

than AWS data and even the AWS data needed to be altered to incorporate the foehn wind effect. However, we include this work here to demonstrate that reanalysis data can be used to force the model and can still provide some information about melt events.

Both ECMWF ERA-Interim data and NCEP reanalysis data were available for use. However, given the much finer resolution of the ERA-Interim data this was chosen as it enabled a grid point to be chosen that was directly in an area of Larsen C where lakes have been observed so is more likely to capture the foehn wind effect and have realistic conditions for lake formation.

The model was run from the beginning of 2011 to the end of 2015, running over this data twice to allow for a five year spin up period following that used for the sensitivity studies. Although this is not a time where lakes have been observed in MODIS imagery (see Figure 4.2), it is interesting to see the evolution of the firn profile during this time and to investigate if the model suggests melting did occur and if so the effect that it had on the firn.

Figure 6.9 shows that in fact the model suggests that very shallow lakes formed during this period. However, this may not be incorrect; not only are the lakes shallow enough that they may well not show up in MODIS imagery, they are also covered by a frozen lid for a large proportion of their existence (see Figure 6.10) which would also prevent them from being visible.

Figure 6.11 shows the evolution of the firn density profile over the final five years. If we look to the left of the figure we can see layers of higher density near the surface, that have remained from melt that occurred during the spin up period but did not lead to lake formation. Further down in the firn we can see a large yellow band of high density firn; this was caused by the high melt rate in the 2011-12 melt season in the first year of the model run and we can see that as the model loops over this data again the firn becomes fully saturated and a large layer of high density firn occurs again near the surface. This demonstrates that only one year of high melt is needed to saturate the firn and that this can lead to lake formation in several subsequent years as long as the melt rate can melt though any new snowfall.

This large feature of dense ice is especially significant as it was observed within the firn in Cabinet Inlet by Hubbard *et al.* (2016) using an optical televiewer. This feature has

also been observed using ground penetrating radar, as shown in Figure 6.12.[5]

[5]Thank you to Adam Booth of the University of Leeds for providing this figure and analysis.

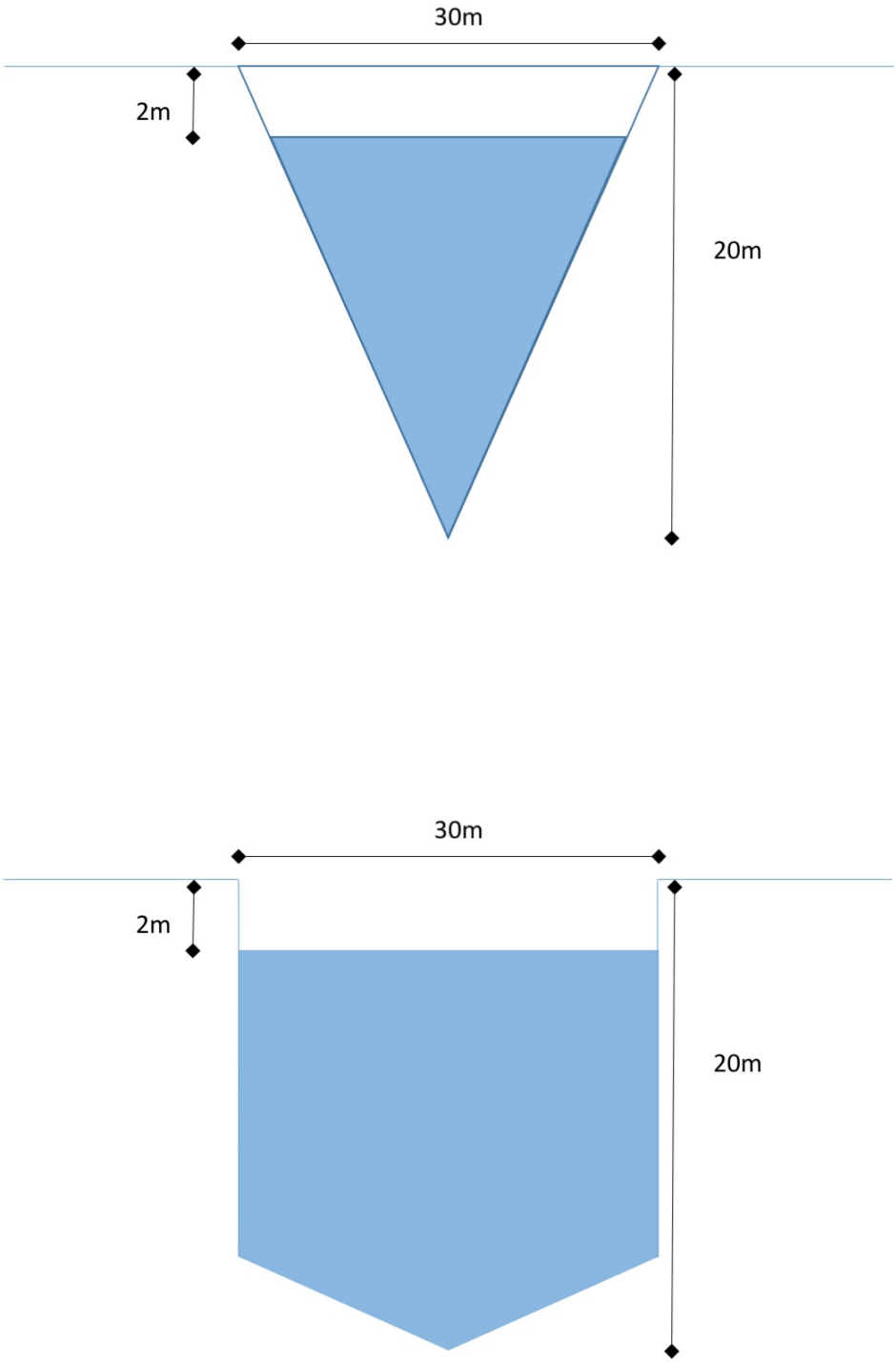

Figure 6.8: Two idealised crevasses in an ice shelf, 90% filled with meltwater. The upper is a purely triangular crevasse, the lower is a rectangular crevasse with a triangular tip.

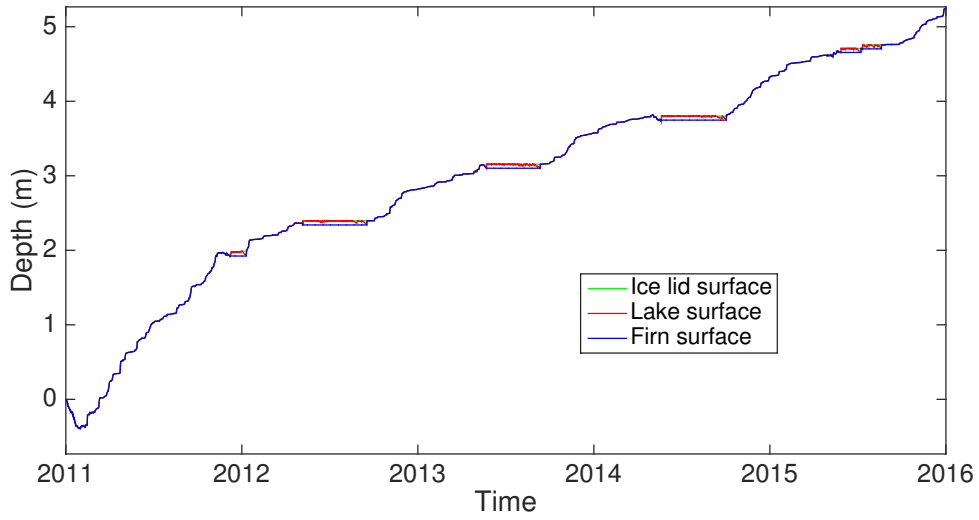

Figure 6.9: The evolution of very shallow lakes that occur during the final five years of a simulation using ERA-Interim data. The lakes are so shallow that the refrozen lid is hard to distiguish here, although they do refreeze completely each year. The lid can clearly be distiguished in Figure 6.10.

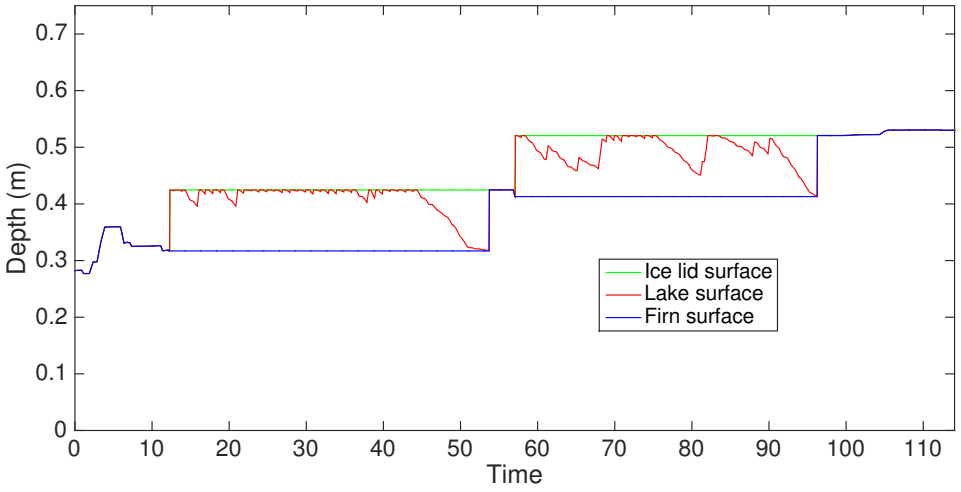

Figure 6.10: A zoomed in version of the final lake shown in Figure 6.9. Here a timescale of days and a depth scale of meters are given to show size. We can see here that the lake surface is barely exposed and at one point freezes over completely before reforming again.

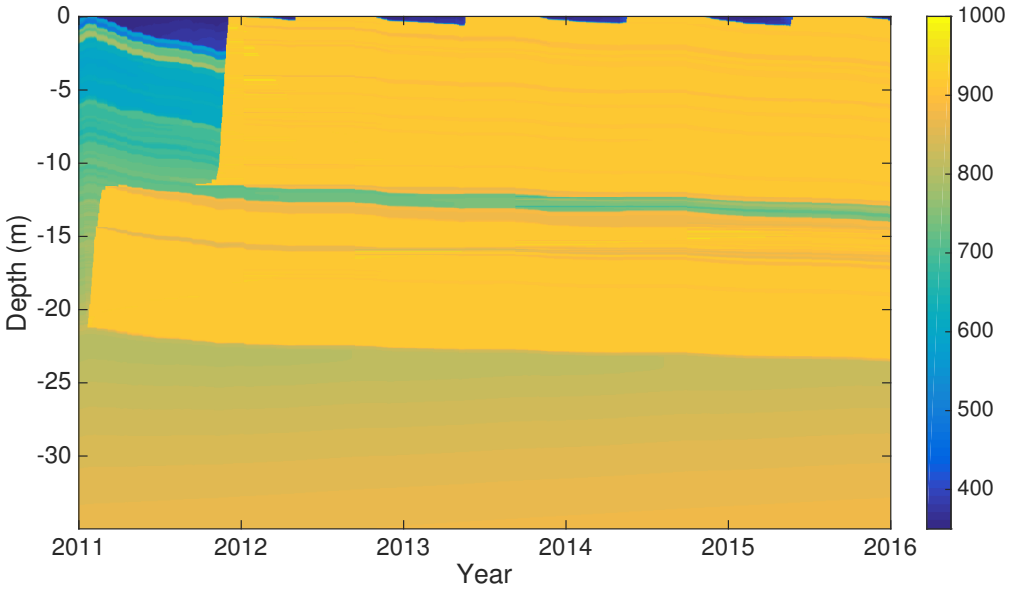

Figure 6.11: The evolution of the firn density profile over the final five years of a simulation using ERA-Interim data. The colour bar shows density. Here the layer of high density that is concurrent with observations is visible near the surface as the large yellow band.

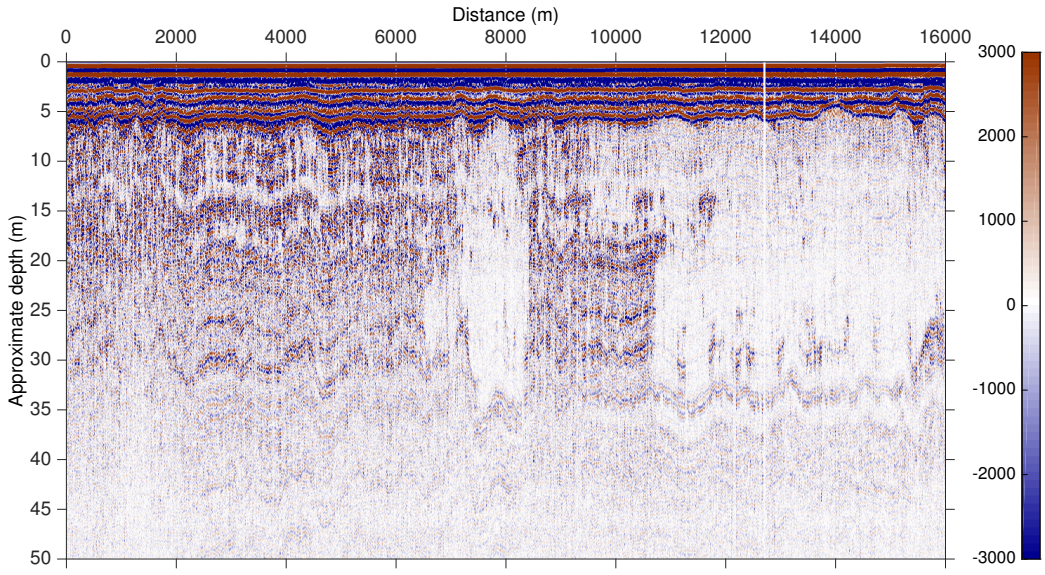

Figure 6.12: The firn structure of Cabinet Inlet, Larsen C imaged using ground penetrating radar. The colour bar gives the amplitude; this is the strength of the radar reflection which is proportional to the density contrast across a given layer. Therefore the transparent section of the image is the area of more homogenised densities where the layer of solid ice is present.

Chapter 7

Conclusion

The appearance of surface melt lakes on an ice shelf can drastically alter the ice shelf, both through altering the surface energy balance due to the change in albedo caused by the lake and through the possibility of the lakes affecting the stability of the ice shelf through mechanisms such as crevasse propagation.

Here we have presented a one-dimensional model for surface melt on an ice shelf. The model calculates the transfer of heat through the upper ice shelf using a heat equation and also incorporates the percolation and refreezing of meltwater through the firn. The effects of foehn winds and also transport of water from a catchment area surrounding a lake basin are considered. The formation and development of a surface melt lake are modelled, as well as the refreezing of this lake.

It was found that the formation of solid ice lenses within the firn due to the refreezing of meltwater enabled the formation of melt lakes, and then these lakes once refrozen acted as ice lenses in subsequent years and enabled the formation of exposed lakes more rapidly. Both the foehn wind effect and lateral transport of meltwater from a catchment area surrounding the lake were found to be essential for lakes to form on Larsen C under current conditions.

The formation of ice lenses was found to be consistent with observations made on the Larsen C Ice Shelf. Furthermore, the depth of lakes simulated by the model agree well lake depths calculated from Landsat data. The model is also able to reproduce the large layer of high density firn found by Hubbard *et al.* (2016) on the Larsen C Ice Shelf when run with reanalysis data.

Sensitivity studies show that the value chosen for the effective catchment area plays a key role in determining lake depth. In addition to this, air temperature and shortwave radiation are also key parameters in influencing lake depth.

Possible future conditions on the Larsen C Ice Shelf were modelled by increasing the snowfall and the air temperature independently. It was found that increasing the snow-

fall led to deeper lakes but only up to a certain amount. If the snowfall was increased too much then it prevented saturation of the firn and delayed lake exposure, preventing the formation of deep lakes.

Increasing the air temperature also increased lake depths but again only up to a limit. Increasing the air temperature by 0.5 K led to deeper lakes than the base case simulation but increases above this prevent the lakes from refreezing, making lakes in subsequent years smaller as there is less snowfall on top of the frozen lake to melt, which limits the depth of these subsequent lakes.

The depth of the lakes modelled even for current conditions on the Larsen C Ice Shelf may be sufficient for crevasse propagation but this is dependent on lake size and crevasse orientation.

7.1 Future work

There are several possible ways in which the model could be improved to make increasingly accurate simulations of lake formation. As lateral transport of meltwater is key to lake formation but is also one of the biggest uncertainties in this work this is a pertinant area for future work. One area for potential model development would be to track the progress of meltwater through the firn. Currently it is assumed that all meltwater will percolate as far through the firn as it can before it has refrozen, reached an impermeable layer or is retained due to capillary forcing, following Ligtenberg *et al.* (2011). However, as stated in Section 2.1.3.1 the time taken for water to percolate through the whole 35 m of the model domain used here is longer than one timestep. Although the water would not percolate quite this deep into the firn it would take longer than one timestep for meltwater to reach the level at which it has been shown to be forming ice lenses in these calculations, yet here the changes in temperature and density due to this meltwater refreezing happen within one timestep. It is thought that it would be very unlikely for this to materially affect results as the temperature changes that would happen within the surface layers of the firn would not affect the lower layers of the firn over these timescales. However, to be certain of this and to ensure a greater level of physical accuracy the model could be improved by slowing down this percolation to a more realistic speed.

When considering meltwater transport from the catchment area we have not con-

sidered that meltwater will likely take preferential channels through the firn and so may actually be able to contribute to lens formation within the lake basin. This may also mean that meltwater can move faster into the lake, or from further away than the catchment area considered here. Although this would be impossible to model directly using a two column one-dimensional model it would at least be possible to investigate this further by varying the timing at which water from the catchment area starts to be transported into the lake basin.

Alternatively the routing of meltwater could be examined using an approach such as that of Banwell *et al.* (2012b) as discussed in Chapter 1 where a DEM and surface routing algorithm could be used to determine more accurately the catchment area for individual lakes.

A further improvement would be to include a two stream radiation model such as that used in Taylor and Feltham (2004). This would then allow the model to account for radiation reflected back from the lake-firn boundary, which is currently not accounted for. Furthermore, it would be a useful exercise to compare what happens if we do not assume that radiation is absorbed only at the surface of the firn before a lake is present, for example by following an approach such as that taken by Sergienko and MacAyeal (2005). In this thesis we made the assumption that the firn surface is highly scattering and, as Sergienko and MacAyeal (2005) note, 'usually melting occurs first at about 5 cm below the surface' and so melt would likely occur in our top grid cell anyway. However, this may not always be the case; Kuipers Munneke *et al.* (2012a) state that radiation penetration would change the amount of melt, and we may need to account for melt below the top 5 cm.

In this thesis we have excluded any snowfall that would fall into an exposed lake. However, this snow would act as heat energy sink as latent heat would be needed to melt it once it is in the lake and this process may therefore speed up the refreezing of melt lakes, but also deepen them which would counteract this somewhat as a deeper lake will take longer to refreeze.

A development that would be useful for certain locations would be to consider a catchment area with an albedo other than that of snow. In the case of Larsen C, lakes form near the Peninsula mountains, and both dust and exposed rocks have been observed (Ed King, personal communication, 2015). This will significantly change the albedo of the

catchment area as a whole and may lead to greater amounts of melting. This could also be the case for other ice shelves, for example the McMurdo where there is a lot of debris on the surface (Doug MacAyeal, personal communication, 2016).

Among the most challenging processes that are of most interest in dealing with the albedo change to debris cover is the 'cleaning' of debris from ice surfaces that have standing and running water, and transport of debris into more localised areas. The possibility exists that debris-enhanced melting one year could lead to a cleaner surface in subsequent years, and this would limit the lifespan of a given lake under some circumstances.

A further assumption we have made that could be investigated is that ice lenses formed in the firn are totally impermeable to water. It has been observed in Greenland that ice lenses can in fact be slightly 'leaky' (Tad Pfeffer, personal communication, 2016). Although this is unlikely to be important in years where a refrozen lake is acting as an 'ice lens', it could be an important consideration for example in years where water can remain liquid between melt seasons on top of a smaller ice lens when modelling an ice shelf or sheet where water may remain perennially.

Finally, there is the consideration that the surface topography of ice shelves is affected by a combination of ice flow across grounding lines (for example, ice streams that flow into ice shelves) and local snow accumulation and ablation patterns that can be strongly influenced by atmospheric conditions. These features of an ice shelf determine the character and texture of its surface undulations as well as the patterns of surface crevasses and the presence of subglacial melt channels. Basal crevassing can also influence surface topography (McGrath *et al.*, 2012). These aspects of ice shelf morphogenesis need to be considered in the context of surface hydrological behaviour. Here we have assumed a constant topographical gradient from the catchment area into the melt lake, and in reality the situation is much more complex than this. If we wished to model lake features without prior knowledge of where they should form then at least some aspect of a two or even three dimensional approach would have to be taken.

The model developed here could be used to investigate further ice shelves, either to determine if lakes may develop on them under a future warming climate, or to provide insights into lakes that have already been observed. Several Antarctic ice shelves could be promising candidates for the latter: the Ross Ice Shelf has large lakes up to 80 kilometres long ((Kingslake *et al.*, 2017), the Amery Ice Shelf which presently retains meltwater ((Bell

et al., 2017)) or the George VI Ice Shelf where melt lakes have been present for several decades (Reynolds, 1981).

Although a model of this scale is of far too high a resolution to be applied to general circulation models, the information found can be used in parameterizations, for example to account for the change in surface energy balance as a result of the presence of the lakes.

Despite the limitations of our modelling approach there is still a great deal that can be learned from a one-dimensional model. The design of our model means that it can easily be adapted for other ice shelves or ice sheets and there are many areas in both Antarctica and Greenland where it would be beneficial to learn more about the surface processes that are occurring and the fate of meltwater that is produced on their surfaces and their

Appendix A

Model Summary

The model is summarised in Figure A.1. The steps that it takes are as follows:

1. The module setup takes place, requiring the functions 'ImportSnow' and 'ImportAWS'.
2. For each timestep, the surface boundary conditions are calculated using 'SfcBoundary'. The model then follows one of three paths, 'InitialSurfaceMelt' (no lake present, firn not completely saturated), 'LakeFormation' (no lake, firn fully saturated) or 'LakeDevelopment' (lake present, with or without a lid). For each of these paths, optional functions (connected with orange arrows) may be activated depending on the conditions.
3. Regardless of the path chosen the model will then run three or four functions at the end of each timestep. 'SnowDens', 'RefreezeInFirn' and 'Accumulation' are always run, and 'ResetCombine' is run only when the lake completely freezes over or a prescribed amount of melting occurs on the frozen lid surface.
4. For each timestep, points two and three are repeated.
5. The final output is delivered after the final timestep.

A brief description of the purpose of each function is included in Appendix B.

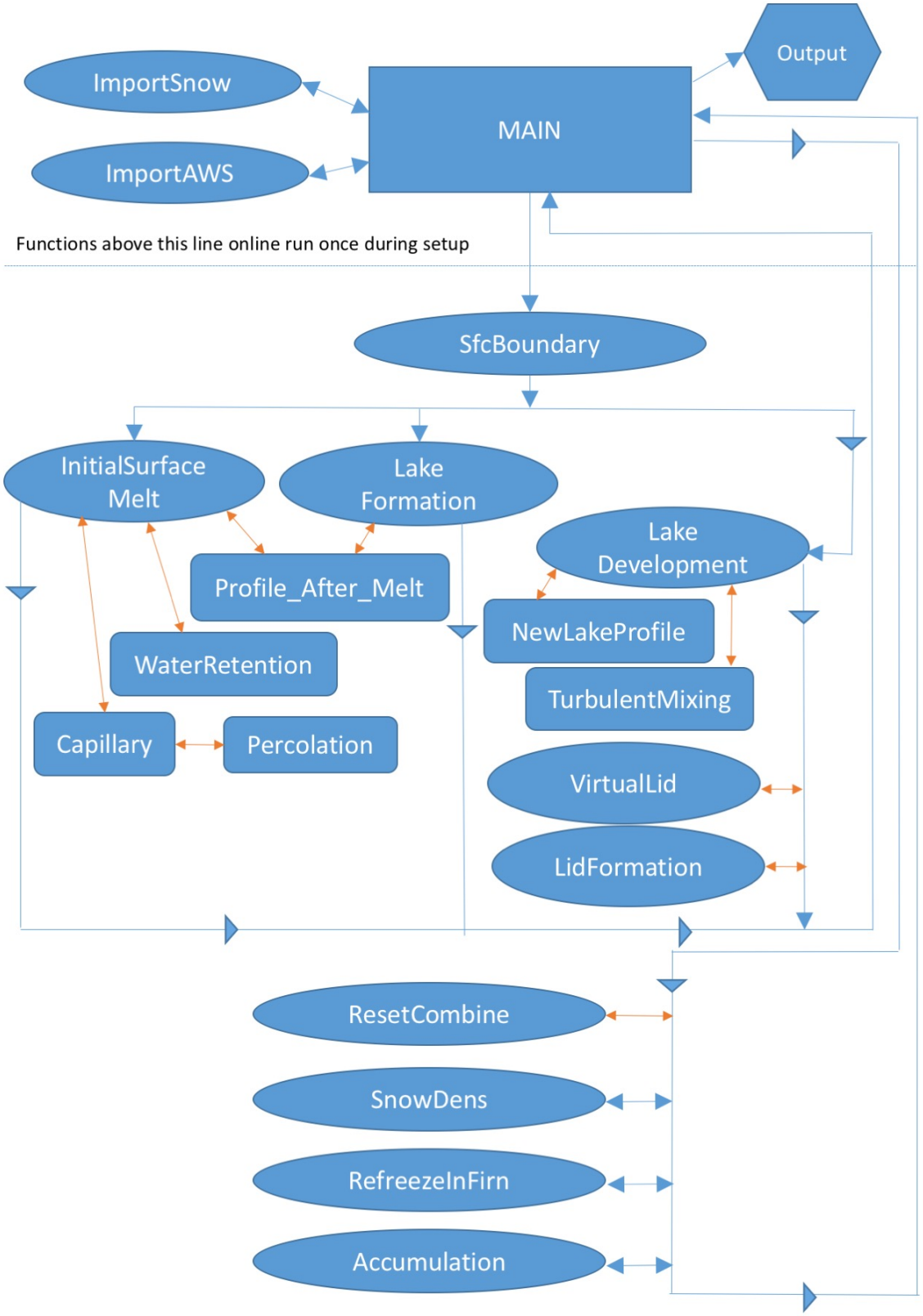

Figure A.1: The functions that comprise the melt lake model and their interactions are summarised above. The model is run from the main module. Orange arrows represent optional paths that are only taken should certain conditions be satisfied (e.g the presence of meltwater).

Appendix B

Model Code Description

Accumulation Adds fresh snow to the top of the firn profile.

Capillary Calculates the volume of water that will remain in each grid cell due to capillary forcing.

ImportAWS Imports the weather station data in a format suitable for the model to be forced with. Foehn winds are also added here.

ImportSnow Imports snowfall data which is used to determine when and how much snow is added to the firn profile.

InitialSurfaceMelt When a lake is not present this function determines if there is surface melt and calls the appropriate functions to determine the fate of this meltwater. This also calls the pde solver to calculate heat transfer through the firn.

LakeDevelopment Calculates the temperature profile of the lake and firn below it and determines the movement of the lake- firn boundary as the firn melts or the lake freezes.

LakeFormation Once the firn is fully saturated this function calculates the amount of surface melt that is taking place, until it is determined that a lake is present.

LidFormation Once a permanent frozen lid has formed on the lake this function calculates the expansion of this lid as the lake below it freezes.

Main The model is run from here.

NewLakeProfile Calculates the new lake temperature profile once it has melted some firn below it, before turbulent mixing occurs.

NewLakeProfile_Freeze Calculates the new lake temperature profile once some of its height has been lost due to the refreezing of the lid.

NewLakeProfile_LidMelt Calculates the new lake temperature profile once it has increased in depth due to melting of the lid from below.

Percolation Calculates the movement of meltwater down through the firn and subsequent refreezing and temperature changes.

Profile_After_Melt Calculates new density and water content profiles after melting has taken place at the surface.

RefreezeInFirn Checks for layers within the firn where the temperature has gone below the freezing temperature and freezes meltwater in this layer as well as calculating the new temperature and density of the layer a a result of this.

ResetCombine Once a lake has completely refrozen this combines the firn and frozen lake density, temperature and water content profiles to make one profile. The lake profile is also included in this if the function is called before the lake has completely refrozen due to a prescribed amount of melting occurring on the refrozen lid.

SfcBoundary Calculates surface fluxes from AWS data.

SnowDens Calculates dry snow densification.

TurbulentMixing This calculates the lake temperature profile once turbulent mixing has occurred.

VirtualLid Once the surface of the lake gets below freezing a 'virtual lid' of ice is formed and allowed to grow or shrink. If it reaches 10 cm in depth it is considered stable and therefore the model switches to a state of a permanent lid on top of the lake.

WaterRetention Once an ice lens has formed or meltwater reaches the pore closure depth further melting will accumulate on top of the ice and saturate the firn from the bottom upwards.

Glossary

Note: units here are written in the standard way (e.g. kgm^{-3} for density). For the case of the model where we are working in one dimension the units actually used in practice may differ, for example, kgm^{-1} for density, but for ease of understanding this has been replaced with the more commonly seen three dimensional form.

c constant (used in calculation of the initial density profile)

$\mathbf{c}_p$ specific heat capacity (J kg^{-1} K^{-1})

$\mathbf{c}_{p_{air}}$ specific heat capacity of air (J kg^{-1} K^{-1})

$\mathbf{c}_p^{total}$ specific heat capacity of a grid cell (J kg^{-1} K^{-1})

$\mathbf{c}_{p_{ice}}$ specific heat capacity of ice (J kg^{-1} K^{-1})

$\mathbf{c}_{p_{liq}}$ specific heat capacity of water (J kg^{-1} K^{-1})

d model sensitivity

f fractional freezing rate

g acceleration due to gravity (m s^{-2})

h height of melt lake (m)

$\mathbf{h}_l$ location of melt lake-firn interface

$\mathbf{h}_u$ location of melt lake-air interface

k thermal conductivity (W m^{-1} K^{-1})

$\mathbf{k}^{total}$ thermal conductivity of a grid cell (W m^{-1} K^{-1})

$\mathbf{k}_{air}$ thermal conductivity of air (W m^{-1} K^{-1})

$\mathbf{k}_{ice}$ thermal conductivity of ice (W m^{-1} K^{-1})

$\mathbf{k}_{liq}$ thermal conductivity of water (W m^{-1} K^{-1})

$\mathbf{q}_{air}$ humidity (g kg^{-1})

t time (s)

u vertical flow speed of meltwater through firn(m s^{-1})

$\mathbf{u}_l$ lateral flow speed of meltwater through firn(m s^{-1})

z height (m)

B parameter value for the sensitivity study

$\mathbf{C}_T$ bulk transfer coefficient

$\mathbf{F}_{LAT}$ latent heat flux (W m^{-2})

$\mathbf{F}_{LW}$ longwave flux (W m^{-2})

$\mathbf{F}_{SENS}$ sensible heat flux (W m^{-2})

$\mathbf{F}_{SW}$ shortwave flux (W m^{-2})

H Initial model domain size; height of firn (m)

$\mathbf{H}_u$ digital elevation model height of firn surface (m)

K hydraulic permeability (m s^{-1})

Q an energy flux (W m^2)

T temperature (K)

$\mathbf{T}_0$ firn surface temperature (K)

$\mathbf{T}_{air}$ air temperature (K)

$\mathbf{T}_{frz}$ the freezing temperature of water, 273.15 (K)

$\mathbf{T}_{sfc}$ lake surface temperature (K)

V volume of meltwater (m^3)

W proportion of a grid cell that is liquid water

α albedo

δ snow grain size (μm)

ε emissivity

η viscosity (Pa s)

κ thermal diffusivity ($m^2\ s^{-1}$)

$\kappa*$ extinction coefficient (m^{-1})

μ cosine for the effective angle for incident sunlight (radians)

ν wind speed ($m\ s^{-1}$)

ξ height (coordinate transformed)

ρ density ($kg\ m^{-3}$)

ρ_a density of dry air ($kg\ m^{-3}$)

ρ_{ice} density of ice ($kg\ m^{-3}$)

ρ_{liq} density of water ($kg\ m^{-3}$)

ϕ solid fraction

Π hydraulic permeability (m^2)

L latent heat of fusion ($J\ kg^{-1}$)

L* latent heat of vaporisation ($J\ kg^{-1}$)

References

Alexiades, V. and Solomon, A. (1993). *Mathematical Modelling of Melting and Freezing Processes*. Hemisphere Publishing Corporation.

Ambaum, M. (2010). *Thermal Physics of the Atmosphere*. Royal Meteorological Society.

Anisimov, O., Vaughan, D., Callaghan, T., Furgal, C., Marchant, H., Prowse, T., Vilhjlmsson, H., and Walsh, J. (2007). Polar regions (Arctic and Antarctic). Climate Change 2007: Impacts, Adaptation and Vulnerability. Contribution of Working Group II to the Fourth Assessment Report of the Intergovernmental Panel on Climate Change, M.L. Parry, O.F. Canziani, J.P. Palutikof, P.J. van der Linden and C.E. Hanson, Eds.

Arnold, N. (2010). A new approach for dealing with depressions in digital elevation models when calculating flow accumulation values. *Progress in Physical Geography*, **34**(6), 781–809.

Arnold, N., Richards, K., Willis, I., and Sharp, M. (1998). Initial results from a distributed , physically based model of glacier hydrology. *Hydrological Processes*, **12**(February 1997), 191–219.

Arthern, R., Vaughan, D. G., Rankin, A., Mulvaney, R., and Thomas, E. (2010). In situ measurements of Antarctic snow compaction compared with predictions of models. *Journal of Geophysical Research*, **115**.

Banwell, A., Arnold, N., Willis, I., Tedesco, M., and Ahlstrøm, A. (2012b). Modeling supraglacial water routing and lake filling on the Greenland Ice Sheet. *Journal of Geophysical Research: Earth Surface*, **117**(4), 1–11.

Banwell, A., MacAyeal, D., and Sergienko, O. (2013). Breakup of the Larsen B Ice Shelf triggered by chain reaction drainage of supraglacial lakes. *Geophysical Research Letters*, **40**.

Barrand, N., Vaughan, D., Steiner, N., Tedesco, M., Kuipers Munneke, P., Van Den Broeke, M., and Hosking, J. (2013). Trends in Antarctic Peninsula surface melting conditions from observations and regional climate modeling. *Journal of Geophysical Research: Earth*

Surface, **118**(1), 315–330.

Batchelor, G. (1974). Transport properties of two-phase materials with random structure. *Annu.Rev. Fluid Mech.*, **6**.

Bell, R., Chu, W., Kingslake, J., Das, I., Tedesco, M., Tinto, K., Zappa, C., Frezzotti, M., Boghosian, A., and Lee, W. (2017). Antarctic ice shelf potentially stabilized by export of meltwater in surface river. *Nature*, **544**(7650), 344–348.

Bevan, S., Luckman, A., Hubbard, B., Kulessa, B., Ashmore, D., Kuipers Munneke, P., O'Leary, M., Booth, A., Sevestre, H., and McGrath, D. (2017). Centuries of intense surface melt on larsen c ice shelf. *The Cryosphere*, **In Discussion**.

Church, J., Clark., P., Cazenave, A., Gregory, J., Jevrejeva, S., Levermann, A., Merrifield, M., Milne, G., Nerem, R., Nunn, P., Payne, A., Pfeffer, W., Stammer, D., and Unnikrishnan, A. (2013). Sea level change. *Climate Change 2013: The Physical Science Basis. Contribution of Working Group I to the Fifth Assessment Report of the Intergovernmental Panel on Climate Change*, pages 1137–1216.

Clason, C., Mair, D., Burgess, D., and Nienow, P. (2012). Modelling the delivery of supraglacial meltwater to the ice/bed interface: Application to southwest Devon Ice Cap, Nunavut, Canada. *Journal of Glaciology*, **58**(208), 361–374.

Colbeck, S. C. and Anderson, E. (1982). The permeability of a melting snow cover. *Water Resources Research*, **18**(4), 904–908.

Crank, J. (1984). *Free and Moving Boundary Problems*. Clarenden Press.

Cuffey, K. (2001). Interannual variability of elevation on the Greenland ice sheet: effects of firn densification, and establishment of a multi-century benchmark. *Journal of Glaciology*, **47**(158).

De Angelis, H. and Skvarca, P. (2003). Glacier surge after ice shelf collapse. *Science (New York, N.Y.)*, **299**(5612), 1560–2.

Domack, E., Duran, D., Leventer, A., Ishman, S., Doane, S., McCallum, S., Amblas, D., Ring, J., Gilbert, R., and Prentice, M. (2005). Stability of the Larsen B ice shelf on the Antarctic Peninsula during the Holocene epoch. *Nature*, **436**(7051), 681–685.

Ebert, E. and Curry, J. (1993). An intermediate one-dimensional thermodynamic sea ice model for investigating ice-atmosphere interactions. *Journal of Geophysical Research*, **98**(C6), 10085–10109.

Forster, R., Box, J., van den Broeke, M., Miège, C., Burgess, E., van Angelen, J., Lenaerts, J., Koenig, L., Paden, J., Lewis, C., Gogineni, S., Leuschen, C., and McConnell, J. (2014).

Extensive liquid meltwater storage in firn within the Greenland ice sheet. *Nature Geoscience*, **7**(2), 1–4.

Fretwell, P., Pritchard, H. D., Vaughan, D. G., Bamber, J. L., Barrand, N. E., Bell, R., Bianchi, C., Bingham, R. G., Blankenship, D. D., Casassa, G., Catania, G., Callens, D., Conway, H., Cook, A. J., Corr, H. F. J., Damaske, D., Damm, V., Ferraccioli, F., Forsberg, R., Fujita, S., Gim, Y., Gogineni, P., Griggs, J. A., Hindmarsh, R. C. A., Holmlund, P., Holt, J. W., Jacobel, R. W., Jenkins, A., Jokat, W., Jordan, T., King, E. C., Kohler, J., Krabill, W., Riger-Kusk, M., Langley, K. A., Leitchenkov, G., Leuschen, C., Luyendyk, B. P., Matsuoka, K., Mouginot, J., Nitsche, F. O., Nogi, Y., Nost, O. A., Popov, S. V., Rignot, E., Rippin, D. M., Rivera, A., Roberts, J., Ross, N., Siegert, M. J., Smith, A. M., Steinhage, D., Studinger, M., Sun, B., Tinto, B. K., Welch, B. C., Wilson, D., Young, D. A., Xiangbin, C., and Zirizzotti, A. (2013). Bedmap2: Improved ice bed, surface and thickness datasets for Antarctica. *Cryosphere*, **7**(1), 375–393.

Fujitai, S., Hirabayashi, M., Goto-Azuma, K., Dallmayr, R., Satow, K., Zheng, J., and Dahl-Jensen, D. (2014). Densification of layered firn of the ice sheet at NEEM, Greenland. *Journal of Glaciology*, **60**(223), 905–921.

Glasser, N. F., Kulessa, B., Luckman, A., Jansen, D., King, E. C., Sammonds, P. R., Scambos, T. A., and Jezek, K. C. (2009). Surface structure and stability of the Larsen C ice shelf, Antarctic Peninsula. *Journal of Glaciology*, **55**(191), 400–410.

Gourmelen, N., Shepherd, A., Jenkins, A., and Houlie, N. (2009). Basal melt rate at the larsen- c ice shelf, poster c21d-0473. AGU Fall meeting 2009, San Francisco, USA.

Griggs, J. A. and Bamber, J. L. (2009). Ice shelf thickness over Larsen C, Antarctica, derived from satellite altimetry. *Geophysical Research Letters*, **36**(19), 1–5.

Henneman, H. and Stefan, H. (1999). Albedo models for snow and ice on a freshwater lake. *Cold Regions Science and Technology*, **29**.

Hock, R., De Woul, M., Radic, V., and Dyurgerov, M. (2009). Mountain glaciers and ice caps around Antarctica make a large sea-level rise contribution. *Geophysical Research Letters*, **36**(7), 1–5.

Holland, D. M. and Jenkins, A. (1999). Modeling Thermodynamic Ice-Ocean Interactions at the Base of an Ice Shelf. *Journal of Physical Oceanography*, **29**(8), 1787–1800.

Holland, P., Corr, H. F. J., Pritchard, H. D., Vaughan, D. G., Arthern, R. J., Jenkins, A., and Tedesco, M. (2011). The air content of Larsen Ice Shelf. *Geophysical Research Letters*, **38**(10), 1–6.

Holland, P. R., Brisbourne, A., Corr, H. F. J., McGrath, D., Purdon, K., Paden, J., Fricker, H. A., Paolo, F. S., and Fleming, A. H. (2015). Oceanic and atmospheric forcing of Larsen C Ice-Shelf thinning. *Cryosphere*, **9**(3), 1005–1024.

Hubbard, B., Luckman, A., Ashmore, D., Bevan, S., Kulessa, B., Kuipers Munneke, P., Philippe, M., Jansen, D., Booth, A., Sevestre, H., Tison, J., O'Leary, M., and Rutt, I. (2016). Massive subsurface ice formed by refreezing of ice-shelf melt ponds. *Nature Communications*, **7**(May), 1–6.

Jansen, D., Kulessa, B., Sammonds, P. R., Luckman, A., King, E. C., and Glasser, N. F. (2010). Present stability of the Larsen C ice shelf, Antarctic Peninsula. *Journal of Glaciology*, **56**(198), 593–600.

Jansen, D., Luckman, A., Cook, A., Bevan, S., Kulessa, B., and Hubbard, B. (2015). Brief Communication: Newly developing rift in Larsen C Ice Shelf presents significant risk to stability. *The Cryosphere*, **9**, 1223–1227.

Jarvis, E. and King, E. (1995). Seismic investigation of the Larsen Ice Shelf, Antarctica: in search of the Larsen Basin. *Antarctic Science*, **7**(2), 181–190.

Khazendar, A., Rignot, E., and Larour, E. (2011). Acceleration and spatial rheology of Larsen C Ice Shelf, Antarctic Peninsula. *Journal of Geophysical Research*, **38**(9).

Khazendar, A., Borstad, C. P., Scheuchl, B., Rignot, E., and Seroussi, H. (2015). The evolving instability of the remnant Larsen B Ice Shelf and its tributary glaciers. *Earth and Planetary Science Letters*, **419**, 199–210.

Kingslake, J., Ely, J., I. Das, I., and Bell, R. (2017). Widespread movement of meltwater onto and across Antarctic ice shelves. *Nature*, **544**(7650), 349–352.

Krinner, G., Magand, O., Simmonds, I., Genthon, C., and Dufresne, J. L. (2007). Simulated Antarctic precipitation and surface mass balance at the end of the twentieth and twenty-first centuries. *Clim Dyn*, **28**(215), 215–230.

Kuipers Munneke, P., Van den Broeke, M., King, J., Grat, T., and Reijmer, C. (2012a). Near-surface climate and surface energy budget of Larsen C ice shelf, Antarctic Peninsula. *The Cryosphere*, **6**.

Kuipers Munneke, P., Picard, G., Van Den Broeke, M. R., Lenaerts, J. T. M., and Van Meijgaard, E. (2012b). Insignificant change in Antarctic snowmelt volume since 1979. *Geophysical Research Letters*, **39**(1), 6–10.

Kuipers Munneke, P., Ligtenberg, S., Van den Broeke, M., and Vaughan, D. (2014). Firn air depletion as a precursor of Antarctic ice-shelf collapse. *Journal of Glaciology*, **60**(220),

205–214.

Leeson, A., Shepherd, A., Palmer, S., Sundal, A., and Fettweis, X. (2012). Simulating the growth of supraglacial lakes at the western margin of the Greenland ice sheet. *Cryosphere*, **6**(5), 1077–1086.

Li, J. and Zwally, H. (2002). Modeled seasonal variations of firn density induced by steady-state surface air-temperature cycle. *Annals of Glaciology*, **34**.

Ligtenberg, S., Helsen, M., and van den Broeke, M. (2011). An improved semi-empirical model for the densification of Antarctic firn. *The Cryosphere*, **5**.

Luckmann, A., Elvidge, A., Jansen, D., Kulessa, B., Kuipers Munneke, P., King, J., and Barrand, N. (2015). Surface melt and ponding on Larsen C Ice Shelf and the impact of foehn winds. *Antarctic Science*, **26**(6), 625–635.

Lüthje, M., Pedersen, L., Reeh, N., and Greuell, W. (2006a). Modelling the evolution of supraglacial lakes on the West Greenland ice-sheet margin. *Journal of Glaciology*, **52**(179).

Lüthje, M., Feltham, D. L., Taylor, P. D., and Worster, M. G. (2006b). Modeling the summertime evolution of sea-ice melt ponds. *Journal of Geophysical Research: Oceans*, **111**(2), 1–17.

Marshall, G., Stott, P., Turner, J., Connolley, W., King, J., and Lachlan-Cope, T. (2004). Causes of exceptional atmospheric circulation changes in the Southern Hemisphere. **31**, 2–5.

Marshall, S. (2012). *The Cryosphere*. Princeton University Press.

MathWorks (2015). pdepe. http://uk.mathworks.com/help/matlab/ref/pdepe.html. Accessed: 2016-01-05.

McGrath, D., Steffen, K., Rajaram, H., Scambos, T., Abdalati, W., and Rignot, E. (2012). Basal crevasses on the Larsen C Ice Shelf, Antarctica: Implications for meltwater ponding and hydrofracture. *Geophysical Research Letters*, **39**(16), 1–6.

McKay, C., Clow, G., Anderson, D., and Wharton Jr., R. (1994). Light transmission and reflection in perennially ice-covered Lake Hoare, Antarctica. *Journal of Geophysical Research*, **99**(C10).

Moaveni, S. (2010). *Engineering Fundamentals: An Introduction to Engineering*. Cengage Learning.

Morris, E. and Vaughan, D. (2003). Spatial and temporal variation of surface temperature on the Antarctic Peninsula and the limit of viability of ice shelves. *Antarctic Peninsula*

Climate Variability: Historical and Paleoenvironmental Perspectives, Anarct. Res. Ser., **79**.

Oerlemans, J. (1991). The mass balance of the Greenland ice sheet: sensitivity to climate change as revealed by energy-balance modelling. *The Holocene*, **1**(1), 40–48.

Paterson, W. (2000). *The Physics of Glaciers*. Butterworth-Heinemann.

Pfeffer, W. and Bretherton, C. (1987). The effect of crevasses on the solar heating of a glacier surface. (170), 191–206.

Pope, A., Scambos, T., Moussavi, M., Tedesco, M., Willis, M., Shean, D., and Grigsby, S. (2016). Estimating supraglacial lake depth in West Greenland using Landsat 8 and comparison with other multispectral methods. *Cryosphere*, **10**(1), 15–27.

Rack, W. and Rott, H. (2004). Pattern of retreat and disintegration of the Larsen B ice shelf, Antarctic Peninsula. *Annals of Glaciology*, **39**.

Rebesco, M., Domack, E., Zgur, F., Lavoie, C., Leventer, A., Brachfeld, S., Willmott, V., Halverson, G., Truffer, M., Scambos, T., Smith, J., and Pettit, E. (2014). Boundary condition of grounding lines prior to collapse, Larsen-B Ice Shelf, Antarctica. *Science*, **345**(6202).

Reynolds, J. (1981). Lakes on George VI Ice Shelf, Antarctica. *Polar Record*, **20**(128).

Rignot, E. (2013). Ice_Shelf Melting Around Antarctica. *Science*, **341**.

Rignot, E., Casassa, G., Gogineni, P., Krabill, W., Rivera, A., and Thomas, R. (2004). Accelerated ice discharge from the Antarctic Peninsula following the collapse of Larsen B ice shelf. *Geophysical Research Letters*, **31**(L18401).

Rott, H., Rack, W., Nagler, T., and Skvarca, P. (1998). Climatically induced retreat and collapse of northern Larsen Ice Shelf, Antarctic Peninsula. *Annals of Glaciology*, **27**.

Rye, C., Arnold, N., Willis, I., and Kohler, J. (2010). Modeling the surface mass balance of a high Arctic glacier using the ERA-40 reanalysis. *Journal of Geophysical Research*, **115**(F2), 1–18.

Scambos, T., Hulbe, C., Fahnestock, M., and Bohlander, J. (2000). The link between climate warming and break-up of ice shelves in the Antarctic Peninsula. *Journal of Glaciology*, **46**(154).

Scambos, T., Hulbe, C., and Fahnestock, M. (2003). Climate-induced ice shelf disintegration in the Antarctic Peninsula. *Antarctic Peninsula Climate Variability, Antarctic Research Series*, **79**.

Scambos, T., Bohlander, J., Schuman, C., and Skvarca, P. (2004). Glacier acceleration and thinning after ice shelf collapse in the Larsen B embayment, Antarctica. *Geophysical*

Research Letters, **731**.

Schytt, V. (1958). Glaciology. A: Snow studies at Maudheim. Glaciology. B: Snow studies inland. Glaciology. C: The inner structure of the ice shelf at Maudheim as shown by core drilling. *Norwegian- British- Swedish Antarctic Expedition, 1949-5*, **IV**.

Scott, F. and Feltham, D. (2010). A model of the three-dimensional evolution of Arctic melt ponds of first-year and multiyear sea ice. *Journal of Geophysical Research*, **46**(154).

Sergienko, O. (2005). *Surface melt in ice shelves and icebergs*. Ph.D. thesis, University of Chicago.

Sergienko, O. and MacAyeal, D. (2005). Surface melting on Larsen Ice Shelf, Antarctica. *Annals of Glaciology*, **40**(1), 215–218.

Shepherd, A., Wingham, D., Payne, T., and Skvarca, P. (2003). Larsen Ice Shelf has progressively thinned. *Science*, **302**.

Shimizu, H. (1970). Air permeability of deposited snow. *Low Temp. Sci., Ser. A,*, **22**.

Shindell, D. and Schmidt, G. (2004). Southern Hemisphere climate response to ozone changes and greenhouse gas increases. **31**, 1–4.

Singh, P. (2001). *Snow and Glacier Hydrology*, volume 37 of Water Science and Technology Library. Springer Science Business Media.

Skeel, R. and Berzins, M. (1990). A method for the spatial discretization of parabolic equations in one space. *Siam J. Sci. Stat. Comput.*, **11**(1).

Skvarca, P., De Angelis, H., and Zakrajsek, A. F. (2004). Climatic conditions, mass balance and dynamics of Larsen B ice shelf, Antarctic Peninsula, prior to collapse. *Annals of Glaciology*, **39**(1), 557–562.

Sturm, M., Holmgren, J., Knig, M., and Morris, K. (1997). The thermal conductivity of seasonal snow. *Journal of Glaciology*, **43**(143), 2641.

Taylor, P. and Feltham, D. (2004). A model of melt pond evolution on sea ice. *Journal of Geophysical Research*, **109**(C12007).

The Engineering ToolBox (2016). Water- Thermal Properties. http://www.engineeringtoolbox.com/water-thermal-properties-d$_1$62.*html*. *Accessed* : $2016 - 12 - 21$.

The MIDAS project (2017). Larsen C Ice Shelf poised to calve. http://www.projectmidas.org/blog/larsen-c-ice-shelf-poised-to-calve/. Accessed: 2017-02-19.

Thompson, D. and Solomon, S. (2002). Interpretation of Recent Southern Hemisphere

Climate Change. **296**(May), 895–899.

Touloukian, Y., Liley, P., and Saxena, S. (1970). Thermophysical Properties of Matter - The TPRC Data Series. Volume 3. Thermal Conductivity - Nonmetallic Liquids and Gases.

Tseng, P., Illangasekare, T., and Meier, M. (1994). Modelling of snow melting and uniform wetting front migration in a layered subfreezing snowpack. *Water Resources Research*, **30**(8), 2363–2376.

van den Broeke, M. (2005). Strong surface melting preceded collapse of Antarctic Peninsula ice shelf. *Geophysical Research Letters*, **32**(12), 1–4.

Vaughan, D. G. and Arthern, R. (2007). 'CLIMATE CHANGE: Why Is It Hard to Predict the Future of Ice Sheets?'. *Science*, **315**(5818), 1503–1504.

Wright, A. P., Wadham, J., Siegert, M., Kohler, A. L. J., and Nuttali, A. (2007). Modeling the refreezing of meltwater as superimposed ice on a high Arctic glacier: A comparison of approaches. *Journal of Geophysical Research: Earth Surface*, **112**(4), 1–14.

Zwally, H. and Li, J. (2002a). Seasonal and interannual variations of firn densification and ice-sheet surface elevation at the Greenland summit. *Journal of Glaciology*, **48**(161), 199–207.

Zwally, H., Abdalati, W., Herring, T., Larson, K., Saba, J., and Steffen, K. (2002b). Surface Melt-Induced Acceleration of Greenland Ice-Sheet Flow. *Science*, **297**(5579), 218–222.